

Lawrence Berkeley National Laboratory

Recent Work

Title

THE USE OF THE STATISTICAL MODEL IN HEAVY-ION REACTION STUDIES

Permalink

<https://escholarship.org/uc/item/1t08w1g8>

Author

Stokstad, Robert.

Publication Date

1981-04-01



Lawrence Berkeley Laboratory

UNIVERSITY OF CALIFORNIA

To be published as a Chapter in Heavy-Ion Science,
D. Allan Bromley, ed., Plenum Publishing,
New York, 1981

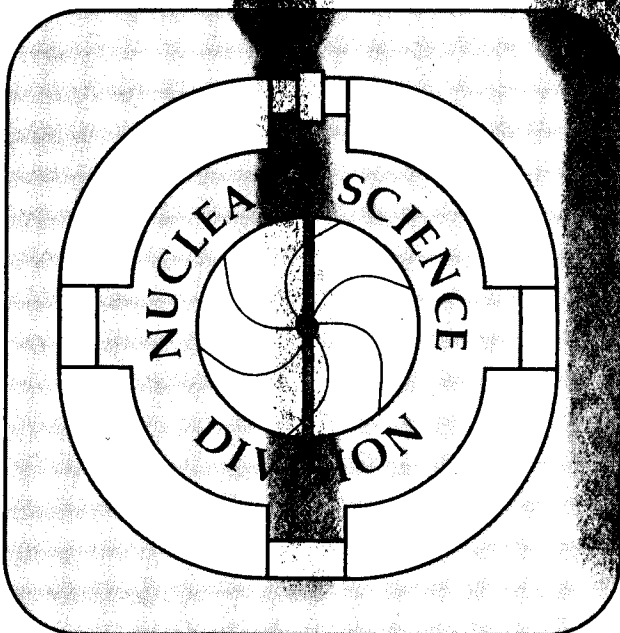
THE USE OF THE STATISTICAL MODEL IN
HEAVY-ION REACTION STUDIES

Robert Stokstad

April 1981

REC'D
LIBRARY
NOV 9 1981

LIBRARY AND
DOCUMENTS SECTION



LBL-12636
c.2

DISCLAIMER

This document was prepared as an account of work sponsored by the United States Government. While this document is believed to contain correct information, neither the United States Government nor any agency thereof, nor the Regents of the University of California, nor any of their employees, makes any warranty, express or implied, or assumes any legal responsibility for the accuracy, completeness, or usefulness of any information, apparatus, product, or process disclosed, or represents that its use would not infringe privately owned rights. Reference herein to any specific commercial product, process, or service by its trade name, trademark, manufacturer, or otherwise, does not necessarily constitute or imply its endorsement, recommendation, or favoring by the United States Government or any agency thereof, or the Regents of the University of California. The views and opinions of authors expressed herein do not necessarily state or reflect those of the United States Government or any agency thereof or the Regents of the University of California.

THE USE OF THE STATISTICAL MODEL IN HEAVY-ION
REACTION STUDIES

Robert Stokstad

Nuclear Science Division
Lawrence Berkeley Laboratory
University of California
Berkeley, CA 94720

ABSTRACT

The statistical models of nuclear structure and nuclear reactions receive wide application in the analysis of heavy-ion reaction data. This article reviews the use of statistical models to describe nuclear level densities and the decay of equilibrated nuclei. Applications are illustrated with examples of gamma-ray decay, the emission of light particles and heavier clusters of nucleons, and fission. In addition to the compound nucleus, the treatment of equilibrated fragments formed in binary reactions is discussed. The statistical model is shown to be an important tool for the identification of products from nonequilibrium decay.

To be published in Heavy Ion Science (D. Allan Bromley, ed.), Plenum, New York (1982).

This work was supported by the Director, Office of Energy Research, Division of Nuclear Physics of the Office of High Energy and Nuclear Physics and by Nuclear Sciences of the Basic Energy Sciences Program of the U.S. Department of Energy under Contract W-7405-ENG-48.

THE USE OF THE STATISTICAL MODEL IN HEAVY-ION
REACTION STUDIES

TABLE OF CONTENTS

1.	INTRODUCTION	1
2.	THE NUCLEAR LEVEL DENSITY	7
2.1	Introduction	7
2.2	Methods for Obtaining the Level Density	8
2.3	The Equidistant-Level Model	9
2.4	Shell Effects and Residual Interactions	12
2.4.1	Nonuniform Single-Particle Spacings	12
2.4.2	Pairing	13
2.4.3	Deformation	14
2.4.4	Effective Residual Interactions	17
2.5	Measurements of Level Densities and Comparison with Theory . .	18
2.6	Compilations of Level-Density Parameters	23
2.6.1	Gilbert and Cameron	24
2.6.2	Gadioli and Zetta	25
2.6.3	Facchini et al.	25
2.6.4	Dilg et al.	26
2.6.5	Holmes	26
2.6.6	Beckerman	26
2.7	Summary	27

3.	THE DECAY OF AN EQUILIBRATED NUCLEUS	29
3.1	Introduction	29
3.2	Modes of Decay	31
3.2.1	Gamma-Ray Decay	31
3.2.2	Emission of Nucleons and Clusters	35
3.2.3	Fission	39
3.2.4	The Total Decay Rate	42
3.3	The Hauser-Feshbach Formulae	44
3.4	A Consistent Treatment of Fission and Evaporation	46
3.5	Practical Calculations, Computer Codes	49
3.6	Summary	52
4.	ILLUSTRATIVE APPLICATIONS	54
4.1	Introduction	54
4.2	Compound Nucleus Reactions	55
4.2.1	The Decay of Light Compound Nuclei	56
4.2.1a	Gamma-Ray Decay	57
4.2.1b	Light-Particle Emission	58
4.2.1c	Emission of Heavy Clusters	60
4.2.1d	High-Spin Selectivity	63
4.2.1e	Evaporation Residues	64
4.2.1f	Two-Particle Correlations	70
4.2.2	Neutron-Gamma Competition	74
4.2.2a	General Features	74
4.2.2b	Gamma-Ray Multiplicity	75
4.2.2c	The Gamma-Ray Continuum	78

4.2.3 Fission-Evaporation Competition	79
4.2.3a Results for Light Ions	79
4.2.3b High Angular Momentum	80
4.2.3c Fission-Barrier Heights	81
4.2.3d A Search for Shell Effects in Hot, High Spin Nuclei	83
4.2.3e Open Questions	86
4.3 Noncompound Reactions	89
4.3.1 Introduction	89
4.3.2 Primary and Secondary Distributions	90
4.3.3 Measurements of Spin and Alignment	90
4.3.4 Energy Equilibration and the Emission of Fast Particles .	93
4.3.4a Nucleon Emission	93
4.3.4b Alpha-Particle Emission	95
4.3.4c Summary of Results	98
4.4 Summary	99
ACKNOWLEDGEMENTS	101
REFERENCES	102
TABLES	120
FIGURE CAPTIONS	125
FIGURES	138

1. INTRODUCTION

Statistical concepts and models have been used to understand the nucleus and its reactions with other nuclei since the beginning of nuclear science. The reason for this is simple. The nucleus is a many body, complex system which, if given even a rather small amount of excitation energy, may experience many different configurations. That is to say, the density of quantum-mechanical states increases rapidly with excitation energy and soon becomes very large. Even at the lowest bombarding energies at which nuclear reactions can be initiated with charged particles, there are many states available for the compound nucleus and, often, many different ways in which it can decay. Given this complexity, statistical methods are not only appropriate, they are essential for the comprehension and prediction of many nuclear phenomena.

The "statistical model", unlike, e.g., the optical model, is not a precisely defined term. There is a statistical model for the average properties of nuclei having a given excitation, energy, and angular momentum. This model is of importance because it predicts the density of levels, something which must be known in order to apply another statistical model, that for the decay of an equilibrated nucleus. This second statistical model, and the one with which we are mainly concerned, assumes that all possibilities for decay are, intrinsically, equally likely and are thus governed by factors such as the density of final states and barrier penetration factors. The probability for a particular decay to occur is thus inversely proportional to the total number of possible decays. This statistical assumption, when combined with

conservation laws and the principle of detailed balance, leads to a statistical model for average cross sections.

Nuclear physics began with neutron and light-ion probes. Thus, the early development of the statistical model was influenced strongly by the type of experimental data characteristic of neutron- and proton-induced reactions. This development proceeded along the two distinct but not unrelated tracks noted above, the studies of nuclear structure and of nuclear reactions. The study of nuclear structure involved the characterization of the many levels near the neutron separation energy in terms of the distribution of their spacings (the Wigner distribution) and widths (the Porter-Thomas distribution). The variation with excitation energy of the density of levels was described by the properties of a gas of noninteracting Fermions. The systematic exploration of these statistical properties throughout the periodic table revealed, of course, many aspects of nuclear structure outside the realm of the gas model.

Nuclear reaction studies concerned the analysis of cross-section data in terms of the statistical model for the formation and decay of the compound nucleus. The early models developed by Bethe, Weisskopf and Ewing (1937-1940) were very successful in explaining a large body of experimental data, acquired in the following two decades, on average neutron cross sections and the evaporation of protons, neutrons and alpha particles. These models, based on Bohr's independence hypothesis for the formation and decay of the compound nucleus nevertheless neglected a direct consideration of angular momentum and parity. These defects were remedied in 1952 by Hauser and Feshbach.

The advent of heavy-ion beams in the late 1950s brought with it new phenomena and a need for new applications of the statistical model. The

introduction of large amounts of angular momentum associated with the large mass of the projectile had many consequences. Processes which can effectively dissipate angular momentum--the emission of α particles, heavier clusters, and fission--gained importance. Not only the compound nucleus, but also the heavy residue which remained after evaporation was complete, was now a rapidly spinning object. Thus, new questions could be asked about the behavior of the nucleus under the stress of centrifugal forces and how its nuclear structure would be reflected in the products of its decay.

With the incorporation of angular momentum in the nuclear level density and in the theory of compound nuclear reactions, the statistical model was in a form suitable for the analysis of heavy-ion induced reactions. The decade beginning in 1960 saw the first applications of compound nucleus theory to evaporation from compound nuclei formed by the fusion of heavy ions. The results were not only encouraging, they were surprisingly good, considering one of the basic approximations made in the derivation of the Hauser-Feshbach formula was violated by the strongly absorbing nature of heavy ions.

The many channels populated in heavy-ion reactions required the development of major computer programs for the prediction and analysis of the various products of compound nucleus data. Gamma-ray emission and fission were included as competing processes. The study of angular momentum effects on the multiplicity of gamma rays and on the probability for fission became a significant enterprise in the late 1960s and continues as such today. Indeed, the period between approximately 1965 and 1975 was one in which many comparisons of the statistical models of

nuclear structure and nuclear reactions were made with experimental data. These comparisons spurred refinements in the techniques of statistical model calculations and brought us to the point where the model became as much an analytical tool as an object of study for its own sake. It can now be used to verify the reaction mechanism, to aid in the identification of compound nucleus formation and decay, to determine angular momenta, and to search for nonstatistical aspects of nuclear structure at high excitation energies and high angular momentum.

Today the statistical model finds wide application outside the area for which it was originally developed, compound nucleus formation and decay. The products emerging from a heavy-ion reaction can include two heavy fragments, one reminiscent of the projectile and the other of the target, which carry excitation energy and angular momentum. Each fragment will, in general, reach equilibrium and therefore qualify for a statistical treatment of its decay. The application of the statistical model to such binary, noncompound reactions makes possible a determination of the properties of the fragment before it decayed and this renders the primary reaction accessible for study. In such a comparison between experiment and an equilibrium model, it also becomes possible to identify the reaction products which originate with nonequilibrium processes and which may probe the early stages of the reaction. Rapid progress has been made in the last few years in the development and application of Monte Carlo statistical model codes for this purpose.

The purpose of this review is to describe the application of the statistical model to the analysis of heavy-ion reaction data. Thus, the emphasis is on how the model is used and how useful it may be. In this

practical approach, the theoretical foundations of the model are necessarily slighted, but this is perhaps excusable given the existence of comprehensive articles on the subject (Er 60, Fe 60, Vo 68, Bo 70) and the recent review by Mahaux and Weidenmüller (Ma 79).

The present article has three main sections which deal with the subjects of level densities, the decay of an equilibrated nucleus, and applications. The density of levels enters into all statistical model calculations. Therefore, section 2 discusses this subject at some length and attempts to show how nuclear structure enters into the density of levels.

Whatever form the particular expression used in a statistical model calculation may take, it can be related to the equations governing the decay of an equilibrated nucleus. Section 3 presents these equations for gamma-ray decay, particle evaporation, and fission. Following a brief discussion of the relationship between the evaporation of large clusters and fission, the methods used in practical calculations are mentioned.

Illustrative examples of the use of the statistical model are given in section 4. The discussion of compound nucleus reactions is organized according to the principal modes of decay. Light nuclei are discussed first. In this case, proton, neutron and α -particle emission are the main competitors. In heavier nuclei, it is the competition between fission and evaporation and then between neutron and gamma-ray emission which is of importance.

The experience gained from the study and successful analysis of compound nuclear reactions provides a solid basis for the application of the statistical model to reactions which do not proceed via compound

nucleus formation. Here, the emission of gamma rays and light particles and fission are again encountered, but the source is assumed to be a fully accelerated and equilibrated fragment emerging from the nuclear collision. The modeling of such post-reaction effects and the associated comparison with coincidence experiments has recently become quite sophisticated and holds considerable potential for the study of nonequilibrium phenomena in heavy-ion induced reactions.

The three sections are intended to be reasonably self contained; while it is logical to read them in the order in which they are presented, it is not essential.

It may be valuable to say what this review does not attempt. Fusion, the reaction mechanism responsible for the formation of a compound nucleus, is not discussed per se but is the subject of a separate chapter by U. Mosel. Similarly, deep inelastic scattering, a mechanism by which equilibrated fragments are produced, and the systematics of fission are not covered here but are reviewed by J.R. Huizenga and H.J. Specht, respectively.

There is an important aspect of the statistical model which, regrettably, it has not been possible to include: the energy dependence of the reaction cross section, i.e., fluctuation phenomena. The statistical model which predicts average cross sections can also predict the width of the distribution of cross sections about this average. Particularly in light nuclei, statistical analyses of the narrow structure often seen in excitation functions for heavy-ion induced reactions have provided important clues to the nature of the reaction mechanism and the properties of the compound nucleus.

2. THE NUCLEAR LEVEL DENSITY

2.1. Introduction

A glance at any compilation of nuclear level schemes shows that the density of levels increases rapidly with increasing excitation energy. It is also readily apparent that the density of levels near the ground state varies markedly depending on an odd or even number of neutrons and protons, the vicinity of a closed shell, and the spherical or deformed nature of the nucleus. The accurate calculation of the decay products of an excited nucleus requires the ability to describe not only these variations in level density at low excitation but also to extrapolate the level density into regions of excitation energy, angular momentum, and nuclear shape for which we have little direct experimental knowledge. Thus, characterization of the level density will have to be in large part phenomenological. A basic and simple theoretical model will provide the energy and angular momentum dependence in terms of parameters which can be adjusted to provide agreement with known level densities.

Apart from our rather practical needs, the theoretical study of the nuclear level density provides a fundamental insight into an important average property of nuclei and how it is affected by the microscopic, i.e. shell-related, aspects of nucleonic motion.

The literature on nuclear level densities is extensive, and there are a number of review articles and conference proceedings available for the interested reader (Er 60, Ga 72, Hu 72, Hu 72a, Da 80).

After mention of the theoretical methods used to obtain the level density, the results of the simplest model will be discussed. The various effects of shell structure and residual interactions are then described and experimental determinations of the level density and comparisons with theory overviewed. A partial list of compilations of nuclear level-density parameters will be given at the end of this section.

2.2. Methods for Obtaining the Level Density

The calculation of a nuclear level density amounts to determining the number of different ways in which individual nucleons can be placed in the various single-particle orbitals such that the excitation energy lies in the range E to $E + dE$. It is thus a combinatorial problem in which the physics is contained in the specification of the single particle orbitals if the nucleons are noninteracting and requires specification of the residual interaction if they do interact.

There are three main methods of obtaining the level density from the single particle levels. The first and oldest method, which might be called the thermodynamic approach, uses the mathematical techniques of statistical mechanics (Be 36). A grand partition function, which contains the essential statistical information, is written down in terms of the single-particle levels. When the single-particle level densities have certain simple properties, the solution is analytic. The second method relies on a large computer to determine all the combinations and sort them according to excitation energy and angular momentum for a restricted number of excited nucleons and available orbitals (Gr 67, Hi 69, Wi 72, Hi 74). These two methods start from the same basis (the single particle levels) and differ only in the mathematical methods used to obtain the level density. The

combinatorial approach is more accurate when the level density is low, i.e. near the Yrast line. The third and most recently introduced method, that of spectral distributions, uses the observation that shell-model state densities are very nearly Gaussian and only the lowest moments of the nuclear Hamiltonian are needed to describe them (Ch 71, Gi 73, Ay 74, Gi 75).

2.3. The Equidistant-Level Model

The simplest possible single-particle level distribution is that of equally spaced levels separated by an energy g^{-1} MeV. (See Fig. 1a.) This represents an excellent approximation to a system of noninteracting particles, i.e., a Fermi gas, in which the single-particle level spacing decreases with the square root of energy (Hu 72). The density of states[†] for a gas of two components in this equidistant model is

$$\omega(E) = \frac{\sqrt{\pi}}{12} \frac{\exp 2\sqrt{aE}}{E^{5/4} a^{1/4}} \quad (2.1)$$

where $a = \frac{\pi^2 g}{6}$ and g is the sum of the neutron and proton single particle level densities of a Fermigas, evaluated at the Fermi surface (Hu 72). Expressions of the type (2.1) are thus referred to as the Fermi-gas level density.

Bohr and Mottelson have given a very useful exposition of the approximations made in the derivation of this formula and the physical meaning of the

[†]A level of total angular momentum J has $2J + 1$ degenerate magnetic states M . The state density ω thus counts all states (J,M) , whereas the level density ρ counts only states of different J . $\omega(E,J) = (2J + 1)\rho(E,J)$.

quantities involved (Bo 69). Summarizing their discussion: Eq. (2.1) is valid over the range $\epsilon_F/A \ll E \ll \epsilon_F A^{1/3}$ where ϵ_F = Fermi energy (≈ 37 MeV) and $A = Z + N$ = the total number of nucleons. The nuclear temperature T defined by

$$\frac{1}{T} = \frac{d \ln \omega}{dE} \quad (2.2)$$

is given by

$$\frac{1}{T} = \sqrt{\frac{a}{E}} - \frac{5}{4E} \quad (2.3)$$

and is the region around the Fermi energy in which the average occupation number of an orbital differs substantially from 1 or 0 (see Fig. 1a). Also, T is (roughly) the average energy per excited nucleon. In addition to the nuclear temperature T , a statistical or thermodynamic temperature t can be defined by the relation $t \equiv \frac{dS}{dE}$ where S is the entropy. In the limit of large excitation energies, $gE \gg 1$, the thermodynamic temperature $t = \sqrt{\frac{E}{a}}$ and T become equal. The average number of nucleons removed from ground state orbits is $n_{ex} \approx gT$. Table I gives values of these quantities for several typical cases. The rapid increase of $\omega(E)$ with E and the degenerate nature of the Fermi gas, in that only relatively few nucleons are excited even at high excitation energies, are illustrated there.

Since $a \approx \frac{E}{T^2}$, the argument of the exponential (which is the main factor governing the energy dependence of ω) is proportional to $\frac{E}{T}$. It turns out that the experimental low energy level density is often well described by the expression

$$\rho(E) = C \exp \frac{E}{T} \quad , \quad (2.4)$$

in which T is a constant. Equation (2.4), thus, is referred to as the constant temperature formula. Its application for the case of ^{20}Ne is illustrated in Fig. 2.

In general, the densities of positive and negative parity states are assumed to be equal.

In most statistical model calculations, and certainly in those involving heavy-ion reactions, it is the density of levels for a given angular momentum which must be known. Bohr and Mottelson (Bo 69) describe the derivation (Be 36) of the level density formula for a given angular momentum and both parities, $\pm\pi$:

$$\rho(E, I) = \frac{2I+1}{12} \sqrt{a} \left(\frac{\hbar^2}{2J} \right)^{3/2} \frac{1}{(E - E_{\text{rot}})^2} \exp\left\{2\sqrt{a(E - E_{\text{rot}})}\right\} \quad (2.5)$$

where $E_{\text{rot}} = \frac{\hbar^2}{2J} I(I+1)$. The rigid body moment of inertia, J , is related to the average of the squares of the single-particle angular momentum projections, $\langle m^2 \rangle$, by $J = g \langle m^2 \rangle$. Often the spin distribution is expressed in terms of a spin cutoff factor $\sigma^2 = \frac{Jt}{\hbar^2}$.

The obvious interpretation of eq. (2.5) is that energy in the form of rotation is unavailable for the random or thermodynamic excitation of the system and therefore does not contribute to what might be called the "intrinsic" level density.

The formula (2.5) differs in one respect from that used by others (La 65, Gi 70, Hu 72) in that the rotational energy is subtracted from the excitation energy appearing in the denominator as well as in the argument of the exponential. However, eq. (2.5) is only valid for $E \ll E_{\text{rot}}$ so the two expressions are equivalent in their region of validity. With this limitation, $E \ll E_{\text{rot}}$, the approximation

$$\begin{aligned} \exp 2\sqrt{a(E - E_{\text{rot}})} &\approx \exp 2\sqrt{aE} \exp\left(\frac{-E_{\text{rot}}}{t}\right) \\ &= \exp 2\sqrt{aE} \exp\left(\frac{-I(I+1)}{2\sigma^2}\right) \end{aligned} \quad (2.6)$$

is frequently used. Note that the often-encountered formula

$$\rho(E) \propto \frac{\exp(2\sqrt{aE})}{E^2}$$

corresponds to the density of levels with spin 0.

Formulae for the density of levels as a function of isospin can be derived in complete analogy with the treatment of angular momentum (Hu 72, Ki 73). As is the case with parity, isospin is generally not given specific consideration in practical statistical model calculations involving heavy ions (see Sect. 2.5).

2.4. Shell Effects and Residual Interactions

2.4.1. Non-Uniform Single-Particle Spacings

In Sec. 2.3 it was shown that only a relatively few single-particle levels in the vicinity of the Fermi surface contribute to the level density. Thus, the major shell effect we may expect at moderate excitation energies is a variation of the parameter g (or a) as nucleons are added and the location of the Fermi surface E_F moves from regions of low single particle density at magic numbers to regions of high single-particle density at mid-shell nuclei. The transition from a uniform to a nonuniform spacing as given by the shell model (Ma 55) is illustrated schematically in Figs. 1a and 1b). On the average, "a" will vary as the number of nucleons A but will show large deviations from this average near closed shells.

Figure 3 illustrates directly in terms of an experiment how dramatic an effect on the level density is had by the closure of a major shell (Mi 80). Resonances observed in (p,p) elastic scattering are shown for three targets,

^{44}Ca , ^{42}Ca , and ^{40}Ca . Note the reduction in the density of resonances the fewer the number of nucleons outside the double closed shell at $Z = N = 20$. Values of the level density parameter as obtained from an analysis of 265 nuclei are shown in Fig. 4 (Ho 76, Wo 80). The rapid decrease of "a" near shell closures is evident. The straight line, which approximates the average trend, corresponds to $a = A/9$.

Given a particular nucleus A, with Fermi surface E_F , the spacing of single particle levels will no longer be uniform and thus the energy dependence of $\rho(E)$ should no longer be given by expressions of the type (2.1) or (2.4). Certain types of nonuniform spacings, viz those which are periodic, produce an energy dependence like eq. (2.1) at high excitation energies, except that the excitation energy E is replaced by an effective excitation energy $E^* = E - \Delta$ (Ka 66). The value of Δ is positive for a nucleus with its ground state near a closed shell and is negative for a mid-shell nucleus. Thus, if a and Δ are regarded as parameters which may be adjusted for a given nucleus, it may be possible to reproduce approximately the energy dependence of ω for actual nuclei exhibiting quite different shell structures. The values of "a" shown in Fig. 4 were obtained by fitting the density of levels near the ground state and at the neutron threshold with eq. (2.1) and $E^* = E - \Delta$ (Ho 76). Allowing for an energy dependence $a \rightarrow a(E)$, corresponding to the washing out of shell effects at high excitation energies would, of course, introduce even greater flexibility in reproducing shell effects over a wide range of energy.

2.4.2. Pairing

Up to now we have considered cases in which the nucleons occupying the different single-particle levels of a spherical potential do not interact

with each other. Residual interactions will alter the energy dependence of the density of levels, the most visible of these interactions being the pairing interaction. The effect of pairing is to (partially) block levels near the Fermi surface such that unpaired nucleons cannot occupy them, thus reducing the density of levels. The effects of pairing are weakened, however, by temperature and angular momentum. Moretto (Mo 72) has calculated the critical temperature T_c and angular momentum M_c for which pairing effects vanish and the energy dependence of ρ reverts back to the Fermi-gas formula. Again, above these critical values, an effective excitation energy $E^* = E - \Delta_p$ is used where $\Delta_p = 1/2 g \Delta_0^2$ is related to the energy gap Δ_0 associated with the pairing correlation in the ground state (Mo 72). The critical temperature and angular momentum are given by

$$T_c \approx \frac{2}{3.5} \Delta_0 \quad (M = 0)$$

and

$$M_c \approx g \Delta_0 |m| \quad (T = 0)$$

where $|m|$ is the average angular momentum projection of the single-particle levels. Increased angular momentum lowers T_c below the above estimate and, also, it appears that pairing effects are small by the time the neutron threshold is reached (La 63).

2.4.3. Deformation

The spacing and order of single-particle levels depend on the shape of the nuclear potential. That deformation is a shell effect may be seen quite vividly by comparing the sequence of single-particle levels for a spherical nucleus (Fig. 1b) with those for a nucleus with varying deformation (Fig. 1c) (Bo 75). In the case of a deformed nucleus, large gaps in the spacing

of single particle levels occur for certain ratios of the major and minor axes. Thus, the density of intrinsic single-particle levels at the Fermi surface depends on the deformation. The excitation energy available for distributing nucleons among the available single particle orbitals is measured with respect to the ground state of the deformed system.

The relationship of nuclear shape, potential energy of deformation, and energy of rotation for a hypothetical cold nucleus with uniformly spaced intrinsic single particle levels (i.e. with no shell effects) is given by the rotating liquid drop model (Co 74). Microscopic calculations of the single-particle levels and their associated level densities for deformed nuclei have been reported by several workers (Mo 70, Ra 70, Mo 72c, Va 72, Wi 72). These calculations are of particular importance in the understanding of fission, a process governed in large part by the density of levels at the saddle point. The saddle point represents the maximum deformation energy of a nuclear system along its path to fission and thus shell effects can be expected to play a particularly important role. Recently, Bertsch has examined the change in the density of states as a function of the deformation (Be 80).

Another consequence of deformation for the level density in addition to its effect on the single-particle spacing is the introduction of levels associated with collective degrees of freedom, i.e. rotational levels. For small collective rotational energies, $E_{rot} \ll E$, the levels of the rotational bands built on the intrinsic states should be included to obtain the total level density (Er 58). [However, if the rotational energy becomes a large fraction of E , the intrinsic level density will have an energy dependence governed by $E - E_{rot}$ as in Eq. (2.5).]

The specification of the level density for an axially symmetric nucleus now involves two moments of inertia: \mathcal{J}_{\parallel} , the moment of inertia about an axis parallel to the symmetry axis, and \mathcal{J}_{\perp} , the moment about the perpendicular axis. The level density is obtained by summing over all intrinsic states with an angular momentum projection K on the symmetry axis for which $|K| \leq J$ (Er 58, Bo 75). Assuming a normal distribution of states with respect to K and defining $\sigma_K = \mathcal{J}_{\parallel} T / \hbar^2$,

$$\rho_{\text{intr}}(E, K) = \frac{1}{\sqrt{2\pi}\sigma_K} \exp \left\{ -\frac{K^2}{2\sigma_K^2} \right\} \rho_{\text{intr}}(E) \quad (2.7)$$

and

$$\rho(E, I) = \frac{1}{2} \sum_{K=-I}^I \rho_{\text{intr}}[E - E_{\text{rot}}(K, I), K] .$$

Thus,

$$\rho(E, I) =$$

$$\frac{1}{\sqrt{8\pi}\sigma_K} \rho_{\text{intr}}(E) \times \sum_{K=-I}^I \exp \left\{ -\frac{1}{T} \left(\frac{\hbar^2}{2\mathcal{J}_{\perp}} \right) I(I+1) + \left(\frac{\hbar^2}{2\mathcal{J}_{\parallel}} - \frac{\hbar^2}{2\mathcal{J}_{\perp}} \right) K^2 \right\} \quad (2.8)$$

For not-too-large angular momenta, it may be shown (Hu 74, Hu 74a) there is an enhancement of ρ by a factor $\sigma_{\perp}^2 = \mathcal{J}_{\perp} T / \hbar^2$ over the intrinsic density for an equivalent spherical nucleus at the same excitation. This factor, which is of the order of the number of rotational levels with rotational energy $\leq T$, is significant, ranging from 35 to 65 for nuclei with A -values ranging from 150 to 250, assuming rigid-body moments of inertia and excitation energies at the neutron binding energy.

Microscopic calculations of level densities for deformed (Hu 74, Dø 74) and spherical nuclei (Hu 74a) and comparison with experimental level densities from neutron resonances indicate the need for including the collective levels. Grimes has emphasized that the effect of deformation (indeed of all shell effects) is to redistribute the level density, not to create new levels which would otherwise not appear (somewhere) in the spectrum of a noninteracting Fermi gas (Gr 80). Thus, the collective levels must exist at the expense of higher-lying intrinsic excitations. However, it appears that the error made in neglecting the contribution of collective levels at low excitation energies would be more serious for most practical statistical model calculations than the inclusion of spurious extra levels at high excitation.

Deformation itself is a collective degree of freedom which can couple to, and be excited by, the intrinsic thermal excitations. This effect, studied by Moretto (Mo 72a), causes a reduction in the average deformation at high intrinsic excitation energies. Thus, intrinsic thermal motion washes out the shell effects producing deformation. For a number of cases considered between $A = 170$ and 200 , the shell effects (defined as a high probability of finding the nucleus in a narrow region of deformation) vanished by the time the excitation energy reached 50 MeV.

Calculations by Mosel et al. (Mo 74) using a temperature-dependent Hartree-Fock formalism have also shown this tendency of a deformed nucleus to become spherical as the temperature increases.

2.4.4. Effective Residual Interactions

The density of levels is determined exactly if the energy eigenvalues of all possible levels are calculated individually. This is feasible by combinatorial methods for the case of noninteracting particles (Gr 67, Hi 69,

Wi 72, Hi 74) but requires (with the exception of the pairing interaction) the diagonalization of the two-body residual interaction in the space of the single-particle Hamiltonian when nucleons are allowed to interact. Such calculations have shown, however, that the spectrum of eigenvalues for a given number of valence particles in a restricted space of single-particle levels has a Gaussian distribution. From this has developed the method of spectral distributions in which only the lowest moments of the eigenvalue distribution are calculated from averages and moments of the appropriate operators. This can be done for any desired residual interaction [e.g., those of Kuo and Brown (Ku 68) or of Kahana et al. (Ka 69)], without diagonalizing the Hamiltonian. The method is tested by comparison with large-scale exact shell-model calculations, and the agreement is remarkable. Such a comparison is shown in Fig. 5 (Gi 75). While this method enjoys accuracy and the ability to incorporate sophisticated residual interactions, it is limited to relatively low excitation energies because the level density of a real nucleus never reaches a maximum as does a Gaussian distribution for a finite subspace of orbitals. For obvious reasons, it is also best applied where the number of valence nucleons is large enough to give good statistics but small enough to yield a manageable calculation. Most calculations done so far are for $A < 70$ (Gi 73, Ay 74, Gi 75).

2.5. Measurements of Level Densities and Comparison with Theory

The most straightforward method of determining a level density is to count individual levels. This is possible at low excitation energies where

the levels are well spaced and easily resolved by a variety of techniques including γ -ray and charged particle spectroscopy. A narrow region of energy at the neutron threshold is accessed by neutron resonance spectroscopy. Levels spaced by only a few eV can be resolved this way, and there is a systematic body of data for hundreds of nuclei. More recently, proton resonance scattering has been done with sufficiently high resolution (~ 300 eV) to reveal individual compound nuclear resonances in nuclei with $A \lesssim 70$ (Bi 76, Mi 80) (See Fig. 3.) These types of measurements have played the major role in revealing shell effects (see Fig. 4).

Level densities of nuclei at excitation energies well above the neutron or proton separation energy, however, can only be studied through less direct approaches which involve models for the formation and decay of the compound nucleus. The spectra of protons, neutrons and alpha particles evaporated by a compound nucleus, as we shall see in the following sections, are sensitive to the density of levels in the residual nucleus. The average widths Γ of overlapping levels in a compound nucleus can be determined through an analysis of fluctuations in the energy dependence of cross section populating individual final states. Provided the total number of open channels, N , can be calculated accurately, the density of levels in the compound nucleus may be obtained from the statistical model relation

$$\rho = \frac{N}{2\pi\Gamma}$$

The determination of N , however, requires the knowledge of the level density in the residual nuclei reached by the decay. The quantity $\Gamma\rho$, or equivalently Γ/D , can also be determined from experiment by measuring the energy averaged compound nucleus cross section for the population of an

isolated level of known spin and parity and by comparing this with the Hauser-Feshbach expression (Sec. 3). The latter depends basically on transmission coefficients and N . Thus, a measurement of a fluctuation width and an average cross section can determine the density of levels in the compound nucleus.

Comparisons of theoretical and experimental level densities are shown in Fig. 6 for the nucleus ^{56}Fe . The experimental data are derived at low energies from counting levels, at high energies from fluctuation measurements (i.e., measurements of Γ and Γ/D), and at other energies from fitting the spectra of evaporated charged particles (Lu 72). Figure 6a shows a theoretical calculation by Hillman and Grover in which the single-particle levels were taken from Seeger (Se 57) and pairing was included. Level densities obtained from the single-particle levels calculated by Seeger (Se 57) and also by Nix (Bo 72) are shown in Fig. 6b, with pairing included in both cases. In Fig. 6a, the mathematical technique used was combinatorial; in Fig. 6b, statistical mechanical. In the former case, structure appears at low energies, while the latter case necessarily shows a smooth energy dependence. The results are similar and in both cases the agreement with experiment is excellent. The solid line in Fig. 6b also represents the Fermi-gas level density with $a = 6.2 \text{ MeV}^{-1}$, $\Delta = 1.0 \text{ MeV}$, and a rigid-body moment of inertia. Thus, the Fermi-gas formula is able (both in this case and in general) to reproduce the energy dependence predicted by microscopic calculations provided a , Δ , and σ^2 are adjustable parameters.

The density of levels as a function of angular momentum, expressed in terms of the spin cutoff factor σ [Eq. (2.6)], is perhaps a more difficult quantity to determine experimentally because it involves, implicitly, a measurement of angular momentum. Information on σ is obtained through measurements of angular distributions of particles evaporated by a compound nucleus, and isomer ratio measurements (Hu 72). Examples of experiments in which the level density parameters Δ (the energy shift), a and σ^2 are determined by fitting compound nucleus reaction data (i.e., yields, energy spectra, angular distributions and fluctuation widths) are found in refs (Lu 72, Go 76). The determination of σ^2 for nuclei near mass 60 yielded values consistent with $\sigma^2 = 2/5 mR^2$ and $R = 1.2 A^{1/3}$ fm. In much lighter nuclei, at high excitation energy, a larger moment of inertia with $R \approx 1.4A^{1/3}$ seems to be preferred (Go 76). A value of $r_0 = 1.4$ is much larger than the half-density radius of a spherical nucleus, which suggests that a significant deformation of the compound nucleus may be involved. Microscopic calculations of σ^2 at neutron capture excitation energies also indicate a sensitivity to shell structure effects (Hu 74a) and particularly to the pairing energy (Lu 72).

The relative widths for neutron emission and fission are governed by the relative densities of levels at two different deformations, that corresponding to the minimum potential energy and that corresponding to the saddle point. These can in turn be expressed in terms of the ratio of single particle densities a_f/a_n . In the absence of shell effects $a_f/a_n \rightarrow 1.0$, i.e. the nucleus is described by a Fermi gas with constant level spacing independent of deformation. Microscopic calculations (Wi 72) have shown some success in explaining the deviations from unity of values of a_f/a_n deduced from experiment (Va 73).

Spin cutoff factors have been calculated with the spectral distribution method for a number of light nuclei (Ay 74) and compared with values used in Hauser-Feshbach analyses of compound nuclear reactions in that mass region (Ha 74). This comparison is shown in Fig. 7a,b (Ay 74). With the exception of ^{28}Si , the spin cutoff factors calculated microscopically are even larger than the rigid body values calculated with a radius parameter $r_0 = 1.4-1.5$ fm. (This does not mean, however, that the shell model predicts anomalously large moments of inertia.) The variation among the level densities calculated with the KLS interaction [with s-d and $f_{7/2}$ orbits (Ka 69)], the Kuo interaction (s-d orbits only (Ku 68)], and empirical Fermi-gas parameters (Fa 68) is quite large.

The effects of the isospin dependence of the nuclear level density can be observed in a number of ways (Lu 72, Gr 72, Va 72a, Ro 73, Ro 75, Ay 74, St 74). They are more pronounced for light-ion induced reactions and have indeed been studied by comparing reactions for $(\alpha, \alpha') (p, p') (\alpha, p)$ and (p, α) (Lu 71, Mi 72, Va 72a). The formalism for the formation and decay of a compound nucleus can also be extended to include isospin (Gr 72, Ro 73, Ro 75, Ha 77), in order to examine the importance of isospin conservation or isospin mixing (Ha 77). There are indications that isospin is conserved in compound reactions involving complex projectiles and light targets (Ru 72, St 74), and this can have important consequences for isospin forbidden transitions. Another case of possible importance concerns the use of empirically determined level densities. Those obtained from proton-induced resonance reactions can contain $T_>$ and $T_<$ states[†], whereas those from slow

[†]The rotation $T_<$ and $T_>$ refers to state of isospin with $T = T_z$ and $T = T_z + 1$, respectively.

reaction resonance reactions will contain only $T_{<}$ states. If the compound nucleus reaction under study permits population of $T = 0$ states only, then only the $T_{<}$ states (in nuclei reached by α emission) should be counted in determining the number of open channels.

In heavy nuclei, which have a large neutron excess, the levels of residual nuclei populated in heavy ion x-n reactions and in slow neutron resonance reactions will have the same isospin. Thus, the neglect of isospin selection rules will not have serious consequences. Grover (Gr 77a) has pointed out that population of $T_{>}$ states by neutron decay could lead to a situation in which isospin selection rules would then favor proton decay. However, the probability for this to occur is reduced by a factor of $\rho(T_{>})/\rho(T_{<})$ and there does not seem to be any evidence that this effect is of practical importance in heavy-ion reactions.

Thus, even though level densities do depend on isospin and isospin appears to be conserved in heavy-ion induced compound reactions, isospin generally is not considered explicitly in statistical model analyses. Isospin certainly does not have the importance of angular momentum. Except for a few special cases mentioned above, neglect of isospin is a reasonable procedure.

2.6. Compilations of Level-density Parameters

The systematic synthesis and analysis of level-density information for a wide range of nuclei serves several purposes. It reveals the effects of nuclear structure on continuum properties, provides experimental values against which theoretical predictions may be compared, enables the

determination of unmeasured level-density parameters through interpolation, and, perhaps most important, provides a convenient source of essential parameters for use in calculations of the statistical decay of an equilibrated nucleus. For each of the compilations briefly described below, we give the mass range covered, the type of experimental data included, the level-density formula used to fit the data, and the treatments of the energy shift and spin cut-off factor.

2.6.1. Gilbert and Cameron (Gi 65, Gi 65a) and Reffo (Re 80)

Masses from ~ 25 to ~ 230 are considered. Individual levels are counted at low excitation (from decay schemes) and near the first particle threshold (from neutron and proton resonances). A composite level density formula is used. At excitation energies below a value E_x , a constant temperature formula

$$\rho_1 = \frac{1}{T} \exp \frac{E-E_0}{T} \quad (2.9)$$

is applied. This formula matches at $E = E_x$ the Fermi-gas formula for the density of levels of all J and both parities,

$$\rho_2(U) = \frac{\sqrt{\pi}}{12} \frac{\exp(2\sqrt{a}U)}{a^{1/4} U^{5/4}} \frac{1}{\sqrt{2\pi}} \sigma \quad (2.10)$$

The effective excitation energy U is defined by $U = E - P(N) - P(Z)$ where the pairing corrections are determined from odd-even mass differences. The spin cutoff factor, $\sigma^2 = 0.0888 \sqrt{a}U A^{2/3}$, corresponds to a rigid body moment of inertia with $r_0 \approx 1.1$ fm if $A/a = 8$. The spin distribution for both parities is given by

$$\begin{aligned} \rho(U, J) &= \rho(U) \frac{2J+1}{2\sigma^2} \exp[-(J + 1/2)^2/\sigma^2] \\ &= \frac{2J+1}{12} \sqrt{a} \left(\frac{\hbar^2}{2J}\right)^{3/2} \frac{\exp(2\sqrt{a}U)}{U^2} \exp \frac{-(J + 1/2)^2}{2\sigma^2} \end{aligned} \quad (2.11)$$

Reffo (Re 80) has incorporated recent data and updated the analysis of Gilbert and Cameron.

2.6.2. Gadioli and Zetta (Ga 68)

Slow neutron resonances, statistical reaction spectra, and fluctuation widths were analyzed for nuclei with $A \leq 70$. The formula used here was derived by Lang (La 63) and Lang and LeCouteur (La 54),

$$\rho(U, J) = \frac{2J+1}{12} \sqrt{a} \left(\frac{\hbar^2}{2J}\right)^{3/2} \exp \frac{(2\sqrt{a}U)}{(U+t)^2} \exp \frac{-[J(J+1)]}{2\sigma^2}, \quad (2.12)$$

and is identical to eq. (2.11) except for the factor $(U + t)$ in the denominator and the relationship of the effective excitation energy U and thermodynamic temperature t which, for eq. (2.12), becomes $U = at^2 - t$. A discussion of the relative merits and correctness of eqs. (2.11 and 2.12) is found in Ga 68 and Gi 65. In brief, Eq. (2.11) is correct, but eq. (2.12) seems to fit the data better at lower excitation energies. The pairing energies of Gilbert and Cameron were used, with the addition of a slowly varying "backshift", $U = E - \Delta + \frac{70}{A} \text{MeV}$, and the moment of inertia was calculated assuming $r_0 = 1.25 \text{ fm}$.

2.6.3. Facchini et al. (Fa 68, Fa 68a)

A similar range of nuclei as in Gilbert and Cameron was considered, and the same formula, eq. (2.11), and pairing energies were used. The main difference is that statistical reaction spectra at high energies were considered, and low-lying levels near the ground state were not.

Furthermore, the spin-cutoff factor used was about a factor 1.6 larger than that of Gilbert and Cameron.

2.6.4. Dilg et al. (Di 73)

Whereas Gilbert and Cameron fixed the energy shift Δ to be the pairing energy obtained from ground state mass differences, Dilg et al. leave this quantity, along with the parameter "a", as a parameter for each nucleus. This procedure is referred to as the back-shifted Fermi-gas model. The result is that densities at energies near the ground state and at the neutron separation energy can be fit with one formula [eq. (2.12)]. The masses for which Δ and "a" are compiled extend from mass 40 to mass 240, and the radius parameter for σ^2 was 1.25 fm.

2.6.5. Holmes (Ho 76a)

A back-shifted Fermi-gas analysis similar to that of Dilg et al. has been carried out for a larger number of nuclei (265 vs 220) by J.A. Homes (Ho 76, Ho 76a) (see Fig. 4). Differences with the analysis of Dilg et al. include the use of eq. (2.11) instead of eq. (2.12) and semiempirical expressions for the N and Z dependence of "a" and Δ .

2.6.6. Beckerman (Be 77)

Beckerman has analyzed low-lying individual levels, neutron and charged particle resonance reactions, and particle transfer experiments to determine level densities for nuclei with $23 \leq A \leq 40$. A simplified Fermi-gas formula for the density of levels of all J,

$$\rho(E) = C \exp 2\sqrt{aE}$$

was used, effectively absorbing the energy dependent denominator U^2 or $(U + t)^2$ into the constants C and a. The spin cutoff factor employed $r_0 = 1.2$ fm.

2.7. Summary

Our first-hand knowledge of the density of levels is confined to a rather small region of excitation energy and angular momentum. For excitation energies not too far above the first particle-decay threshold, a parameterization in terms of the Fermi-gas formula, which is fit to experimentally-determined levels, provides a rather accurate representation of the level density. The various nuclear structure effects present at low excitation energies--pairing, shell closures, deformation, etc.,--are contained in the phenomenological mass dependence of the parameters "a", Δ and σ . Our understanding of these variations in terms of microscopic nuclear structure is good. Calculations of level densities employing realistic spherical or deformed shell model single-particle levels, and residual interactions have been successful in reproducing experimental data on level densities. Mathematical techniques have been developed which enable the calculation of the level density for effective residual interactions without diagonalizing the Hamiltonian. In some cases, these microscopic theories provide more detailed dependences of, e.g., spin-cutoff factors on mass and excitation energy than can be determined independently in an experiment.

The concepts of single particle motion, the nuclear shape degrees of freedom, angular momentum, and pairing are all interdependent in their determination of the level density. All these various shell effects are predicted to decrease and then vanish at sufficiently high intrinsic excitation energies. [These qualitative considerations are illustrated schematically in Fig. 8 (Vi 80).] In this limit, the independent particle

Fermi-gas model, with $a \propto A$, should become valid. The limit of large angular momentum has different consequences than the limit of high excitation energy. While decreasing the pairing interaction, it cools the nucleus by placing energy in a collective form which is unavailable for intrinsic or thermal excitation. Thus, a rapidly rotating nucleus can be quite sensitive to shell effects (variations in the local single particle density) which can change rapidly with angular momentum and deformation. The potential energy associated with these shell effects must also be known in order to establish the zero energy reference point for the intrinsic excitation. All these effects, or uncertainties, are present in the phenomenon of fission in which the density of levels in a highly deformed and, often, rapidly rotating system governs the fate of the nucleus. It is in these limits, excitation energy and angular momentum, that our experimental knowledge is very limited.

Since the density of levels plays an important role in determining statistical decay, it is possible to convert some of this a priori ignorance into a posteriori knowledge if one accepts the models and methods which are thought to describe the decay of an equilibrated nucleus. These models and methods are the subject of Sec. 3.

3. THE DECAY OF AN EQUILIBRATED NUCLEUS

3.1. Introduction

It is possible in many situations involving the interaction of heavy ions to consider one stage of a reaction independently of other stages except for the conservation of total energy, total angular momentum and parity. The classic example of this factorization is, of course, the compound nucleus for which Niels Bohr hypothesized that the decay was independent of formation. In the case of compound nuclear reactions, there is a theory for the entire reaction, i.e., for both initial and final stages. In other cases this independence may be only an approximation made either for convenience or out of necessity. The model of statistical decay is now being used in applications other than compound nucleus reactions and in cases where a detailed reaction theory may not exist. In fact, any nuclear reaction which produces, or is thought to produce, a nucleus in the exit channel which reaches a degree of equilibrium by the time it decays is a candidate for application of the statistical model. We therefore assume for the following discussion that we are presented with a nucleus in statistical equilibrium having a specified excitation energy E_i and total angular momentum J_i . Parity and isospin will be ignored in the formalism with the realization that the extension of the theory to keep track of these quantities is straightforward and can be done in those cases where it might have a recognizable effect.

The statistical model, which follows on the assumption of equilibrium, rests on the premise that all decay channels which are "open" are, on the average, equally likely to be populated. By an open channel we mean a particular final state, specified by all quantum numbers including the

magnetic quantum number, which can be reached from the initial state without the hindrance of barrier penetration. (If a centrifugal, Coulomb or other type of potential barrier is present, the probability of the population of that channel is simply reduced by the barrier-penetration probability.) The statistical model thus says that the probability of decay to a particular channel (or group of channels n) is just $1/N$ (or n/N) where N is the total number of open channels. In any given measurement at a specific bombarding $E \pm \Delta E$, individual channels will not exhibit the same cross section or probability of population; rather, the cross sections will be distributed about a mean value. The width of this distribution will narrow as the energy averaging interval ΔE increases. The important point to keep in mind is that the statistical model described below predicts only the mean of a distributed quantity.

The procedure will be to first consider for each mode of decay the transition rate from the initial state of specified E_i and J_i to the final state of the emitted particle and residual nucleus having the specified values, E_f , j . This will serve to illustrate the basic features of the statistical model. Practical calculations will involve distributed values of E_i and J_i in the initial state and summations over all the final states of interest. The following represents but one of a variety of ways of presenting the statistical model. Other articles which the reader may find interesting and helpful are (Er 60, Fe 60, Th 68, Vo 68, Ma 79).

3.2. Modes of Decay

The modes of decay are labeled by the type of radiation emitted or type of products produced. We consider γ -ray decay, the emission of nucleons (p,n) and clusters of nucleons (d,t, α ,etc.), and fission. It is convenient to consider initially the partial rates of decay (i.e. decays per second) for the different channels and modes. These rates can then be converted to normalized probabilities once the total decay rate or total number of open channels has been obtained.

The connection of the decay of an equilibrated nucleus to its mode of formation (compound nucleus, quasielastic reaction, deep inelastic scattering, etc.) will be considered in the illustrative examples in Section 4.

3.2.1 Gamma-Ray Decay

The average rate at which an ensemble of nuclei with initial excitation energies in the range E_i to $E_i + dE$, angular momentum J_i and level density $\rho(E_i, J_i)$ emits gamma radiation of energy E and multipolarity λ to produce nuclei with final state energies E_f to $E_f + dE$ and angular momenta j may be written (Sa 67, Gr 67a)

$$R(E_i, J_i; E_f, j)(dE) = \left[C_\lambda(\epsilon) \right]_A \left[\epsilon^{2\lambda+1} \right]_B \left[\frac{\rho(E_f, j)}{\rho(E_i, J_i)} \right]_C dE \quad (3.1)$$

Qualitatively, these factors may be explained as follows: Factor A represents an average squared intrinsic matrix element which may have some dependence on $\epsilon = E_i - E_f$. The next factor, B, arises from the long wavelength limit $\frac{\lambda_\gamma}{R_{Nuc}} \gg 1$ which causes the rate of emission to increase rapidly with the γ -ray energy, ϵ_γ . (The nucleus is a poor antenna for

electromagnetic radiation in the γ -ray spectrum!) The third factor represents the phase-space ratio of the initial and final densities of levels which is associated with reciprocity. The angular momenta J_i and j are related by $\vec{J}_i = \vec{\lambda} + \vec{j}$.

The factor C has also been derived by considering the one-body nature of the electromagnetic operator (B1 52) which requires the wavefunction of the initial state to differ from that of the final state in the coordinates of only one particle. The one-particle component in the initial (higher energy) state will be diluted proportionately to the density of neighboring levels, whence $R \propto \rho(E_i)^{-1}$.

An energy dependence of $C_\lambda(\epsilon_\gamma)$ can arise if the distribution of radiative strength (for a given multipole) is not uniform. The giant dipole and giant quadrupole resonances represent a concentration of radiative strength which introduces an energy dependence into $C_\lambda(\epsilon_\gamma)$. Statistical gamma radiation begins to compete with particle emission only for excitation energies below those where the giant resonance reaches its maximum strength. Thus, as the energy of the γ -ray transition increases, the greater the fraction of the dipole (or quadrupole) strength it is likely to have. One way of incorporating this is to write (Sa 72)

$$C_1(\epsilon_\gamma) = \frac{E_d^2 + \frac{1}{4} \Gamma^2}{(\epsilon_\gamma - E_d)^2 + \frac{1}{4} \Gamma^2} C_1^i \equiv G(\epsilon_\gamma) C_1^i \quad (3.2)$$

where $E_d \approx 32A^{-1/3}$ MeV is the energy of the giant dipole resonance, Γ is its width, and C_1^i represents an energy-independent average matrix element. Another formulation, which has been derived using a Fermi-gas model for the distribution of single particle levels leads to (Li 78)

$$C_{\lambda}(\epsilon_{\gamma}) = \epsilon_{\gamma} C'_{\lambda}$$

The absolute normalization of eq. (3.1) can be stated in terms of a single particle proton transition rate (Mo 64) and a hindrance factor H which is the factor by which the transition rate is reduced below the single-particle estimate (Sa 72).

$$C_{E1}(\epsilon_{\gamma}) = \frac{1.6}{H_{E1}} \times 10^{15} G(\epsilon_{\gamma}) \text{ decays/sec} \quad (3.3)$$

$$C_{E2}(\epsilon_{\gamma}) = \frac{1.8 \times 10^{10}}{H_{E2}} \text{ decays/sec} \quad (3.4)$$

where $G(\epsilon_{\gamma})$ is defined by eq. (3.2) and ϵ_{γ} is in MeV. If these rates are converted to widths, the above numerical factors are $\sim \frac{1 \text{ eV}}{H_{E1}}$ for dipole radiation and $\frac{10^{-5}}{H_{E2}}$ eV for quadrupole radiation.

The absolute normalization can in principle be obtained by measuring either the cross section for photonuclear absorption and invoking reciprocity or from a knowledge of the radiative widths of slow neutron resonances which decay by a known and unique multipolarity. In practice these latter widths are mainly of dipole character. Given that the hindrance factors are large and can be different for E1 and M1 radiation, it becomes difficult to obtain a reliability much better than a factor of 10. In general, dipole radiation tends to be hindered by a factor of from 10^2 to 10^3 below the single-particle estimate. Electric quadrupole widths on the other hand tend to be enhanced by similar factors when the transitions arise from collective quadrupole motion such as rotation or vibration. Quadrupole transitions of a statistical nature (i.e., proceeding via a fragmented single-particle strength rather than via a change in a collective coordinate) presumably exist with hindrances similar to those for E1

transitions. In practice, therefore, the absolute normalizations of the different types of γ radiation (statistical dipole, statistical quadrupole, and collective quadrupole) need to be determined by comparison with the results of the experiments one is attempting to analyze. Through this, a systematic empirical determination of these strengths can be gained which enables predictions for other cases. Average electromagnetic transition rates for $A \leq 40$ have been compiled by Skorka et al. (Sk 66).

The angular distribution of the radiation can be calculated provided the distribution of magnetic quantum numbers, i.e., the orientation of J_i , is known. The expressions for the angular distributions are particularly simple when the emitting nucleus is produced with and maintains full alignment. If, as is the case for compound nucleus formation, all angular momenta are aligned perpendicular to the beam axis, the angular distributions for stretched transitions, $j = J_i - \lambda$ in the limit $J \gg \lambda$ are (Da 80a)

$$\begin{aligned} W(\theta) &= \frac{3}{8} (2 + \sin^2\theta) \quad , \quad \lambda = 1 \\ W(\theta) &= \frac{5}{4} (1 - \frac{3}{8} \sin^4\theta) \quad , \quad \lambda = 2 \end{aligned} \tag{3.5}$$

where θ is the polar angle with respect to the beam axis.

In the case of complete alignment along an axis perpendicular to the reaction plane,

$$\begin{aligned} W(\alpha) &= \frac{3}{4} (1 + \cos^2\alpha) \quad , \quad \lambda = 1 \\ W(\alpha) &= \frac{5}{4} (1 - \cos^4\alpha) \quad , \quad \lambda = 2 \end{aligned} \tag{3.6}$$

for stretched transitions and large spin (Wo 78).

The importance of considering γ -ray emission in heavy-ion reactions arises from several factors. There is usually a large amount of angular momentum which has to be dissipated as well as excitation energy. Emission of α -particles, which accomplishes this so well in light nuclei, is inhibited by the Coulomb barrier when $A \gtrsim 150$. Neutrons are not very effective in removing angular momentum and thus sequential quadrupole emission becomes an efficient decay mode, especially for deformed nuclei. The competition between neutron or particle emission, statistical E1, collective E2 radiation can be treated in the statistical model; this brings us to the consideration of particle decay.

3.2.2 Emission of Nucleons and Clusters

Consider an ensemble of nuclei in equilibrium with energies E_i to $E_i + dE_i$ and angular momenta J_i which emits particles μ with kinetic energy ϵ , spin s , orbital angular momentum ℓ , and leaving the residual or daughter nuclei with excitation energies E_f to $E_f + dE$ and spin j . The average rate of emission, summed over orbital angular momentum, is (Th 64)

$$R_\mu(E_i, J_i; E_f, j, s) dE = \frac{1}{h} \sum_{S=|j-s|}^{j+s} \sum_{\ell=|J_i-S|}^{J_i+S} T_\ell(\epsilon) \frac{\rho(E_f, j)}{\rho(E_i, J_i)} dE \quad (3.7)$$

where $\vec{S} = \vec{j} + \vec{s}$ is the channel spin. (Spin orbit coupling (Sa 67) is neglected here.) The energies E_i and E_f are related by $E_i = E_f + S_\mu + \epsilon$, where S_μ is the separation energy for particle type μ . $T_\ell(\epsilon)$ is the optical model transmission coefficient for formation of a compound nucleus in a time reversed reaction of the emitted particle and the residual nucleus

with excitation energy E_f and angular momentum j . In practice, the transmission coefficient is computed for $E_f = 0$, $j = 0$. Similarly, the level density $\rho(E_f, j)$ is taken to be that of the residual nucleus when the emitted particle is at infinite separation.

The quantity T_ℓ incorporates the effects of Coulomb, V_c , and centrifugal barriers, V_ℓ , and the nuclear potential, V_N , on the probability for a particle to be emitted. If, at the nucleon surface, $V_c + V_\ell + V_N \ll \epsilon$, then $T_\ell \approx 1/2$; for ϵ significantly above the barrier, $T_\ell \rightarrow 1$. The double sum in eq. (3.7) in this case is thus of order J . Comparing eq. (3.7) with eqs. (3.1 and 3.3), we see that particle emission is favored over (unhindered) dipole emission by a factor of $\sim 10^7$. Thus, γ -ray emission will be important only in the later stages of decay in which thresholds, centrifugal barriers or Coulomb barriers severely inhibit particle emission.

A complete discussion of the reciprocity relation and inverse cross sections has been given by Thomas (Th 64). The transmission coefficients governing the decay rate also determine, as noted above, the cross section for the inverse reaction, $\sigma_{fi}(E_i, J_i)$ which is for the formation of a compound nucleus with excitation energy E_i and total angular momentum J_i . Thus,

$$\sigma_{fi}(E_i, J_i) = \frac{\pi}{k_f^2} \frac{2J_i+1}{(2s+1)(2j+1)} \sum_{S=|j-s|}^{j+s} \sum_{\ell=|J_i-S|}^{J_i+S} T_\ell(\epsilon) \quad (3.8)$$

and

$$\begin{aligned} & R(E_i, J_i; E_f, j, s) dE \\ &= \frac{(2s+1)}{h} \frac{k_f^2}{\pi} \sigma_{fi}(E_i, J_i) \frac{(2j+1)\rho(E_f, j)}{(2J_i+1)\rho(E_i, J_i)} \end{aligned} \quad (3.9)$$

The angular distribution of particles emitted by a nucleus depends on the spin and orientation of the nucleus before decay. In general, the angular distribution may be written as

$$W(\vec{\Omega}) = \sum_{\lambda, q} (2\lambda + 1) \rho_{\lambda}^q A_{\lambda} Y_{\lambda q}(\vec{\Omega}) \quad (3.10)$$

where $\vec{\Omega}$ is the direction with respect to some axis of quantization, ρ_{λ}^q is a tensor describing the orientation of the initial nucleus, and A_{λ} is an angular momentum recoupling coefficient (St 71). The $Y_{\lambda q}$ are the spherical harmonics. If we take the axis of quantization to be along the direction of the initial angular momentum J_i and $M_J = J_i$ then eq. (3.10) becomes

$$W(\nu) = \sum_{\lambda} A_{\lambda} B_{\lambda} P_{\lambda}(\cos \nu) \quad (3.11)$$

where

$$A_{\lambda} = (2J_i + 1)^{1/2} (2\ell + 1) \langle \ell 0 \ell 0 | \lambda 0 \rangle \mathcal{K}(\ell \ell J_i J_i | \lambda S) \quad (3.12)$$

and

$$B_{\lambda} = 2(2J_i + 1)^{1/2} \langle J J J - J | \lambda 0 \rangle .$$

The symbols P_{λ} , $\langle | \rangle$ and \mathcal{K} denote the Legendre polynomials, Clebsch-Gordan coefficients, and Racah coefficients, respectively, and ν is the polar angle of the emitted particle with respect to the polar axis (see Fig. 9). The summation over λ extends to the smaller of 2ℓ or $2|J_i - j|$.

When large angular momenta are involved, a semi-classical approximation to eq. (3.11) is useful. Defining $\Delta = |J_i - S|$,

$$W(\gamma) = \frac{(\ell - \Delta)!}{(\ell + \Delta)!} |P_{\ell}^{\Delta}(\cos \nu)|^2 \quad (3.13)$$

where P_{ℓ}^{Δ} is the associated Legendre polynomial. For an extensive discussion of a semi-classical treatment of the angular distribution of evaporated particles with respect to the initial angular momentum, see Catchan et al. (Ca 80).

Classically, the direction in which a particle is emitted must be perpendicular to its orbital angular momentum. Ericson and Strutinsky (Er 58a) have derived an expression for the angular distribution of particles

$$W(\nu) = \frac{1}{\sqrt{\sin^2 \nu - \cos^2 \nu_{\ell}}} \quad (3.14)$$

in which ν_{ℓ} is the polar angle of the orbital angular momentum $\vec{\ell}$. This angle is defined by the triangle $\vec{J}_i = \vec{j} + \vec{\ell}$ (see Fig. 9). Note that this classical approximation neglects the intrinsic spin s of the emitted particle as well as the quantum mechanical aspects of angular momentum coupling.

In the case of compound nucleus formation, the initial direction of the total angular momentum is perpendicular to the direction of the beam provided the ground-state spins of projectile and target are small compared with the orbital angular momentum. This is nearly always a good approximation in heavy-ion reactions. In the classical limit, particles are emitted in a plane perpendicular to J_i (the flywheel effect) and are thus focused at 0° and 180° with respect to the beam. The angular distribution in this case becomes

$$W(\theta) = (2\pi^2 \sin \theta)^{-1} \quad (3.15)$$

where θ is the polar angle with respect to the beam. Comparing expression 3.15 with 3.13, we see that the $(\sin \theta)^{-1}$ approximation will be valid only for angles $\theta \gtrsim \pi / (\min J_i, \ell)$. Expression 3.15 works quite well for heavy emitted particles which carry large orbital angular momenta.

The angular correlation of two particles evaporated in succession has been discussed by Kuang-Hsi et al. (Ku 79). The coincidence rate R_c for particles emitted in a plane perpendicular to the beam depends on the correlation angle θ_c between them, and $R_c(\theta_c)$ turns out to be quite sensitive to the distribution of angular momenta in the compound nucleus.

3.2.3 Fission

In apparent contrast to the decay modes considered so far, the decay rate for fission does not depend on the densities of levels or other statistical properties of the residual nuclei, which are the fission fragments at infinite separation. Rather, it depends (Bo 39) on the properties of the compound nucleus at the point where the nucleus becomes committed to fission. This point, called a transition state, is the saddle point configuration. Here the angular-momentum-dependent potential energy associated with the shape of the nucleus $E_B(J_i)$ has reached a maximum. The fissioning nuclear system thus passes through a transition state where most of the energy has gone into deformation and the energy available for intrinsic excitation and the density of intrinsic levels may be quite small (Bo 56). This is illustrated schematically in Fig. 10. Thus, fission is treated in a manner almost analogous to light particle decay if in Eq. (3.7) we understand the final state whose energy is denoted by E_f to be one of the transition states. Similarly, in evaluating the intrinsic or thermal excitation energy which determines the density of states, it is the kinetic energy at the transition state or saddle point, ϵ^S , and not the asymptotic relative kinetic energy, ϵ , which must be considered.

The transmission coefficients are taken to be unity if the total available energy is in excess of the fission barrier and zero otherwise.

This generally is a good approximation in heavy-ion induced fusion-fission reactions.* Thus

$$R_f(E_i, J_i; E_f, j) \sim \frac{2J_i + 1}{h} \frac{\rho(E_f, j)}{\rho(E_i, J_i)} \quad (3.16)$$

and

$$E_f = E_i - E_B(J_i) - \epsilon^S \quad (3.17)$$

$E_B(J_i)$ is the fission barrier or saddle point energy, which now depends explicitly on the angular momentum. The factor $2J_i + 1$ arises from a summation over the transmission coefficients which we have set equal to 0 or 1. We should emphasize the importance of the angular momentum j of the transition-state levels and in particular, the enhancement of the level density because of low-lying collective rotations. [Recall the discussion in Section 2.4.3 and eq. (2.8).] The moments of inertia required in eq. (2.8) [and the fission barrier $E_B(J_i)$] may be taken from the rotating liquid drop model (Co 74). Practical aspects of the introduction of these collective enhancements in the calculation of fission widths have been discussed by Vigdor (Vi 80).

The direction of the fission fragments is assumed to lie along the symmetry axis of the nucleus in its prolate saddle-point configuration (Fig. 11). Furthermore, the assumption is made that the projection K of the total

*If penetration of the fission barrier is important, it may be included by adding a factor $1 + \exp\left(\frac{-2\pi}{h\omega} E_f\right)$ in the denominator of eq. (3.16). Here, $h\omega$ is the characteristic energy of a harmonic oscillator with the same curvature as the barrier.

angular momentum J_i onto the nuclear symmetry axis is a constant of the motion once the nucleus has passed through the saddle point. The angular distribution of the fission fragments is expressed in terms of the rotational wave functions by

$$W_{M_i, K}^{J_i}(\theta) = \frac{2J_i + 1}{2} d_{M_i, K}^{J_i}(\theta)$$

and the axis of quantization in compound nucleus reactions is customarily taken along the direction of the beam. The projection K is defined only for a deformed nucleus, so that it is clearly a quantum number which "develops" with the evolution of the nucleus from an initial (and possibly spherical) shape to its saddle-point shape. While J_i and M_i are determined by the reaction mechanism which produces the nucleus, K is a property of the fissioning nuclear system. If all the initial orbital angular momentum of the projectile and target is converted into orbital angular momentum of the fragments, then $K = 0$. It is also clear from Fig. 11 that $K = 0$ corresponds to the minimum of rotational energy since $J_{\perp} > J_{\parallel}$. For fixed values of E , t and J_i the statistical distribution of levels with projections K is (Va 73)

$$\rho(K) \propto \exp \left[-\frac{\hbar^2 K^2}{2Jt} \left(\frac{1}{J_{\parallel}} - \frac{1}{J_{\perp}} \right) \right] \quad (3.18)$$

We may define, in analogy to $\sigma^2 = \frac{J_{\text{rigid}} t}{\hbar^2}$,

$$\sigma_K^2 = \frac{J_{\text{eff}} t}{\hbar^2}$$

where $J_{\text{eff}} = \frac{J_{\perp} J_{\parallel}}{J_{\perp} - J_{\parallel}}$

$$\text{and } \rho(K) = \exp \frac{-K^2}{2\sigma_K^2}, K \leq J_i$$

$$0, K > J_i$$

The angular momentum of fission fragments can thus be expressed in terms of two parameters J_i and σ_K^2 . Under the approximation that projectile and target spins can be neglected and $M_i = 0$, the angular distribution of fragments emitted in a compound nucleus reaction is

$$W_{M_i=0}^{J_i}(\theta) \propto \exp \left[-\left(J_i + \frac{1}{2} \right)^2 \sin^2 \theta / 4\sigma_K^2 \right] J_0 \left[i \left(J_i + \frac{1}{2} \right)^2 \sin^2 \theta / 4\sigma_K^2 \right] \quad (3.19)$$

where J_0 is the zero-order Bessel function with imaginary argument and θ is the angle with respect to the beam (Va 73). As is the case with particle emission, for large angular momenta (relative to σ_K) the angular distribution is well approximated by $(\sin \theta)^{-1}$ over most of the angular range. The value of σ_K^2 is determined by the anisotropy, $W(180^\circ)/W(90^\circ)$.

The angular correlation of fission fragments from a nucleus fully aligned with respect to an axis of quantization has been treated in detail by Back and Bjornholm (Ba 78). Such situations are encountered in the deep inelastic scattering of heavy nuclei, in which case the nucleus before fission can have an angular momentum aligned perpendicular to the reaction plane (Dy 77).

3.2.4 The Total Decay Rate

The average total rate $R(E_i, J_i)dE$ at which levels (E_i, J_i) decay is the sum of the rates for all possible transitions which depopulate the levels. These may be summed for each mode of decay as follows.

$$R_{\gamma dE} = \sum_{\lambda} \sum_{J} \int_{\epsilon=0}^{E_i} R_{\lambda}(E_i, J_i; E_i - \epsilon, j) d\epsilon, \quad (3.20)$$

$$R_{\text{evap}} dE = \sum_{\mu} \sum_{J, S} \int_{\epsilon=0}^{E_i - S_{\mu}} R_{\mu}(E_i, J_i; E_i - S_{\mu} - \epsilon, j, s) dt \quad (3.21)$$

$$R_{\text{fission}} dE = \sum_j \int_0^{E_i - E_B(J_i)} R_f(E_i, J_i; E_i - E_B(J_i) - \epsilon^S, j) d\epsilon^S. \quad (3.22)$$

Thus,

$$R(E_i, J_i) = R_{\gamma} + R_{\text{evap}} + R_{\text{fission}}. \quad (3.23)$$

The probability that any given channel, x , will be populated, $P(E_i, J_i; x)$ is just

$$P(E_i, J_i; x) = \frac{R(E_i, J_i; x)}{R(E_i, J_i)}. \quad (3.24)$$

The cross section for the population of a given channel may be written

$$\sigma(x) = \sum_{J_i} \sigma(E_i, J_i) P(E_i, J_i; x) \quad (3.25)$$

where $\sigma(E_i, J_i)$ is the cross section for production of an equilibrated nucleus with excitation energy and angular momentum E_i and J_i , respectively.

Equations (3.20)-(3.25) are the basis for the statistical model of nuclear decay and represent the fundamental hypothesis that all open channels are equally likely to be populated. The important physical quantities in these equations are the level densities and transmission coefficients.

3.3. The Hauser-Feshbach Formulae

Since many of the applications of the statistical model involve compound nucleus formation and decay, it is useful to give the formulae which pertain specifically to this case. For a recent review of the theory of compound nucleus formation, see the article by Mahaux and Weidenmüller (Ma 79).

Let all quantum numbers which specify the colliding nuclei and the two nuclei in the exit channel be denoted by α and α' , respectively. Similarly, $\vec{\ell} + \vec{S} = \vec{J} = \vec{\ell}' + \vec{S}'$, $\vec{S} = \vec{I} + \vec{i}$ and $\vec{S}' = \vec{I}' + \vec{i}'$ denote the angular momentum coupling for orbital angular momentum ℓ , channel spin S and intrinsic angular momenta I and i . We have then (Vo 68)

$$\sigma_{\alpha\alpha'} = \pi \chi_{\alpha}^2 \sum_J \frac{2J+1}{(2I+1)(2i+1)} \frac{\left\{ \sum_{S\ell} T_{\ell}(\alpha) \right\}^J \left\{ \sum_{S'\ell'} T_{\ell'}(\alpha') \right\}^J}{\left\{ \sum_{\alpha'', S''\ell''} T_{\ell''}(\alpha'') \right\}^J} \quad (3.26)$$

for the angle integrated cross section and

$$\frac{d\sigma_{\alpha\alpha'}}{d\Omega} = \sum_L \frac{\chi^2}{4} \sum_J \frac{1}{(2I+1)(2i+1)} \frac{\left\{ \sum_{S\ell} T_{\ell}(\alpha) \right\}^J \left\{ \sum_{S'\ell'} T_{\ell'}(\alpha') \right\}^J}{\sum_{\alpha'' S''\ell''} \left\{ T_{\ell''}(\alpha'') \right\}^J} \times Z(\ell J \ell J; S L) Z(\ell' J \ell' J; S' L) (-)^{S-S'} P_L(\cos\theta) \quad (3.27)$$

for the differential cross section. T_{ℓ} denotes the optical model transmission coefficient and Z is an angular momentum coupling coefficient (Fe 60).

Equation (3.26) may be obtained from eqs. (3.8) and (3.25). The inclusion of angular momentum recoupling coefficients [Eq. (3.10)] to give the differential cross section [eq. (3.27)] is straightforward. The fundamental difference between the Hauser-Feshbach theory (Ha 52) and the

earlier Weiskopf-Ewing (We 40) theory of compound nucleus formation and decay is the neglect of proper angular momentum coupling in the latter. This difference is crucial for heavy-ion induced reactions.

Although eqs. (3.26) and (3.27) are written in terms of a single final state, application to problems involving the continuum are made simply by multiplying by the density of levels and performing the appropriate integration.

These equations may also be derived from the theory of resonance reactions. The requirements for a rigorous derivation are not always met, especially in heavy ion reactions (Ma 79). Nevertheless, these formulae "work" well even though the criteria governing their derivation are not completely satisfied (Mo 64a, Mo 75a).

Useful statistical model relations encountered in the derivation of eq. (3.26) are as follows.

$$T_{S\ell}(\alpha) = 2\pi \left\langle \frac{\Gamma(\alpha\ell S|J)}{D_J} \right\rangle \quad (3.28)$$

where $\Gamma(\alpha\ell S|J)$ is the partial width for a transition from the entrance channel α, ℓ, S to the compound nucleus of spin J . D_J is the average spacing between levels of angular momentum J . This is valid provided $T_{S\ell}(\alpha) \ll 1$.

In the R-matrix theory of nuclear reactions, $\langle \Gamma(\alpha\ell S|J) \rangle = \langle \gamma^2 P_\ell \rangle$, where P_ℓ is a penetrability and γ^2 is the reduced width for decay into channel α, ℓ, S . The statistical model has as one of its basic assumptions that the individual γ_i for each resonance i are randomly distributed with a most probable value of 0. Thus, the transmission coefficient is more than just a probability of barrier penetration, it is a probability for compound nucleus

formation which, itself, is the product of a barrier penetrability times an average reduced width.

The total number of open channels is given by

$$N = \left\{ \sum_{\alpha, S, \ell} T_{\ell}(\alpha) \right\}_J = 2\pi \left\langle \frac{\Gamma_J}{D_J} \right\rangle \quad (3.29)$$

where Γ is the average width of levels in the compound nucleus. In most cases involving heavy ion reactions, $\Gamma_J/D_J \gg 1$, in which case the derivation of eq. (3.28) is no longer justified (Fe 60, Bo 70).

3.4. A Consistent Treatment of Fission and Evaporation

In principle, the treatments of the evaporation of light particles and fission given in the preceding sections are inconsistent. This is because the only difference between fission and evaporation is in the relative size of the emitted particle and the residual nucleus. A straightforward extension of the Hauser-Feshbach formula to heavier and heavier "evaporated" particles leads ultimately to a situation in which the rate of fission into equal mass fragments would be determined not by the density of levels at the saddle point but rather by the densities of levels of the residual fission fragments at infinite separation. This is clearly inappropriate for the fission of a heavy nucleus.

Another approximation customarily made in the application of the Hauser-Feshbach formula also fails in the limit of fission, viz. the assumption that the transmission coefficient may be calculated by the optical model for spherical nuclei in their ground states. (The principle of detailed balance would require the T_{ℓ} to be calculated for deformed fragments colliding to form a system at a saddle-point configuration.) On

the other hand, the transition-state method (Bo 39) and Hauser-Feshbach formula (Ha 52) give the same result for neutron evaporation. This is because the transition state in the latter case consists of the neutron just outside the (spherical) residual nucleus and the "fission-barrier" energy may be identified with the neutron separation energy [see eqs. (3.21) and (3.22)].

Moretto (Mo 72b, Mo 75) has pointed out and discussed the inconsistency described above and has proposed that evaporation be treated in the same manner as fission. Swiatecki has also discussed this problem (Sw 80) from a slightly different point of view and has come to the same conclusion. A self-consistent treatment of statistical decay would involve the following ingredients which we may express schematically as follows

$$R(E_i, J_i) \propto P(\epsilon^S) \frac{\rho(E_t, J_t)}{\rho(E_i, J_i)} \quad (3.30)$$

in which the thermal excitation energy of the transition state is given by $E_t = E_i - E_B(J_i) - \epsilon^S$ where, as usual, $E_B(J_i)$ is the energy required to bring the system from the ground state into the transition-state configuration. The quantity ϵ^S is the energy associated with the translational kinetic energy of the separation coordinate at the transition state configuration. $\rho(E_t, j)$ is the corresponding density of levels for the nuclear system in this configuration. The probability that the system will in fact separate when approaching the transition state or saddle point is denoted by $P(\epsilon^S)$. For energies $\epsilon^S < 0$, $P(\epsilon^S) < 1/2$ and barrier penetration is necessary, where for $\epsilon^S \gg 0$, $P(\epsilon^S) \rightarrow 1.0$. This is in direct analogy to

the behavior of the transmission coefficient, evaluated at energies below, at, and above the barrier. (The kinetic energy at infinite separation is ϵ .)

For neutron emission, we have to good approximation $E_B(J_i) = S_n$, $\epsilon^S = \epsilon$, and the saddle-point configuration consists of a residual nucleus having the same shape as the compound nucleus. Thus,

$$E_t = E_i - E_B(J_i) - \epsilon^S = E_i - S_n - \epsilon .$$

For an alpha particle, we may approximate the transition state as an alpha particle just touching the surface of the residual nucleus, such that the separation of centers is R . In this case,

$$E_B(J_i) \approx S_\alpha + \frac{\hbar^2}{2\mathcal{J}(R)} (J_i^2) + V_n(R) + V_{\text{Coul}}(R)$$

where the last three terms represent a centrifugal, nuclear and Coulomb potential, respectively. However, the saddle-point and asymptotic kinetic energies are related approximately by

$$\epsilon^S \approx \epsilon - \frac{\hbar^2 J_i^2}{2\mathcal{J}(R)} - V_n(R) - V_{\text{Coul}}(R) \quad (3.31)$$

and thus, $E_t \approx E_i - S_\alpha - \epsilon$. To the extent that

(i) an α -particle, when just outside the nuclear surface, does not strongly polarize or deform the shape of the adjacent residual nucleus and

(ii) dissipative effects, which convert potential and rotational energy at the saddle point into heat rather than kinetic energy, as given by eq. (3.31), are small,

then the Hauser-Feshbach and transition state methods give identical results. This is probably why the Hauser-Feshbach method works so well for the evaporation of particles as heavy as helium.

It is apparent that the practical (as opposed to conceptual) differences between the transition-state method and the Hauser-Feshbach method lie partly in how well the saddle-point configuration can be approximated by touching spheres having an effective moment of inertia $\mathcal{J}(R) \approx \mu R^2$, where μ is the reduced mass for the touching-sphere configuration, which interact through a nuclear potential $V(R)$ arising from tangential surface contact. These differences, therefore, are contained in the formation of a neck, deformation of the nuclei in contact, shell effects on the level density associated with these shape changes, and dissipation of kinetic energy between the saddle point and scission.

It will be interesting in the illustrative examples to see whether the above effects, neglected in nearly all statistical model treatments of light-particle emission, might be important.

3.5. Practical calculations, computer codes

There are many different quantities which can be measured in those heavy-ion induced reactions which produce equilibrated nuclei. First of all there are the different decay products, γ rays, light particles, heavy residual nuclei, and fission products. In each of these cases relative yields as a function of charge and mass, continuous energy spectra, and angular distributions may be observed. Sometimes it will be the differential cross section to a resolved, low-lying state in a residual nucleus which is of interest. Reactions not proceeding through a compound nucleus but which

nevertheless are thought to produce fragments which do reach equilibrium before decay also present a variety of observables for study, including the effect of particle evaporation on the spin (magnitude and direction) of a fragment before it begins to emit γ rays. These examples are mentioned to show why a variety of computer codes have been developed over the years.

The types of calculation and computer code may be classified as follows.

- 1) Single step (SS) calculations. Either the excited nucleus has energy sufficient for one decay only or it is only the emission of the first particle which is of interest. In the case of compound nucleus formation and decay, eqs. (3.26) and (3.27) then determine angle-integrated cross sections and differential cross sections, i.e., angular distributions, respectively. Eqs. (3.22)-(3.25) would be used for fission.
- 2) Multi-step (MS) calculations. In this case the spectra of γ rays and light particles contain contributions from successive decays, and the distribution of heavy residues is arrived at through several or many successive decays. This problem is treated in two ways. The first method involves the construction of a grid in Z and A and, for each nucleus, a population distribution over a two-dimensional grid in excitation energy and angular momentum. Given the initial distribution of E and J for the compound nucleus, the populations of the various daughter nuclei are calculated. The size of the grid in Z and A continues to expand for successive daughter nuclei until further decay is energetically forbidden.

The advantage of the grid calculation is that the yields of very weakly populated residual nuclei may be calculated with precision. A disadvantage is that such codes generally do not calculate angular distributions of emitted particles or residues. This multi-step, gridded method will be denoted

MSGR. The second method (MSMC) follows the decay of individual compound nuclei in an initial ensemble by Monte Carlo techniques until the residual nucleus can no longer decay. In this case, the accuracy with which any given quantity can be predicted will depend on how likely that quantity is to occur and how many cases or events, i.e., compound nuclei, are calculated. Thus, the yields of infrequently populated residues are calculated less accurately. The great advantage of the Monte Carlo method is that it can predict energy spectra, angular distributions and multi-particle correlations, in the laboratory system.

The vast majority of all applications of the statistical model to experimental data requires a numerical calculation, and either a computer code must be written for the specific case at hand or, if possible, an existing code may be used. Many codes have been developed and circulated among the practitioners of statistical analyses and among nonpractitioners who wish only to estimate a production cross section for some isotope of interest. These codes are frequently referred to by name in the literature. However, of necessity, they are frequently modified, improved and sometimes renamed by users having specific needs. Nevertheless, it may be useful for some readers to have a list of the more frequently encountered codes, which quantities they calculate, and references where more detailed information can be found.

The list of computer codes is contained in Table 2 along with the type, authors, references and an indication whether the code includes γ -ray competition, fission, and whether angular momentum coupling is neglected (W.E. denotes Weisskopf-Ewing), or included (H.F. denotes Hauser-Feshbach).

All codes calculate fission barrier heights with the rotating liquid drop model (RLDM).

One of the important features of any code will be its treatment of the level density of the residual nuclei. Since this is subject to frequent modification, it, as well as other features, is not included in the list but is left for the interested reader to glean from the accompanying references.

One important fact to keep in mind with respect to the use of statistical model computer codes is that they are merely vehicles for converting input information (in terms of initial population distributions, transmission coefficients, and level densities of residual nuclei) into cross sections. The old adage, "garbage in, garbage out" applies here. Furthermore, referring to a code simply by name does not specify the calculation; the input parameters must be stated explicitly when quantitative comparisons with data or with other codes are made.

3.6. Summary

The basic problem in the application of the statistical model to cases of practical interest is to calculate the distribution of products (their charges, masses, energies and angular momenta) obtained from the decay of an ensemble of identical excited nuclei in equilibrium having a known excitation energy and angular momentum. Given the statistical model hypothesis that all open channels are equally likely to be populated, expressions for the rates of decay by γ -ray emission, evaporation of light particles and fission were obtained. These expressions depend on transmission coefficients (or analogous quantities) and on the densities of levels in the residual or transition nuclei. Expressions for the angular

distribution of the products were given. The total decay rate is the sum of all individual decay rates and is simply related to the total number of open channels. Probabilities or cross sections for the population of individual channels are obtained as branching ratios [eq. (3.24)] or as cross sections for the production of a distribution of equilibrated nuclei multiplied by an appropriate branching ratio [eq. (3.25)]. For the case of compound nucleus formation and decay by evaporation of light particles, the Hauser-Feshbach formula is widely used. It may also be derived from a general theory of nuclear reactions, albeit within certain approximations which are not valid for heavy ions. There is a conceptual difference between the Hauser-Feshbach theory for evaporation and the transition state theory for fission which is evident when the former is used to calculate the "evaporation" of heavy particles. Practically, the two methods give equivalent results when applied to the evaporation of neutrons or other particles which are small compared to the emitting nucleus. The agreement between the two formalisms in any particular case should depend on the actual shape of the transition state (deformed nuclei or touching spheres) and on the nature of the descent from saddle point to scission (i.e., on the presence of dissipative processes). Finally, the different types of computer codes used in practical applications were categorized and listed.

4. Illustrative Applications

4.1. Introduction

In sections 2 and 3 we have presented the statistical model for the decay of equilibrated nuclei. We now wish to apply this tool to the analysis of heavy-ion reactions. The emphasis here will be on how well this model works and on what we can learn from those cases in which it appears to be valid.

In the early days of the statistical model and its application to heavy-ion reactions, the questions were centered around the elucidation of the basic reaction mechanism. Most all applications of the statistical model were therefore of intrinsic interest. We shall see that this stage has been passed, except in cases where extremes of bombarding energy and angular momentum are encountered. The success of the statistical model in many applications has thus changed it from an object of study to a valuable tool for investigating the properties of nuclei (or nuclear systems) produced through the collision of complex nuclei.

Characteristically different features are encountered in the decay of equilibrated nuclei depending on their mass and charge and the amount of angular momentum they possess. In light nuclei the Coulomb barrier, which otherwise inhibits the evaporation of charged particles, is small. Thus protons and α particles compete favorably with neutrons and, if the angular momentum of the nucleus is high, the lower centrifugal barrier seen by α particles may make them the favored mode of decay. Gamma-ray emission will only take place when the available excitation energy (or the centrifugal barrier) prevents particle emission, i.e., near and below the

lowest particle separation energy. Fission is generally inhibited because the surface energy is large compared to the small Coulomb energy.

All three modes of decay can be important in medium weight nuclei. Fission may compete with neutron decay when the angular momentum is high. Charged particle emission, while inhibited by the Coulomb barrier, is not altogether absent, especially for those neutron-deficient nuclei which can have quite low proton or α -particle separation energies. For nuclei which survive fission, neutrons first remove excitation energy but little angular momentum. Quadrupole gamma radiation then becomes the only effective way to remove the remaining angular momentum.

Heavy nuclei are characterized by high fissility and low fission barriers. Since the emission of light charged particles is now strongly hindered, only neutron emission and fission compete. With little additional angular momentum, a heavy nucleus can have a fission barrier less than the neutron separation energy, and fission becomes the dominant decay mode. Gamma-ray decay will occur only in the post-scission deexcitation of the fission fragments.

This section on applications is organized along the following lines. The decay of nuclei produced in compound nucleus reactions will be considered first, beginning with light nuclei and following with the neutron-gamma and fission-evaporation competition found in medium-weight and heavy nuclei. Examples of the application of the statistical model to non-compound reactions and a summary are given in the last two subsections.

4.2. Compound Nucleus Reactions

Reactions in which a compound nucleus is formed are the simplest cases for the application of the statistical model. This is true not only

in the sense that the term compound nucleus implies equilibration and therefore the applicability of statistical methods, but for the reason that the charge, mass, and excitation energy of the compound nucleus are known. Within reasonable assumptions, the distribution of angular momenta is also known. In the case of non-compound reactions, the charge, mass, and excitation energies of primary fragments are distributed quantities, and more assumptions must be made about them and the distribution of angular momenta before a statistical calculation can be made.

4.2.1. The Decay of Light Compound Nuclei

Heavy-ion reactions among light nuclei (e.g., p and s-d shell nuclei) which proceed via formation and decay of a compound nucleus are studied for a number of reasons. The cross section for compound nucleus formation, σ_{fus} , and how it depends on the mass and charge of the projectile and target and on the bombarding energy, is itself of general interest. Contained in these cross sections is information on the maximum, or limiting, angular momentum with which a compound nucleus can be formed. This limit in turn may depend on properties of the compound nucleus at high excitation energy and high angular momentum (the yrast line) or on dynamical aspects of the entrance channel. In the latter case, σ_{fus} may depend on the shell structure of the target and projectile nuclei. The distribution in charge and mass of the evaporation residues contains information on the distribution of angular momentum in the entrance channel leading to fusion.

The residual nuclei produced after further particle decay is no longer possible are often in high spin states, a fact that opens up a whole area of spectroscopy. In some cases it is possible to place

quantitative limits on the spins of the states by comparison of measured cross sections with the Hauser-Feshbach theory.

The statistical model is used in pursuit of all the above studies (St 74). In the following, we organize examples of its application in a practical manner according to the type of radiation detected rather than by the motivation for a given experiment.

It is not possible (or even desirable) to give the details of each of the statistical model calculations which will be mentioned in the following discussion. In general, they make use of equations (3.26) and (3.27) (the Hauser-Feshbach expressions) and Fermi-gas level densities with corrections for pairing. The more precise calculations, which are generally those done after 1970, use level densities obtained from one of the compilations discussed in section 2.6. The spin cutoff factor or moment of inertia which determines the spin dependence of the level density is sometimes an adjustable parameter with r_0 varying between 1.2 and 1.5 fm. Transmission coefficients are usually taken from optical model calculations with parameters based on fits to elastic scattering.

4.2.1a Gamma-Ray Decay

Gamma-ray decay in the extreme, i.e. heavy-ion radiative capture, is an extremely weak process, with cross sections in the nano-barn range (Fe 69). High-energy γ -decay in cases such as $^{12}\text{C}(^{12}\text{C}, \gamma)^{24}\text{Mg}$, may also be of collective rather than statistical character (Sa 78).

Searches for statistical γ -ray decay, unaccompanied by particle decay, in the fusion of $^{14}\text{N} + ^{12}\text{C}$, $^{14}\text{N} + ^{30}\text{Si}$ and $^{14}\text{N} + ^{27}\text{Al}$ have yielded upper limits of $\sim 0.5 \mu\text{b}$ (Vi 79). Studies of $^{16}\text{O} + ^{27}\text{Al}$ and $^{16}\text{O} + ^{93}\text{Nb}$ have also produced only upper limits for pure radiative

decay (Br 78) and these have been shown to be consistent with statistical model estimates using the formulation given in section 3.2.1.

Gamma-ray decay which is preceded by particle emission and which occurs at the end of the decay process is, in contrast, quite intense. Geoffrey et al. have studied the multiplicity of γ -radiation from residues produced in the fusion of 107, 155 and 197 MeV ^{12}C with Al and Ni targets (Ge 78). The average multiplicities were 2.7 ± 0.2 and 9.3 ± 0.9 γ -rays per residue for the Al and Ni targets, respectively. Only ~ 6 and ~ 13 MeV of energy were removed by γ -ray emission in these respective cases, and the multiplicity was found to be insensitive to the range of bombarding energies used in the experiment. This indicates again that particle emission is by far the dominant mechanism for the removal of excitation energy and angular momentum in the decay of light compound nuclei. The observed properties of the continuum radiation, average multiplicity, average energy, and energy spectra were reproduced rather well by a statistical model calculation of the type developed by Grover and Gilat (Gr 67a) and described in section 3.2.1.

Gamma radiation between resolved levels can serve as an identification of the heavy residual nucleus and will be discussed in section 4.2.1.e.

4.2.1b Light-Particle Emission

The emission of protons, neutrons and α -particles forms the dominant mode of decay for light compound nuclei. Consequently, there are many examples in the literature where statistical model calculations are compared with measurements of light-particle yields.

One of the earliest detailed comparisons was made by Vogt for the $^{12}\text{C} + ^{12}\text{C}$ reaction (Vo 68). Because of the low bombarding energy (Al 64) and tightly bound reactants, the number of open channels is small and most of these channels are levels of known excitation and spin in the residual nuclei. Thus, the calculation was not very dependent on assumptions about level densities. The agreement between theory and experiment was quite good and presaged many similar comparisons (Sh 69, Gr 72a, Gr 75).

The angular distributions of protons to discrete low-lying states observed in the reaction $^{12}\text{C}(^{14}\text{N},\text{p})^{25}\text{Mg}^*$ are shown in Fig. 12 for two bombarding energies (Ol 74). The quantities entering into the calculation have not been adjusted to fit the data. The agreement obtained here is not atypical; on the average the theoretical predictions agree with the data to within about 50%. Note that the angular distributions display only an average symmetry about 90° c.m. If the data were averaged over bombarding energy, the observed asymmetries would be damped. The states with higher spin show larger cross sections corresponding to their $2J + 1$ magnetic substates. Deuterons were observed in the same experiment. Levels of comparable spin in ^{24}Na , populated by deuteron emission, showed angular distributions of similar shape and magnitude. This reflects the fact that discrete states of the same or comparable spins constitute the same number of open channels.

One of the most extensively studied reactions is $^{12}\text{C}(^{16}\text{O},\alpha)^{24}\text{Mg}$. Greenwood et al. (Gr 72a) extended earlier measurements by Halbert et al. (Ha 67) to higher energies and made absolute comparisons with statistical model cross sections. The angular distributions of α particles, summed

over a large number of excited states in ^{24}Mg , are shown in Fig. 13. Note the steeper rise of $d\sigma/d\Omega$ at forward angles as compared with Fig. 12. Because of the larger angular momenta carried in by $^{12}\text{C} + ^{16}\text{O}$ at these energies and out by $\alpha + ^{24}\text{Mg}$, compared to $^{12}\text{C}(^{14}\text{N},p)^{25}\text{Mg}^*$, the angular distributions may be approximated by a $1/\sin\theta$ function over an angular range extending much closer to 0° and to 180° than in the case shown in Fig. 12. [Recall that eq. (3.15) is valid over angles $\theta \gtrsim \pi / (\min J_i, \ell)$.] The total yield of α particles shown in Fig. 13 agrees to within about 15% with the Hauser-Feshbach prediction using independently determined level densities and transmission coefficients. Energy-averaged angular distributions for discrete, low-lying states in ^{24}Mg are also well reproduced (Mi 79).

4.2.1c Emission of Heavy Clusters

Clusters heavier than α particles are also observed (Ru 72), and it is interesting to see whether their emission can reasonably be interpreted in terms of an evaporative process. Typically, the yields of these clusters represent only a few percent of all particles evaporated (St 74). An interesting comparison of the evaporation of complex particles by nuclei and of molecules by water droplets has been made by Cohen (Co 60). The importance of statistical degeneracy in the nuclear case as the cause of cluster emission is pointed out.

Both the reactions $^{10}\text{B}(^{16}\text{O}, ^6\text{Li})^{20}\text{Ne}$ and $^{12}\text{C}(^{14}\text{N}, ^6\text{Li})^{20}\text{Ne}$ have been investigated over a wide range of energies and can be compared not only with statistical model predictions but with measured yields of light clusters (α particles, deuterons, etc.). The angular distributions of ^6Li particles populating discrete states in ^{20}Ne show symmetry

about 90° (Be 73a) and agree in magnitude with absolute statistical model calculations as shown in Fig. 14 (Ha 74). Comparisons of deuteron yields and ${}^6\text{Li}$ yields produced in the ${}^{12}\text{C} + {}^{14}\text{N}$ reaction (Kl 74) and of α -particle and ${}^6\text{Li}$ yields (Go 74, Fo 74, Lo 76) all show good agreement with the Hauser-Feshbach theory.

The above results are not peculiar to ${}^6\text{Li}$ but extend to similar heavy clusters such as ${}^7\text{Be}$. Figure 15 compares the yields ${}^7\text{Be}$ with those of protons, neutrons and α particles (in terms of the associated residues)(Ho 73). The solid lines correspond to the same Hauser-Feshbach calculation (Ha 74) which reproduces the yields of ${}^6\text{Li}$.

The probability that a relatively massive particle will be emitted depends sensitively on the maximum angular momentum with which the compound nucleus is formed. It was found that a critical angular momentum for fusion, J_c , which is less than the grazing angular momentum in the entrance channel, must be introduced, in order to obtain agreement with experiment for the ${}^6\text{Li}$ yield. If one assumes a priori that ${}^6\text{Li}$ emission can be described by the Hauser-Feshbach theory, then this becomes a means for determining the magnitude and energy dependence of J_c (St 74, Kl 75). On the other hand, J_c can be determined independently and, it is found, is of the right size to produce the agreement indicated in Figs. 14 and 15. This fact can be used to justify the application of the Hauser-Feshbach method.

Thus, the Hauser-Feshbach treatment of the evaporation of clusters such as α particles, ${}^6\text{Li}$ and ${}^7\text{Be}$ nuclei works remarkably well, at least for not-too-high bombarding energies (St 77).

Several reactions have been studied in which the mass of the emitted cluster approaches or is equal to half the mass of the compound nucleus (La 63a, Va 67, Ru 72, Wi 74). In these cases, which are more appropriately named "fission", it would seem that the transition state theory would be required and that the Hauser-Feshbach description should be inappropriate.

Rudy et al. (Ru 72) studied a number of reactions induced by 42 MeV α particles on ^{12}C and ^{16}O targets. While they found strong direct reaction components in the forward angle yields of ^6Li , ^7Li , and ^7Be , which is not surprising, the large-angle yields were generally within the upper and lower limits of a Hauser-Feshbach calculation. Two cases in which no direct reaction component is to be expected are the reactions $^{20}\text{Ne}(\alpha, ^{12}\text{C})^{12}\text{C}$ and $^{28}\text{Si}(\alpha, ^{16}\text{O})^{16}\text{O}$, observed by Lassen (La 63a) and by Vandenbosch et al. (Va 67), respectively. Comparison of the measured differential cross section (at only one bombarding energy) with the Hauser-Feshbach theory in the latter case showed an agreement within a factor of two. The former reaction, for which an excitation function exists, shows large compound-nucleus fluctuations (see Fig. 16) and an energy-averaged cross section which agrees within typically 30% with a statistical model calculation that also reproduces the yields of α particles.

Compound elastic scattering, viz. when the compound nucleus decays back to the entrance channel in which it was originally formed, represents another form of heavy cluster emission. In this case, however, there will be a large direct reaction component from potential scattering. The component which proceeds via the compound nucleus can be identified and

its average strength determined by an analysis of the fluctuations in the energy dependence of the cross section. The $^{12}\text{C} + ^{12}\text{C}$ system is one of the few systems where the total number of open channels is small enough that the effects of compound elastic scattering are easily seen. Analysis by Bondorf (Bo 73) of the scattering at lower energies $7 \leq E_{\text{c.m.}} \leq 14$ MeV and by Shapira et al. (Sh 74) at higher energies $13.5 \leq E_{\text{c.m.}} \leq 37.5$ MeV have shown the magnitude of compound elastic scattering deduced from fluctuation analysis of the narrow (~ 100 - 300 MeV wide) structure in $\frac{d\sigma(E)}{d\Omega}$ and the predictions of the Hauser-Feshbach theory to be consistent.

We are thus led to the conclusion that, for light compound nuclei, the Hauser-Feshbach treatment of the emission of heavy clusters agrees with experiment. That is to say, it gives the right answer for the fission of light nuclei. A probable explanation for this is found in the discussion in section 3.4 and in the rotating liquid-drop model calculations of Cohen, Plasil and Swiatecki (Co 74). The nuclei undergoing fission here have angular momenta which are significantly lower than that for which the fission barrier vanishes. Thus, their saddle point configurations very nearly approximate those of two touching spheres. In this case, the phase space available for the decay of the compound system into fission mode is the same (see section 3.4) in the transition state theory as in the Hauser-Feshbach theory.

4.2.1d. High-spin Selectivity

Most heavy-ion compound nuclear reactions show a selective population of high spin states. [The few exceptions occur in cases like $^{14}\text{N} + ^{14}\text{N} \rightarrow ^{24}\text{Mg} + \alpha$ (Mi 70) where there is a large positive Q-value which drastically increases the excitation energy in the compound nucleus and

the number of open channels (Gr 72a).] A typical spectrum of α particles from such a selective reaction, $^{10}\text{B}(^{16}\text{O},\alpha)^{22}\text{Na}$, is shown in Fig. 17 (Go 74). The angular distributions for these particle groups, together with the statistical model predictions, are given in Fig. 18. When the parameters entering into the Hauser-Feshbach calculation are fixed, the predicted cross sections for the high spin states are sufficiently sensitive to the spin of the residual level that an assignment can be made. When uncertainties in these parameters, especially the spin cutoff factor, are taken into account, an error of $\pm 1 \hbar$ is typical. In the yrast region, however, where the high spin states are well spaced, this is often sufficient to identify a member of a band.

Comparisons such as these, especially when taken together with the results of shell model calculations, have enabled the identification of a number of rotational bands in s-d shell nuclei with levels having spins up to $10 \hbar$. The rotational band structure of ^{22}Na as seen in the $^{10}\text{B}(^{16}\text{O},\alpha)^{22}\text{Na}$ reaction (Go 74) and as compared with shell model calculations (Ha 71) is shown in Fig. 19. This powerful technique has been exploited widely and further examples may be found in refs. (Fo 74, Kl 74, Co 75, Go 75, Kl 75a, Sz 78, Sc 79, Sz 79, Kl 80).

4.2.1e. Evaporation Residues

The heavy residues remaining after particle emission has ceased are distributed in mass and atomic number in a manner reflecting the different types of light particles (p,n, α ,etc.) emitted. Furthermore, their energies and angles in the laboratory system represent a folding of recoil velocities imparted to the residue at each stage of the evaporation. Thus, information complementary to that given by light particle emission

can be obtained from the observation of evaporation residues. If it is mainly the fusion cross section which is of interest, evaporation residues have the distinct advantage of there being exactly one residue per compound nucleus formed (unless, of course, the compound nucleus fissions).

Evaporation residues may be detected either indirectly through characteristic γ rays (and/or x rays in heavier nuclei) or by direct observation and counting of the residues. The gamma-ray method is appropriate when knowledge of the mass alone is sufficient to determine that the nucleus in question is an evaporation residue. At lower bombarding energies, where the number of open channels is much smaller, the yield is concentrated in a smaller number of different residues and the gamma-ray method provides a quick and sensitive way to obtain an angle-integrated cross section. The statistical model enters into the analysis of the data because the population of levels below the particle threshold (and the gamma-ray branching ratios) must be known in order to obtain the number of residues from the type and number of discrete gamma-ray lines. Many measurements and analyses have been made using this technique, a few examples of which are found in refs. (Ol 74, Sp 74, Cu 76, Da 76, Ko 76, Sw 76, Ko 77, Sw 77).

The direct observation of residues using ΔE -E counter telescopes to determine Z and time-of-flight techniques to determine A has become the most frequently used method for measuring fusion cross sections for light nuclei at energies above the Coulomb barrier. The fusion of a heavy-ion projectile with a target of comparable mass imparts a substantial velocity to the compound nucleus. The recoil momenta accompanying the emission of

protons, neutrons and alpha particles are sufficient to deflect the residue to relatively large angles, making them easy to detect.

The interpretation of mass distributions of evaporation residues formed in heavy-ion fusion reactions has been described by Pühlhofer (Pu 77). In particular, he has analyzed the mass distributions of residues formed in the reactions $^{19}\text{F} + ^{12}\text{C}$, $^{19}\text{F} + ^{27}\text{Al}$ and $^{16}\text{O} + ^{27}\text{Al}$ with the Hauser-Feshbach formula and a multi-step, grid calculation. A careful treatment of the level densities, particularly at low excitation, is the main ingredient responsible for the overall good agreement between calculated and measured mass distributions.

The calculations provide an insight into the distribution of decay modes in the excitation energy, angular momentum plane. Figure 20 illustrates the regions in which a mode of decay corresponds to more than half of the total decay probability for the case of ^{44}Sc (Pu 77). The characteristic features of statistical decay in light nuclei are evident here: the predominance of α -particle emission for states of high angular momentum and the importance of γ decay mainly at and below particle thresholds. (There is a small extension of γ -decay probability in the region along the yrast line which is more significant for heavier nuclei.) The decay chains typical for each region of angular momentum are also indicated. A more precise indication of the dependence of the final mass distribution on the initial angular momentum of the compound nucleus is given in Fig. 21. Here again one notes the predominance of nucleon emission for low angular momenta. When the distributions for different initial angular momenta are appropriately weighted and combined, a distribution in good agreement with experiment is obtained.

An examination of the sensitivity of the predicted mass distributions to various assumptions made on the level densities in the region of high excitation (>15 MeV) showed that the retention of the shell effects, present at low excitation, in the region of high excitation had little observable effect (Pu 77). Thus, values of $a(E_x)$ in the range $A/9 \leq a \leq A/7$ for $E_x > 15$ MeV all gave equivalently good fits. On the other hand, unreasonable values such as $A/12$ did not fit the data. The value of the moment of inertia used in determining the spin cutoff factor, expressed in terms of the rigid-body radius parameter, corresponded to $r_0 = 1.2$ fm in the region $4 < E_x < 10$ MeV and to $\sim 1.29(1 + 5 \times 10^{-4} J_i^2)^{1/2}$ fm at higher excitations. This parameter is important in determining the relative amounts of nucleon and α -particle emission; the parametrization employed by Pühlhofer at high excitation energies corresponds to a liquid-drop model prediction (Co 74). The importance of allowing for nuclear deformation at large angular momenta was also borne out in a comparison of statistical model calculations using shell model level densities with experimental data on the decay of ^{56}Ni (Ca 79). The compound nucleus was formed in the reaction $^{32}\text{S} + ^{24}\text{Mg}$.

The sensitivity of the predicted mass distribution to the initial distribution of angular momentum has been used to search for a particular effect in heavy-ion fusion predicted by the time-dependent Hartree-Fock (TDHF) theory (Bo 78). This effect, referred to as the "low- ℓ window", is a predicted absence of fusion for central collisions, that is, for partial waves below a critical ℓ value. Analyses of mass distributions for $^{16}\text{O} + ^{16}\text{O}$ by Kox et al. (Ko 80) and for $^{28}\text{Si} + ^{27}\text{Al}$ by Barrette et al. (Ba 80a) have indicated that a low- ℓ window, if present at all, is much smaller than predicted by the TDHF.

A comparison of the energies and angular distributions of the evaporation residues with statistical model predictions is often important in establishing that complete fusion occurred and that the observed products have properties consistent with the decay of an equilibrated nucleus. For this purpose, Monte Carlo calculations are necessary (Ei 77, Go 79, Co 80, Ga 80, Go 80a). These properties can be predicted rather well, as is evidenced in Figs. 22 and 23 (Co 80). Shown here are measured energy spectra for residues of the reaction $^{20}\text{Ne} + ^{12}\text{C}$ (Fig. 22) and angular distributions from two different reactions which populate the same compound nucleus, ^{32}S (Fig. 23). The effect of α emission on the energy spectrum of ^{27}Si (α, n emission) is dramatic when compared with the spectrum of ^{29}Si ($2p, n$ emission). Note also in Fig. 22 how the two separate kinematic peaks, corresponding to α emission in the forward and backward directions, are joined as additional nucleon emission increases the number of recoil impulses received by the residue. The predictions of the statistical model (solid lines) reproduce these features very well. Similar good agreement is found in the comparison with the angular distributions. Note in particular the broad angular distribution for ^{24}Mg , which is produced by the emission of two α particles.

The foregoing illustrations have involved reactions in which the bombarding energy is low enough that the lightest residues are still heavier than either projectile or target. Gomez et al. have studied the reactions of ^{14}N with ^{12}C and ^{16}O with ^{10}B up to energies for which the masses of the residues are comparable to or less than that of the projectile or target. In cases such as these, a comparison with a Monte Carlo statistical model calculation can provide guidance in the methods used to identify the evaporation residues.

The problem encountered at high energies is illustrated in Fig. 24 (Go 79) which shows two-dimensional ΔE - E spectra obtained at two different bombarding energies, 44 MeV and 178 MeV. At the lower bombarding energy, the residues are well separated from the projectile, while this is no longer true at 178 MeV. The right-hand panel of Fig. 25 shows energy spectra for reaction products with $Z = 6, 7$ and 8 . There are two components present, one with an energy corresponding closely to the velocity of the projectile. The lower energy component has a mean velocity equal to that of the compound nucleus. The histograms are the results of Monte Carlo calculations and show quite clearly that the lower velocity group has the mean velocity and width expected for residues. The left-hand panel shows the angular distributions of the lower energy products identified as residues. The histogram is the statistical model calculation. The properties of the residues from the reactions $^{12}\text{C} + ^{14}\text{N}$ and $^{10}\text{B} + ^{16}\text{O}$ agree quite well with Hauser-Feshbach Monte Carlo calculations over a range of bombarding energy extending from ~ 20 to ~ 115 MeV c.m. (Go 79, Go 79a). This suggests that complete fusion and the formation of a compound nucleus which attains a measure of equilibration occur in light nuclei at bombarding energies approaching 20 MeV/A.

The generally good agreement between experimental charge and mass distributions of residues and the statistical model predictions, as indicated in this subsection, is typical of comparisons with data using codes (see sect. 3.5) such as GROGI (We 76, Fe 78), CASCADE (Co 77, Ko 77a, He 81), JULIAN (Ei 77, Ts 78), LILITA (Go 78, He 81) and LANCELOT (Co 80). The following two points must be borne in mind, however, in discussing this agreement. (i) There is always some room for reasonable adjustment of parameters in these analyses, even when every effort is made to establish

a priori the input parameters from independent information. While such adjustment of parameters is legitimate, it should not be concluded that calculations done in advance of the acquisition of experimental data will necessarily show as good agreement as can be found in post facto analyses described in the literature. (ii) As a part of their analysis of evaporation residues from the $^{13}\text{C} + ^{48}\text{Ti}$ reaction, Dumont et al. (Du 80) conducted the following interesting "experiment". The attempted, insofar as possible, to give the same input quantities to several different evaporation codes (ALICE, JULIAN (various versions), CASCADE, and LILITA). The results showed agreement in overall trends, but the discrepancies were nevertheless surprising. This comparison demonstrates that the use of different level-density formulae, different parameterizations for transmission coefficients, and different numerical approximations in the calculations has important consequences. The differences among the various predictions need to be understood and, if possible, remedied. The authors (Du 80) are pursuing this. In the meantime, one should not conclude that statistical model calculations are a matter of routine!

4.2.1f. Two-Particle Correlations

The angular correlation between light particles emitted in an evaporation cascade is a more sensitive indicator of the compound nucleus angular momentum than is the singles angular distribution (Ku 79). In the latter case, angular distributions for continuum α particles tend to $1/\sin\theta$ as soon as the angular momentum in the compound nucleus becomes appreciable (the "flywheel effect"). Two-particle correlations, even among α particles in the continuum, show a degree of anisotropy which reflects directly the maximum angular momentum in the compound nucleus.

The measurement of such correlations has also been proposed as a method to look for the presence of a low- ℓ fusion window (Ba 80).

Measurements and calculations of light particle, light particle correlations (pp , $p\alpha$, $\alpha\alpha$) have been made by Kuang-Hsi et al. for the reactions $^{16}\text{O} + ^{27}\text{Al}$, ^{40}Ca , ^{58}Ni (Ku 79). The measured correlations for $^{16}\text{O} + ^{27}\text{Al}$ are shown in Fig. 26. Both particles are detected in a laboratory plane perpendicular to the beam ($\theta_1 = \theta_2 = 90^\circ$) and $\phi_1 - \phi_2$ denotes the azimuthal angle between the two detectors. Since α particles are preferentially emitted by the higher spin states of the compound nucleus, and since they carry away more angular momentum than protons, one expects to see a concentration in the reaction plane ($\phi_1 - \phi_2 = 180^\circ$) which is more pronounced for α particles than for protons. This is the classical flywheel effect, again, and its presence is borne out in Fig. 26. A comparison of the measured α - α correlation with the predictions of the statistical model is given in Fig. 27. The value of $J_0 \text{ max} = 47/2$ agrees with the value deduced from the measured fusion cross section using the sharp cutoff approximation (Ku 79).

At moderate and high bombarding energies, there are several reaction mechanisms which can produce light particles and which do not involve fusion-evaporation. The existence of several mechanisms can complicate the interpretation of yields of light particles if they are observed in inclusive experiments. (This problem has been discussed in connection with Li and Be yields in ref. (St 77).) Coincidence experiments enable the study of the light particles most likely originating with compound nuclei (that is, in coincidence with evaporation residues) and make possible either a more stringent verification of the compound nucleus mechanism or identification of noncompound processes.

The prediction of correlations between emitted light particles and residues requires Monte Carlo techniques when multiple decay is possible. Several experimental studies and comparisons with statistical model predictions have been reported for residue, light-particle correlations (Go 80, Go 80a, Ho 80, Os 80, Na 81). As an example, we consider recent work by Namboodiri et al. on the reaction $^{20}\text{Ne} + ^{27}\text{Al}$ at $E(^{20}\text{Ne}) = 120$ MeV (Na 81). Alpha particles and protons were detected in plane and out-of-plane in coincidence with heavy residues ($Z \gtrsim 15$) at $\theta = 15^\circ$ and $\theta = 20^\circ$. Comparisons of their experimental results and the Hauser-Feshbach Monte Carlo predictions are shown in Figs. 28-30. The energy spectra of α particles at a forward angle and a backward angle are presented in Fig. 28. The solid curve is the statistical model prediction. This comparison shows that the higher energy particles observed at the more forward angle are associated with a kinematic effect--the addition of velocities of the moving compound nucleus and the evaporated α particle. Nonequilibrium or preequilibrium emission of α particles is thus not required as an explanation for the emergence of beam-velocity α particles at forward angles in this reaction. Experiments at higher bombarding energies and with lighter projectiles can show such nonequilibrium effects, however (Ho 80, Go 80).

The in-plane angular correlations, shown in Fig. 29, are also well reproduced by the statistical model calculation. These correlations peak on the side of the beam opposite (negative angle) to that on which the heavy-ion detector is placed (positive angle). Again, this is a simple kinematic effect: in order for the residue to emerge at a finite angle with respect to the beam direction, it must emit an α particle or series of particles with a net momentum in the opposite direction.

A particularly graphic comparison of the experimental data and the calculation is made in the velocity contour plot of Fig. 30. The velocity vector V_{FR} denotes the direction of the fusion residue while the straight lines indicate angles at which coincident α particles were observed. A ridge, corresponding to the emission of α particles with energies at the centrifugal-plus-Coulomb barrier, is evident in both the experimental data (Fig. 30a) and in the calculation (Fig. 30b). The overall agreement shown here in Fig. 30 and also found in several other comparisons of measured and calculated correlations between light particles and evaporation residues (Os 80) shows the power of Monte Carlo techniques in the analysis of heavy-ion reaction data. Indeed, such an analysis is a prerequisite to the demonstration of any non-equilibrium phenomena.

4.2.2 Neutron-Gamma Competition

There are two important differences between the phenomena encountered in the decay of light and medium-heavy compound nuclei. The first is the appearance in medium-weight nuclei of large neutron and γ -ray multiplicities. Neutron emission dominates charged particle emission because of the increased Coulomb barrier, and γ -ray emission at the later stages of the decay is enhanced because of the large nuclear charge, possibilities for collective transitions, and need to dissipate large amounts of angular momentum. The second difference, to be considered in section 4.2.3, is the emerging importance of fission.

4.2.2a General Features

There have been many measurements of (HI, xn) cross sections and of γ -ray multiplicities since the papers of Sarantites (Sa 67, 67a,b) and of Grover and Gilat (Gr 67a,b,c) laid down the modern computational basis for the analysis of these data. The salient features of typical energy spectra in this mass region are illustrated in Fig. 31 (Gr 67a). This calculation is for a specific example, $^{140}\text{Ce}(^{16}\text{O}, xn)^{156-x}\text{Dy}$ at $E_{^{16}\text{O}} = 90$ MeV, and shows the dominance of neutron emission, the statistical and collective regions of γ -ray emission, and the protons and alpha particles emerging at energies above their respective Coulomb barriers. (The small peak at $E_{\alpha} = 7.5$ MeV corresponds to a predicted, but not generally observed, emission of α particles from occasional Yrast levels having strongly hindered radiative transitions.)

The neutron spectrum arises from an ensemble of compound nuclei emitting different numbers, x , of neutrons. The observed x -n distribution as a function of bombarding energy is compared in Fig. 32 with a

statistical model calculation for the $^{140}\text{Ce} (^{16}_0\text{n}, \text{xn})$ reaction (Gi 73a). The solid lines represent experimental results while the two calculations, shown as dashed lines, correspond to two different normalizations of the dipole strength [see eq. (3.3)]. Case (a) has a constant normalization factor equal to 10^2 times the value deduced from slow neutron radiative capture widths, while case (b) has a factor $2J + 1$ multiplying this width. Gilat et al. caution against taking this factor of 10^2 , which was necessary to fit the xn distributions, too literally as the gamma-ray competition depends on other quantities and assumptions in the calculation as well (Gi 73a).

The effect of the dipole normalization factor on the neutron-gamma competition is illustrated in another way in Fig. 33. Here are shown the boundary lines in the $E_x - J$ plane, at which the respective probabilities, k_n , k_α , k_γ for neutron, alpha-particle and γ -ray emission are equal to 0.5. Note how the increase of the dipole strength by a factor of 10^2 in case (b) increases the region in which γ rays compete with neutron and α -particle emission. The onset of α emission near the Yrast line is often termed " α -pinch off" and is an effect which arises when the Yrast energy exceeds the Coulomb barrier for α decay. Alpha particles emitted from this region of the $E_x - J$ plane are responsible for the shoulder in the α spectrum (Fig. 31) at $E_\alpha = 12$ MeV.

4.2.2b Gamma-Ray Multiplicity

More information about the decay of the compound nucleus can be obtained by measuring the average number of γ rays emitted, or average gamma-ray multiplicity, $\langle M_\gamma \rangle$. The quantity $\langle M_\gamma \rangle$ can be measured as a function of several variables: (i) the particular xn channel which originated

the cascade, (ii) the average gamma-ray energy, and (iii) the total γ -ray energy emitted. The interest in measuring not only $\langle M\gamma \rangle$ but also the width and higher moments of the multiplicity distribution stems from the strong correlation between the initial angular momentum and the number of γ rays emitted. Thus, it is possible to infer, among other things, the distribution of angular momentum in the initial compound nucleus.

Some of the above considerations are illustrated in the study of the reactions of the tin isotopes with argon ions (Hi 79). The landscape of compound nucleus decay for this reaction is presented in Fig. 34 which shows the results of a statistical model calculation performed for the initial distribution of angular momenta shown at the top. This distribution is ultimately limited at high angular momenta by fission decay. The distribution of excitation energy and angular momentum after the emission of one to five neutrons is indicated. The intensity within a given boundary is shown by the projections onto the abscissa and ordinate. Thus, the 4n channel is predicted to be the most intense, is most strongly populated by an initial angular momentum of $\sim 23\hbar$, and tends to produce a residual nucleus with ~ 14 MeV of excitation. The shaded regions in the 3n, 4n and 5n zones denote where γ -ray emission competes with the emission of an additional neutron.

Measurements were made at a series of bombarding energies (Hi 79) for which $\langle M\gamma \rangle$ and the width of the distribution σ_γ were determined. From these quantities (and from fits to the m-fold coincidence distributions) a series of skewed-Gaussian distributions for $M\gamma$ were determined. These are shown in Fig. 35 (solid lines) along with corresponding statistical model calculations (broken lines). The agreement for the three lower bombarding

energies is seen to be quite good whereas sizeable discrepancies arise at the highest energy. The origin of these discrepancies is thought to lie in noncompound processes (preequilibrium emission or incomplete fusion) rather than in the failure of the statistical model to describe properly the decay of an equilibrated nucleus. Related nonstatistical behavior has also been seen in other reactions as well (Sa 78a, Sa 78b, We 78) when the bombarding energy is high (see section 4.3).

The statistical model also provides a valuable check on the empirical relation between $\langle M_\gamma \rangle$ and the average angular momentum. The formula used to place an angular momentum scale on the top of Fig. 35 was $\ell = 2(M_\gamma - 4)$. Note that the compound nucleus angular momentum (for non-fissioning nuclei) does not exceed $\sim 60-65 \hbar$ for either $^{40}\text{Ar} + ^{122}\text{Sn}$ or for $^{86}\text{Kr} + ^{76}\text{Ge}$, a result which is consistent with the rotating liquid-drop model.

In contrast to the analysis of the x-n data from the reaction $^{140}\text{Ce} (^{16}\text{O}, xn)$ (Gi 73a), the dipole strength was not enhanced over the value deduced from radiative neutron capture reactions. In fact, inclusion of a $2J + 1$ factor in the dipole normalization, which would remedy the discrepancy at high bombarding energies, would destroy the agreement obtained at lower energies. There does not appear to be any satisfactory and universal systematics for the normalization of gamma widths used in statistical model calculations. Each comparison with experimental data seems to be ad hoc. To establish such systematics for highly excited compound nuclei would require self-consistent and detailed analyses of a wide range of experimental data. The enormity of such an undertaking may be the reason why it has yet to be done.

4.2.2c The Gamma-Ray Continuum

The detailed nature of the path by which γ -ray deexcitation takes place is of interest. It was clear from the shape of the γ -ray continuum spectrum that statistical transitions were associated with the higher energy γ rays whose intensity decreased exponentially with increasing γ -ray energy (Si 77). Collective transitions were evident in the large "quadrupole bump" which extended from ~ 0.5 MeV to ~ 1.5 MeV (see Fig. 36). However, it was not known whether, for example, all the statistical E1 γ rays were emitted first or whether they were interspersed with quadrupole transitions within bands. Several studies of this question have been made within the framework of the statistical model (Li 78, Wa 78). Provided one makes the natural assumption that there are many collective rotational bands lying approximately parallel to the Yrast line, the results of the statistical model indicate that the path to the Yrast line is not a direct one. Rather, dipole transitions between bands are intermingled with E2 transitions within a band.

The above examples (Gi 73a, Hi 79) were used to illustrate a comparison of statistical model predictions to experimental data for γ -ray multiplicities. Each of these articles contains a discussion of the sensitivity of predicted quantities to variations in the input parameters. There are a number of other cases in the literature with which the interested reader may wish to become acquainted (Si 77a, Tj 78, Wa 78, Ga 80, Si 81).

4.2.3 Fission-Evaporation Competition

The choice between fission or the evaporation of a light particle is governed by the relative density of levels available for these two processes (see section 3.2.4). For evaporation of a neutron (the main mode of evaporative decay when $A \gtrsim 100$), this level density depends on the thermal energy available in the ground state configuration and on the density of single-particle levels. The available thermal energy is determined in part by the neutron separation energy (Fig. 10). For fission, it is the level density at the transition state which is important. Here, the thermal energy is influenced by the fission barrier height. The single-particle level density parameter a_f may be different from that for the ground state configuration, a_n , because of the different shape of the saddle point. Thus, the competition between fission and evaporation will be governed in the main by the ratio of the single particle level densities a_f/a_n and by the difference between the neutron binding energy and the fission barrier height, $S_n - E_B$.

4.2.3a Results for Light Ions

Measurements of Γ_f/Γ_n , the relative width for fission and neutron evaporation, have been made with a variety of light probes and have produced systematic values of a_f/a_n and E_B (Va 73). The observed mass dependence of these values is understood in terms of the liquid drop model and shell corrections associated with closed shells and with nuclear deformation (Va 73, Mo 74a). The fact that a_f/a_n is generally larger than unity is explained in terms of the interrelationship of deformation and the density of single particle levels at the Fermi surface (Fig. 1c). An equilibrium configuration (minimum potential energy) is produced when the

density of single-particle levels is low: a high density of levels is associated with shapes inbetween stable quadrupole deformations. Since the saddle point is a point of maximum potential energy along the path to fission, it has a higher density of levels associated with it (Va 73). There is also a macroscopic effect, based on the changing (with deformation) ratio of surface to volume, which causes a_f/a_n to exceed unity (Bi 72, Mo 74a, Be 78, Vi 80).

4.2.3b High Angular Momentum

The new dimension added by the use of heavy projectiles is the introduction of large amounts of angular momentum and the resulting production of a rapidly rotating compound nucleus. This affects the fission competition in two ways. First, the centrifugal forces favor fission by reducing the difference in the effective thresholds for neutron emission and fission. Second, the shapes of both the rotating ground state and the rotating saddle point change with increasing angular momentum. The deformation of the former increases while that of the latter decreases (Co 74). Associated with these shape changes will be variations in a_f/a_n (recall Fig. 1c). At some critical angular momentum, J_c , the shapes of the rotating ground state and of the saddle point will merge. In this limit, $a_f/a_n \rightarrow 1$ and $E_B(J_c) \rightarrow 0$. The macroscopic aspects of the shape changes as calculated with the rotating liquid drop model, RLDM (Co 74), are illustrated in Fig. 37 for the compound nucleus ^{149}Tb (P1 75). The critical angular momentum J_c is $\approx 90 \hbar$ in this case.

Not all the energy brought into a collision by a heavy ion will appear as rotational energy. Thus, rapid rotation will also be accompanied by high thermal excitation as well. This in turn may have an effect on a_f/a_n by tending to wash out the shell effects predicted for cold nuclei.

4.2.3c Fission-Barrier Heights

The analysis of heavy-ion induced fission with the statistical model relies on the use of the RLDM to predict the angular momentum dependence of the fission barrier and moments of inertia. Within the context of this very model-dependent procedure, the results of a particular analysis can be expressed in terms of $E_B(J=0)$, the fission barrier predicted by the RLDM for a nonrotating nucleus. In order to fit experimental data, the distribution of angular momentum in the initial compound nucleus must be known as well. This implies a measurement of the fusion cross section $\sigma_{fus} = \sigma_{ER} + \sigma_{fis}$ in order to obtain the maximum angular momentum contributing to fusion, $J_{max}^2 \approx \sigma_{fus}/(\pi\lambda^2)$. Given the initial angular momentum distribution (at each bombarding energy), two parameters, a_f/a_n and a normalization constant k defined by $E_B(J) = kE_B(\text{RLDM})$, are adjusted to fit a measured excitation function for σ_{fis} .

A recent example of such an analysis concerns the fission of the compound nucleus ^{153}Tb produced in the reactions $^{20}\text{Ne} + ^{133}\text{Cs}$ and $^{12}\text{C} + ^{141}\text{Pr}$ (P1 80). The fission excitation functions are shown in Fig. 38 together with statistical model fits to both sets of data for $a_f/a_n = 1.08$ and $k = 0.83$ (or $E_B(0) = 28.5$ MeV). The sensitivity of the prediction to the fission barrier height is shown in Fig. 39 where a_f/a_n and k have been adjusted in each case to reproduce the data point at the lowest excitation energy (P1 80).

The above value of $E_B(0) = 0.83 E_B(\text{RLDM})$ is in agreement with other measurements and analyses in this general mass region (Va 73, p. 236) and with the experience that deduced fission barriers lie in the range 0.8-1.3 times the liquid drop value. Recent analyses by Beckerman, Blann, et al. (Be 77b, Be 78, Bi 77) of data with heavier projectiles have yielded

significantly lower fission barriers, i.e. $k \sim 0.5-0.65$. It has been suggested (Pl 80) that these low barriers arise from the experimental difficulty of excluding the products of strongly damped collisions from fusion-fission for heavier projectiles. However, part of this apparent discrepancy may arise from the manner in which the RLDM fission barriers are adjusted to fit the experimental data: the particular choice of an angular-momentum-independent scaling factor, k , is not unique (Be 78a), and k might be expected to have a mass dependence (Kr 74).

Delagrangé et al. (De 77) have analyzed fusion-fission excitation functions for $^{12}\text{C} + ^{182}\text{W}$, ^{175}Lu , ^{174}Yb and find values of $k \sim 1.0$ and values of a_f/a_n ranging from 1.1 to 1.2. This article gives an extensive discussion of the sensitivity of various predicted quantities to variations in the input parameters. The fusion-fission of $^{16}\text{O} + ^{181}\text{Ta}$ and $^{16}\text{O} + ^{208}\text{Pb}$ has been studied by Videbaek et al. (Vi 77). The respective compound nuclei ^{197}Tl and ^{224}Th are quite different in that $E_B(0)$ (the s-wave barrier for fission) is well above the particle evaporation threshold in the former case and comparable to it in the latter case. Thus, the excitation function for fission of ^{197}Tl is much more sensitive to angular momentum effects on the fission barrier. Analyses of these data yield fission barriers which agree with the RLDM (13.8 MeV for $a_f/a_n = 0.97$) but which disagree with analyses of Γ_n/Γ_f obtained from other measurements (19-23 MeV for $a_f/a_n = 1.10-1.35$) and with microscopic theoretical predictions (Mo 71). The origins of this discrepancy are not known.

The above analyses have all assumed that a_f/a_n is independent of angular momentum. Beckerman (Be 78a) has pointed out that this is not consistent with the fact that the shape of the nucleus is changing with

angular momentum. Indeed we expect a_f and a_n both to vary with (J) but in such a way that $a_f(J)/a_n(J) \rightarrow 1.0$ as $J \rightarrow J_c(E_B = 0)$. The spin independent parameters deduced from an excitation function thus represent effective values averaged over a range of angular momenta. Furthermore, measurements done with lighter ions (i.e. at low angular momenta) and at lower energies will be more sensitive to the differences in shape and level density between the ground and saddle point configurations of a nucleus (Mo 74a). On the other hand, heavy ions and a range of bombarding energies are required if one is to study the angular momentum dependence of E_B .

The above examples show that the statistical model can reproduce the main features of heavy-ion fusion-fission reactions. The level density parameters and fission barrier heights which are deduced through these analyses conform to our general expectations based on independent experimental information and theoretical understanding. However, there can be sizeable errors on some of the deduced quantities; ambiguities (especially when insufficient experimental data are available to constrain the statistical model calculation) are present in the analysis and results occasionally are in conflict. The subject of fission barrier heights is hardly a closed book.

4.2.3d A Search for Shell Effects in Hot, High Spin Nuclei

One of the basic questions which one might hope to answer through a statistical model analysis is whether shell effects (in general) persist at the excitation energies and angular momenta which accompany heavy-ion fusion. This is a difficult question which requires a degree of experimental information and analytical sophistication generally not found in previous studies. Recently, Vigdor, Karwowski, et al. have reported an extensive series of measurements of ${}^6\text{Li}$ -induced fusion and a detailed

statistical analysis specifically designed to address this question (Vi 80). Their experimental data include measurements at three bombarding energies on each of five targets ranging from ^{181}Ta to ^{208}Pb . The cross sections for fission, α -particle and proton emission, x-n evaporation, angular distribution for fission fragments and representative energy spectra for protons and alpha particles were measured. Figure 40 shows the distribution of the yields following compound nucleus formation for the five different targets at each of two bombarding energies. Note how the fission cross section increases with increasing fissility of the compound nucleus. Another indication of the distribution of the total flux in the total reaction cross section, σ_R , is given in Fig. 41. Over half of σ_R is in quasielastic or direct reactions. The distribution over impact parameter given in Fig. 41 is that predicted by the statistical model.

An example of the dependence of the fission fragment angular distribution on the angular momentum of the compound nucleus is shown in Fig. 42. As the angular momentum increases, so does the anisotropy. The formula shown in the figure is empirical and used only for fitting the angular distribution to obtain a cross section and an anisotropy defined as $\gamma_{\text{fiss}} = W(170^\circ)/W(90^\circ)$.

The modifications made by Vigdor et al. to the usual statistical model calculation included the addition of collective rotational levels in the saddle-point level density (eqs. 2.7 and 2.8) with moments of inertia taken from the RLDM (Hagelund and Jensen have also included these effects, Ha 77a). They also included the expression eq. (3.19) for the angular distribution of the fission fragments in a summation over compound nucleus angular momentum and over all fissioning nuclei (i.e. over multiple chance

fission). All moments of inertia in all aspects of the calculation (including the Yrast level density) were treated in a consistent way using the RLDM.

Perhaps the most significant departure from previous analyses has been the philosophy to predict the experimental observables without parameter variation by using a completely macroscopic calculation. That is, all shell effects were consistently eliminated from the calculation. All ground-state masses (except those of the projectile and target which are cold nuclei) were taken from liquid drop model calculations. This is because variations in experimental masses themselves represent shell effects. Pairing was omitted in the Fermi-gas level-density formula, and a_f/a_n was taken to have the value 1.0 plus a correction based on the predicted dependence of "a" on the ratio of surface to volume.

The result of a comparison of this calculation, with all parameters fixed a priori, to all the experimental data was a remarkably good agreement. A portion of this comparison is shown in Fig. 43. Vigdor et al. concluded there was no evidence for the persistence of shell effects. That is, the rotating liquid drop model and the noninteracting Fermi gas are an adequate description of the collective and single-particle aspects of nuclear structure at the excitation energies and angular momenta encountered in their experiments. To observe shell effects, nuclei must be relatively cold.

The above discussion has emphasized the competition between fission and light-particle evaporation in the medium to heavy mass region. Studies of yields, evaporation spectra, angular distributions of protons and α particles have also been made and can provide significant information on

the angular momentum distribution of the compound nucleus. Excellent examples of this are found in the series of papers by Galin et al. (Ga 74, Ga 74a) and in the work of Reedy et al. (Re 69) and Logan et al. (Lo 80a).

4.2.3e Open Questions

There are still a number of fundamental open questions concerning the use of the statistical model. These pertain in the main to the choice of transmission coefficients. Often transmission coefficients are taken from optical model calculations which describe elastic scattering and, therefore, the total reaction cross section. Emphasizing the fact that the transmission coefficient is related to the inverse cross section, i.e., is related to fusion, McMahan and Alexander (Ma 80) have analyzed fusion excitation functions for protons and α particles in order to determine the appropriate transmission coefficients. It is argued that this represents a closer approximation to the true inverse cross section, even though the target nucleus is in its ground state rather than in an excited (and probably deformed) state corresponding to the residual nucleus after particle emission. Others (Vi 80) have suggested that the optical model values should be used because an excited target nucleus would have a higher fusion cross section because of the weakening or absence of the Pauli exclusion principle.

A comparison of measured α -particle evaporation spectra and statistical calculations employing both methods of determining transmission coefficients is shown in Fig. 44. Neither the calculations based on fusion transmission coefficients (labeled HW) nor the optical model calculations reproduces the large number of subbarrier α particles and protons.

A possible explanation for the above discrepancy concerns nuclear deformation. Moretto points out that the emission of an α particle (or nucleon) can cause a shape polarization of the two fragments such that the distance between the centroids of the two charge distributions exceeds that of two touching spheres. As mentioned in section 3.4, this effect is in direct analogy to fission, where the final kinetic energy is well below the Coulomb energy of touching spheres and is treated naturally in the transition state method (Mo 75).

Another possible origin of a lowered Coulomb barrier arises from a shape polarization or deformation caused by rapid rotation of a nucleus. Beckerman and Blann (Be 79, Bl 80) have pointed out (Be 79) the consequences of emission of a charged particle from the tip of a prolate nucleus and have made detailed calculations (Bl 80) of the consequences of the associated enhancement of α -particle emission on the competition for fission. This is illustrated in Fig. 45 for a nucleus of mass ~ 150 with various amounts of angular momenta. The effects are enormous, but only once rather high angular momenta are reached. The α particles emitted from such a rapidly rotating nucleus would not contribute to the subbarrier α particle yield shown in Fig. 44 but rather would have substantial kinetic energies associated with the angular momentum they would remove. Blann points out a number of experimental features which are consistent with this enhanced α -particle emission but suggests that additional experiments should be performed to verify it. It is known that deformation influences the barrier for fusion (St 78, St 81) and therefore it must have consequences for evaporation as well. The question is whether the consequences are as drastic as indicated by the calculations

shown in Fig. 45 (B1 80). It seems that the incorporation of light particle emission into a transition theory in which all barriers are angular momentum dependent and calculated within the context of a rotating liquid drop model would be a worthwhile goal.

4.3 Noncompound Reactions

4.3.1 Introduction

The use of the statistical model is not confined to fusion or compound nucleus reactions. Indeed, the model can be applied to the decay of all equilibrated nuclei, independently of how they were formed. One need only know the initial distribution of nuclei (Z,N) and their distribution of excitation energy and angular momenta. Thus, increasing use has been made of statistical model calculations applied to the individual fragments produced in direct reactions, with deep inelastic scattering comprising the main example.

There are several reasons for making use of the statistical model in the analysis of noncompound reactions. The first is that it provides a means of estimating the effects of postcollision light-particle emission on the properties of the secondary fragments observed by detectors. Thus the distribution of charge, mass, and excitation energy in the primary collision can be deduced from the measured properties of the secondary fragments (Bl 79, Go 79b). Another type of application uses the light particles evaporated by the excited primary fragment to deduce the excitation energy, angular momentum, or alignment of the fragment. Finally, the statistical model is used to attack the question whether the high energy light particles observed in coincidence with various fragments are consistent with postcollision evaporation or whether nonequilibrium processes must be invoked in order to explain their presence.

In the following subsections we will consider examples of these different applications.

4.3.2 Primary and Secondary Distributions

Two examples will suffice to illustrate the role of evaporation on the energy distribution of secondary products. In the case of a heavy system, $^{84}\text{Kr} + ^{124}\text{Sn}$, it was estimated that the secondary Q-value distribution was broadened by about 10% over the primary distribution when the bombarding energy was 440 MeV and by about 30% at the higher bombarding energy, 720 MeV (Bl 79). In contrast, the energy distribution of C ions observed in the deep inelastic scattering of 168 MeV ^{20}Ne by ^{63}Cu was shown to be broadened by a factor of two over the primary distribution. This and the effect of particle evaporation on the observed charge distributions are illustrated in Figs. 46 and 47 (Go 79b).

4.3.3 Measurements of Spin and Alignment

Since the angular correlations of light particles, fission fragments, and gamma rays depend on the direction and magnitude of the angular momentum of the emitting nucleus, measurements of the former can be used to deduce the latter. The experience and understanding which have been gained in the study of compound nuclear reactions can be brought to bear on the excited fragments produced in deep inelastic collisions.

The magnitude of the angular momentum transferred in the deep inelastic scattering of very heavy ions has been measured by observing the out-of-plane angular correlation of fragments from the fission decay of the target-like nucleus (Dy 77, Wo 78, Dy 79, Ha 79, Pu 79, Ra 79). The anisotropy of the angular correlation increases with the angular momentum of the fissioning nucleus and thus becomes a measure of the transferred angular momentum. The angular correlation of fission fragments in the reaction plane should be isotropic if the angular momentum transferred is

completely aligned perpendicular to the reaction plane. Thus, a measure of the alignment can also be obtained. Figure 48 from Dyer et al. presents results from the application of this method to the reaction $\text{Kr} + \text{Bi}$.

The measurement of γ -ray angular distributions has also been used to make inferences about the alignment of the angular momentum transferred in deep inelastic collisions (Da 79, Da 80a, Pu 79a, Pu 80, Wo 80a, La 81). In lighter nuclei complications may arise because of the effects of preceding particle emission and mixed multipolarity (quadrupole/dipole) in the γ decay [see eqs. (3.5) and (3.6)] Careful statistical-model calculations can be used to estimate the former effects, however, and detailed correlations can place limits on the quadrupole/dipole mixing ratio such that useful information may be extracted from the continuum γ -ray angular correlations. With heavier nuclei, these corrections are less of a problem (Pu 80, Wo 80a, La 81).

Catchen et al. (Ca 80) have presented a semiempirical method for estimating fragment spins which is based on proton and α -particle emission (Re 69, Ga 74, Ga 74a, Lo 80a). Both the out-of-plane correlations and the ratio of hydrogen to helium emission can be used independently to deduce a fragment spin. An assumption made in this procedure is that the emitting fragment is aligned perpendicular to the reaction plane. Babinet et al. (Ba 80b) have used these methods in a study of the deep inelastic scattering of ^{40}Ar by ^{58}Ni . They find that the energy spectra of the α particles from each fragment[†] and the out-of-plane anisotropies are

[†]The kinematics of the reaction enables an identification of the origin of the emitted particle.

consistent with the deformed dinuclear complex attaining thermal equilibrium and reaching a sticking configuration before separating.

The question of the alignment of the fragments produced in deep inelastic collisions is of wide interest. The effect of an incomplete alignment, or random angular momentum, on an out-of-plane angular correlation is illustrated in Fig. 49 for the reaction $^{20}\text{Ne} + ^{63}\text{Cu}$ (Go 79b). It was found that γ -ray multiplicity measurements (Da 79, Da 80a) and α , p-heavy ion coincidence results could only be reconciled by having a component of randomly oriented angular momentum which was comparable to the aligned component (Go 79b, Da 81).

An experimental demonstration of the sensitivity of the out-of-plane angular distributions to the angular momentum of the emitting fragment is given in Fig. 50 (So 81). In this study of the $^{84}\text{Kr} + \text{Ag}$ reaction, the γ -multiplicity was recorded simultaneously with α -particle, heavy ion coincidences. The left and right sides of Fig. 50 show the correlations observed without and with a γ -multiplicity requirement. Note that the anisotropies increase as events involving larger angular momenta (higher γ multiplicities) and heavier masses are selected. The analysis of the α -particle angular correlations shown here was done with the transition state formalism of Moretto (Mo 75). By deducing the spin of one fragment (γ multiplicity gives the algebraic sum of the spins of both fragments) and its dependence on fragment mass, rigid rotation of the Kr + Ag dinuclear complex could be demonstrated.

Moretto et al. have derived analytical formulae for the calculation of angular momentum misalignment (Mo 80) in deep inelastic reactions and

the resulting angular correlations of emitted particles and γ rays (Mo 80a, Bl 81). The simplicity of the expressions obtained stems from the use of semiclassical models and the assumption of Gaussian distributions for angular momentum components. This offers a certain advantage over the use of Monte Carlo calculations to accomplish the same task. While the latter involve fewer approximations and therefore are more precise, the semiclassical expressions (Ca 80, Mo 80a, Bl 81) give a complementary insight into the physical processes and, of course, are less expensive to evaluate. In general, the heavier the emitting nucleus, the more appropriate the use of semiclassical theories. For light systems such as Ne + Cu (Go 79b) a Monte Carlo treatment of the Hauser-Feshbach formula is useful and provides a check on the appropriateness of the semiclassical methods.

4.3.4 Energy Equilibration and the Emission of Fast Particles

4.3.4a Nucleon emission

The deep inelastic collisions of very heavy ions produce fragments which, having survived fission, decay mainly by neutron emission. The observation of these neutrons in coincidence with a heavy fragment constitutes a method for determining the distribution of excitation energy among the fragments and, possibly, for probing the early stages of the collision.

Measurements of neutrons emitted in deep inelastic collisions have been made for $^{86}\text{Kr} + ^{166}\text{Er}$ (Ey 80), $^{56}\text{Fe} + ^{165}\text{Ho}$ (Hi 79a), Cu + Au (Ta 79) and Xe + Au (Go 80b). Statistical analyses of the energy spectra and multiplicity of neutrons observed in these reactions were consistent with a sharing of excitation energy according to the respective masses of the fragments and to evaporation from fully accelerated fragments. In particular, no evidence was found for nonequilibrium emission of neutrons.

The situation is different if lighter projectiles are used. Evidence has been obtained for the emission of fast, nonequilibrium neutrons in the fusion of $12.7 \text{ MeV/A } ^{12}\text{C} + ^{158}\text{Gd}$ but not from $8.8 \text{ MeV/A } ^{20}\text{Ne} + ^{150}\text{Nd}$ (We 78). Only very recently have measurements been done which indicate similar effects in deep inelastic reactions. These experiments used $12.7 \text{ MeV/A } ^{16}\text{O}$ on a ^{93}Nb target (Ga 81) and $6 \text{ MeV/A } ^{16}\text{O} + ^{58}\text{Ni}$ (Ge 80). As an example of the type of experimental data and analysis which suggest nonequilibrium emission, Figs. 51 and 52 show the results of Gavron et al. (Ga 81). The neutron energy spectra obtained at angles indicated in the inset and in coincidence with projectile-like deep inelastic fragments with $Z = 6, 7, 8$ are shown as letters corresponding to each neutron detector. The solid curves, each similarly labeled with a letter, are the results of Monte Carlo statistical model calculations which assume emission from fully accelerated fragments with excitation energies shared according to their masses. Note the underestimate of the yields in counters C and D at forward angles and in A and B on the side of the beam opposite the heavy-ion detector. On the other hand, the neutrons observed at a large angle (F) are accounted for by this calculation. The calculations in Fig. 52 include, in addition to the neutrons from the fully accelerated fragments, the existence of an additional source of neutrons, postulated to have a temperature of 1.5 MeV and to be moving along the beam axis with a velocity equal to the average of the projectile-like fragments. It is the direction of this source along the beam which now accounts for the fast neutrons in the detectors on the side of the beam opposite the heavy-ion telescope. The normalization is such that the equilibrated sources and the new source produce equal numbers of neutrons.

The reaction $^{63}\text{Cu}(^{20}\text{Ne}, \text{H.I.}, p)$ has been studied by Schmitt et al. (Sc 81) at the same energy/nucleon (12.7 MeV/A) as the above reaction of $^{16}\text{O} + ^{93}\text{Nb}$. Their results are shown in Fig. 53. The dashed line is a semiclassical, transition-state calculation (Mo 75, Bl 81) which assumes fragments each having a single excitation energy equal to its respective share of the average energy loss. The solid lines, however, assume a spread in excitation energies which are assumed to arise from thermal fluctuations in the division of the excitation energy. The agreement with experiment is quite good in this case. Since thermal fluctuations are an expected part of an equilibrated system, the conclusion is that these data do not require the presence of nonequilibrated source of nucleons. It seems indeed remarkable that the emission of single nucleon (protons or neutrons) in reactions induced by similar projectiles (^{16}O , ^{20}Ne) at the same velocity (12.7 MeV/A) should require a nonequilibrium source in one case and not in the other (Gavron et al. say that the results for $^{16}\text{O} + ^{93}\text{Nb}$ can not be fit by varying the temperature of the P.L.F.) It would be valuable to check the equivalence of the two methods of analysis.

4.3.4b Alpha-Particle Emission

The emission of α particles in coincidence with heavy, residue-like fragments and with projectile-like fragments has been studied by Gonthier et al. and by Ho et al. in the reaction of 20 MeV/A ^{16}O with Ti (Go 80, Ho 80). In each of these cases they observe a strong component of α -particle emission which they cannot account for on the basis of evaporation from an equilibrated compound nucleus or from fully accelerated fragments. Monte Carlo Hauser-Feshbach calculations were the basis for comparison of experiment and statistical theory.

The coincidences with heavy residues ($Z > 16$) revealed an excess of high-energy α particles which was present at angles less than 40° and absent at larger angles (Fig. 54). The multiplicities of this nonequilibrium component were large, being 0.4 ± 0.1 for α particles in coincidence with heavy recoil particles at 20° and 1.1 ± 0.2 for recoils detected at 40° .

Experiments in which fast α particles have been detected in coincidence with heavy residues using a different experimental technique have shown a similar phenomenon (In 77, Zo 78, Si 79). In these cases the experimental technique (observation of discrete γ rays in coincidence with the α particles) allows one to establish that a portion of the projectile did indeed transfer to and fuse with the target. (Hence, the equivalent names "massive transfer" and "incomplete fusion" for these processes.) There seems little doubt that these experiments of Gonthier, Inamura, Zolnowski and K. Siwek-Wilczynska et al. are dealing with the same phenomenon, the emission of energetic α particles at an early stage of the collision.

Turning again to the coincidence of light particles with projectile-like fragments, Fig. 55 shows measured α - ^{12}C coincidences for the reaction $^{16}\text{O} + \text{Ti}$ at 310 MeV (Ho 80). Here, a phenomenon occurs similar to that observed for the neutrons from 204 MeV $^{16}\text{O} + ^{93}\text{Nb}$ (Ga 81), viz, there is an excess (relative to an equilibrium calculation) of measured α particles on the side of the beam opposite the heavy-ion detector. Presumably this excess could be accounted for in large part by an additional source of α particles moving along the beam direction. A similar analysis of the $^{20}\text{Ne} + ^{63}\text{Cu}$ reaction at 8.4 MeV/A

(Go 79b) has also indicated an excess of high energy, forward-peaked α particles in coincidence with projectile-like fragments.

The α particles in coincidence with projectile-like fragments in the reaction 204 MeV $^{16}\text{O} + ^{93}\text{Nb}$, on the other hand, have been accounted for (Yo 80) on the basis of an equilibrium Monte Carlo calculation identical to that used in the analysis of the neutrons emitted in the same reaction (Go 81), and no evidence is found for a nonequilibrium component. Young et al. also analyzed the reaction 96MeV $^{16}\text{O} + ^{58}\text{Ni}$ measured by Ho et al. (Ho 77). The latter authors had concluded there was evidence in their experimental results for $^{12}\text{C} + \alpha$ coincidences for formation and decay of a "hot spot". The Monte Carlo calculations of Young et al., which include all kinematic effects associated with the emission of α particles from moving fragments, showed that the high energy α particles could be explained by evaporation from fully accelerated, equilibrated fragments. This example illustrates the value of first predicting the features expected on the basis of equilibrium before invoking nonequilibrium processes.

Light charged-particle emission from reactions induced by ^{40}Ar ions bombarding a variety of targets Sn-Au has been studied systematically by Delagrange et al. and Logan et al. (De 79, Lo 80, Lo80a) at energies up to 8.5 MeV/A. Their results can be summarized as follows. Alpha particles and protons observed at backward angles in coincidence with evaporation residue or deep inelastic fragments have evaporation spectra with a low temperature characteristic of the usual equilibrium processes. At forward angles there is a high temperature component which cannot be accounted for by equilibrium models. This component is present in coincidence with

fission fragments as well. The characteristics of these spectra, including the ratio of proton to α -particle emission indicate that the fast particles precede fission and precede the decay of the rotating dinuclear system (in the case of deep inelastic scattering).

4.3.4c Summary of Results

The current picture with regard to the nonequilibrium emission of light particles in heavy ion reactions is thus, at best, complicated. There seems to be quite clear evidence for the process of incomplete fusion. Yet the analysis of deep inelastic reactions (i.e., light particles in coincidence with projectile-like fragments) suggests, if all cases are taken at face value, that the presence or absence of nonequilibrium emission depends on the bombarding energy, the projectile type, and the type of particle emitted in a manner which currently seems to defy a simple, systematic explanation. The current situation is summarized (very crudely) in Table 3. The possibility that protons, neutrons, and α particles might be emitted at different stages and times of a heavy ion collision, and therefore may carry different information about the path toward equilibrium, is reflected in the results shown in Table 3. Before definitive conclusions about systematic behavior (or the lack thereof) can be drawn, however, further work and effort must be devoted to refining and standardizing the methods used to determine what constitutes equilibrium behavior. In the next years, we may hope to see a consistent and adequate picture of nonequilibrium phenomena emerge.

4.4 Summary

The purpose of section 4 has been to illustrate the various ways in which the statistical model is used in the analysis of heavy-ion reactions. These ways may be summarized as follows:

- (i) The verification of the reaction mechanism.

The statistical model provides a quantitative description of the products of compound nucleus formation and decay, and of the decay of any equilibrated nucleus. All the (average) characteristics of these products--mass, charge, kinetic energy, momentum, excitation energy, and angular momentum--can be predicted. By comparison of these predictions to the experimental data, one can identify which products of the reaction were produced as a result of equilibrium decay and which products were not. Given the propensity of complex nuclei to reach equilibrium sooner or later, this application of the statistical model--the identification of nonequilibrium processes--is of crucial importance in the study of heavy-ion reactions.

- (ii) Deduction of the primary distribution.

The primary distribution refers to the properties of the primary fragments which have emerged in an excited state from the collision region but which have not yet undergone deexcitation. The experimental apparatus invariably observes secondary products whose mass, charge and kinetic energy have been altered by the deexcitation process. By modeling the decay process, the statistical model can be used to "work backward" from the measured properties of the secondary fragments to deduce those of the primary products. (This is often done in relativistic heavy ion reactions.)

(iii) Quantitative analysis of high spin phenomena

Because high angular momentum is one of the distinguishing features of heavy-ion reactions, the use of the statistical model becomes of paramount importance to analyze and understand a wealth of high spin phenomena. The deduction of spins of selectively populated high-spin states and the measurement of spin distributions in compound nuclei and of the angular momentum (magnitude and direction) of heavy fragments in binary collisions fall in this category. One may refer to much of this activity as "probing the Yrast region", first through analysis of light particle decay and then through the properties of the γ -ray continuum. Changes of the fission barrier and the shape of the nucleus with angular momentum are studied by incorporating the rotating liquid drop model into the statistical model.

(iv) Shell effects

The statistical model enables us to address the question of shell effects--nuclear structure not described by a noninteracting Fermi gas--in nuclei at high excitation and angular momentum. By including (or leaving out) in a calculation the shell effects known from the study of level densities at low excitation, one is able to assess the durability of shell effects as the temperature and shape of the nuclear environment are varied.

(v) Prediction

This is an important aspect of the statistical model which because of its very nature has not been illustrated. Heavy-ion reactions are one means by which exotic nuclei, far from stability, are produced. The statistical model enables an experimenter to estimate in advance what the yield of a given isotope will be and, therefore, to optimize the conditions

for its production. The major applications of the statistical model in the analysis of heavy-ion reactions fall into the above general categories. We expect that new applications will be found in the future as the variety of phenomena produced in heavy-ion reactions continues to expand.

ACKNOWLEDGEMENTS

Stimulating discussions with M. Beckerman, M. Blann, J. Gomez del Campo, L.G. Moretto, W. Swiatecki and S.E. Vigdor are gratefully acknowledged. This work was supported by the Director, Office of Energy Research, Division of Nuclear Physics of the Office of High Energy and Nuclear Physics and by Nuclear Sciences of the Basic Energy Sciences Program of the U.S. Department of Energy under Contract W-7405-ENG-48.

REFERENCES

- Al 64 E. Almqvist, J.A. Kuehner, D. McPherson, and E.W. Vogt, Phys. Rev. 136:B84 (1964).
- Ay 74 S. Ayik and J.N. Ginocchio, Nucl. Phys. A 234:13 (1974).
- Ba 78 B.B. Back and S. Bjørnholm, Nucl. Phys. A 302:343 (1978).
- Ba 80 M. Baldo, R.A. Broglia, and A. Winther, Phys. Lett. 94B:473 (1980).
- Ba 80a J. Barrette, O. Hansen, M.J. Levine, C.J. Lister, H.E. Wegner, and P. Braun-Munzinger, Proc. Int. Conf. on Nuclear Physics, Berkeley, California (1980), Vol. 1, p. 521.
- Ba 80b R. Babinet, B. Gauvin, J. Girard, J.M. Alexander, T.H. Chiang, J. Galin, B. Gatty, D. Guerreau, and X. Tarrago, Z. Physik A 295:153 (1980).
- Be 36 H.A. Bethe, Phys. Rev. 50:332 (1936).
- Be 73 A.N. Behkami and J.R. Huizenga, Nucl. Phys. A 217:78 (1973).
- Be 73a T.A. Belote, N. Anyas-Weiss, J.A. Becker, J.C. Cornell, P.S. Fischer, P.N. Hudson, A. Menchaca-Rocha, A.D. Panigiotou, and D.K. Scott, Phys. Rev. Lett. 30:450 (1973).
- Be 77 M. Beckerman, Nucl. Phys. A 278:333 (1977).
- Be 77a M. Beckerman, Phys. Lett. 69B:389 (1977).
- Be 77b M. Beckerman and M. Blann, Phys. Rev. Lett. 38:272 (1977);
Phys. Lett. 68B:31 (1977).
- Be 78 M. Beckerman and M. Blann, Phys. Rev. C 17:1615 (1978).
- Be 78a M. Beckerman, Phys. Lett. 78B:17 (1978).
- Be 79 M. Beckerman and M. Blann, Phys. Rev. Lett. 42:156 (1979).
- Be 80 G. Bertsch, Phys. Lett. 95B:157 (1980).
- Bi 72 C.J. Bishop, I. Halpern, R.W. Shaw, Jr., and R. Vandenbosch, Nucl. Phys. A 198:161 (1972).

- Bi 76 E.G. Bilpuch, A.M. Lane, G.E. Mitchell, and J.D. Moses, Phys. Reports 28:145 (1976).
- Bi 77 J. Bisplinghof, A. Mignerey, M. Blann, P. David, and W. Scobel, Phys. Rev. C 16:1058 (1977).
- B1 52 J.M. Blatt and V.F. Weisskopf, Theoretical Nuclear Physics, Wiley, New York (1952).
- B1 66 M. Blann, Nucl. Phys. 80:223 (1966).
- B1 72 M. Blann and F. Plasil, Phys. Rev. Lett. 29:303 (1972).
- B1 79 M. Blann, R.H. Stokes, B. Erkkila, H.C. Britt, P.D. Goldstone, R.L. Ferguson, F. Plasil, and H.H. Gutbrod, Phys. Rev. C 19:1288 (1979).
- B1 80 M. Blann, Phys. Rev. C 21:1770 (1980).
- B1 81 S.K. Blau and L.G. Moretto, Lawrence Berkeley Laboratory report LBL-10926 (1980).
- Bo 39 N. Bohr and J.A. Wheeler, Phys. Rev. 56:426 (1939).
- Bo 56 A. Bohr, in Proceedings U.N. Int. Conf. Peaceful Uses of Atomic Energy 2:151 (1956).
- Bo 63 J.P. Bondorf, Advanced Course on Nuclear Physics, Kjeller, Norway (1963) unpublished.
- Bo 69 A. Bohr and B. Mottelson, Nuclear Structure, Volume I, Benjamin, New York (1969).
- Bo 70 M. Böhning, in Nuclear Reactions Induced by Heavy Ions (R. Bock, ed.), North-Holland, Amsterdam (1970), p. 633.
- Bo 72 M. Bolsterli, E.O. Fiset, J.R. Nix, and J.L. Norton, Phys. Rev. C 5:1050 (1972).
- Bo 73 J.P. Bondorf, Nucl. Phys. A 202:30 (1973).

- Bo 75 A. Bohr and B. Mottelson, Nuclear Structure, Volume II, Benjamin, New York (1975).
- Bo 78 P. Bonche, B. Grammatikos, and S. Koonin, Phys. Rev. C 17:1700 (1978).
- Br 78 D. Branford and S.G. Steadman, Phys. Rev. C 18:2560 (1978).
- Ca 79 M.J. Canty, P.A. Gottschalk and F. Pühlhofer, Nucl. Phys. A 317:495 (1979).
- Ca 80 G.L. Catchen, M. Kaplan, J.M. Alexander, and M.F. Rivet, Phys. Rev. C 21:840 (1980).
- Ch 71 F.S. Chang, J.B. French, and T.H. Thio, Ann. Phys. 66:137 (1971).
- Co 60 B.L. Cohen, Phys. Rev. 120:925 (1960).
- Co 74 S. Cohen, F. Plasil, and W.J. Swiatecki, Ann. Phys. 82:557 (1974).
- Co 75 E.R. Cosman, T.M. Cormier, K. Van Bibber, A. Sperduto, G. Young, J. Erskine, L.R. Greenwood, and O. Hansen, Phys. Rev. Lett. 35:265 (1975).
- Co 77 T.M. Cormier, E.R. Cosman, A.J. Lazzarini, H.E. Wegner, J.D. Garrett, and F. Pühlhofer, Phys. Rev. C 15:654 (1977).
- Co 80 A.J. Cole, N. Longequeue, J. Menet, J.J. Lucas, R. Ost, and J.B. Viano, Nucl. Phys. A 341:284 (1980).
- Cu 76 B. Cujec and C.A. Barnes, Nucl. Phys. A 266:461 (1976).
- Da 76 R.A. Dayras, R.G. Stokstad, Z.E. Switkowski, and R.M. Wieland, Nucl. Phys. A 265:153 (1976).
- Da 79 R.A. Dayras, R.G. Stokstad, C.B. Fulmer, D.C. Hensley, M.L. Halbert, R.L. Robinson, A.H. Snell, D.G. Sarantites, L. Westerberg, and J.H. Barker, Phys. Rev. Lett. 42:697 (1979).

- Da 80 B. Dalton, S. Grimes, J. Vary, and S. Williams, eds., Theory and Applications of Moment Methods in Many Fermion Systems, Plenum Press, New York (1980).
- Da 80a R.A. Dayras, R.G. Stokstad, D.C. Hensley, M.L. Halbert, D.G. Sarantites, L. Westerberg, J.H. Barker, Phys. Rev. C 22:1485 (1980).
- Da 81 R.A. Dayras, K.A. Geoffrey, D.G. Sarantites, J.H. Barker, D. Shapira, D.C. Hensley, R.G. Stokstad, and M.L. Halbert, to be published.
- De 77 H. Delagrangé, A. Fleury, and J.M. Alexander, Phys. Rev. C 16:706 (1977).
- De 79 H. Delagrangé, D. Logan, M.F. Rivet, M. Rajagopalan, J.M. Alexander, M.S. Zisman, M. Kaplan, and J.W. Ball, Phys. Rev. Lett. 43:1490 (1979).
- Di 73 W. Dilg, W. Schantl, H. Vonach, and M. Uhl, Nucl. Phys. A 217:269 (1973).
- Do 59 I. Dostrovsky, Z. Fraenkel, and G. Friedlander, Phys. Rev. 116:683 (1959).
- Dø 74 T. Døssing and A.J. Jensen, Nucl. Phys. A 222:493 (1974).
- Du 80 K. Dumont, A. D'Onofrio, M.G. Saint-Laurent, F. Terrasi, B. Delaunay, J. Delaunay, and D. Rizzo, in Proc. Int. Winter Meeting on Nucl. Phys., Bormio, Italy (January 1980).
- Dy 77 P. Dyer, R.J. Puigh, R. Vandenbosch, T.D. Thomas, and M.S. Zisman, Phys. Rev. Lett. 39:392 (1977).
- Dy 79 P. Dyer, R.J. Puigh, R. Vandenbosch, T.D. Thomas, M.S. Zisman, and L. Nunnolley, Nucl. Phys. A 322:205 (1979)

- Ei 77 Y. Eisen, I. Tserruya, Y. Eyal, Z. Fraenkel, and M. Hillman, Nucl. Phys. A 291:459 (1977).
- Er 58 T. Ericson, Nucl. Phys. 6:62 (1958).
- Er 58a T. Ericson and V. Strutinski, Nucl. Phys. 8:284 (1958);
Nucl. Phys. 9:689 (1958-59).
- Er 60 T. Ericson, Adv. in Phys. 9:425 (1960).
- Ey 80 Y. Eyal, A. Gavron, I. Tserruya, Z. Fraenkel, Y. Eisen, S. Wald, R. Bass, C.R. Gould, G. Kreyling, R. Renfordt, K. Stelzer, R. Zitzmann, A. Gobbi, U. Lynen, H. Stelzer, I. Rode, and R. Bock, Phys. Rev. C 21:1377 (1980); Phys. Rev. Lett. 41:625 (1978).
- Fa 68 U. Facchini, M.G. Marcazzan, L. Milazzo-colli, and E. Saetta-Menichella, Phys. Lett. 26B:278 (1968).
- Fa 68a U. Facchini and E. Saetta-Menichella, Energia Nucleare 15:54 (1968).
- Fe 60 H. Feshbach, in Nuclear Spectroscopy, Part B, Academic Press, New York (1960), p. 625.
- Fe 69 W. Feldman and D.W. Heikkinen, Nucl. Phys. A 133:177 (1969).
- Fe 78 B. Fernandez, C. Gaarde, J.S. Larsen, S. Pontoppidan, and F. Videbaeck, Nucl. Phys. A 306:259 (1978).
- Fo 74 J.L.C. Ford, J. Gomez del Campo, R.L. Robinson, and P.H. Stelson, Z. Phys. 269:147 (1974).
- Ga 68 E. Gadioli and L. Zetta, Phys. Rev. 167:1016 (1968).
- Ga 72 J.B. Garg, ed., Statistical Properties of Nuclei, Plenum, New York (1972); Proceedings of the International Conference on Statistical Properties of Nuclei at Albany, NY (August 1971).

- Ga 74 J. Galin, B. Gatty, D. Guerreau, C. Rousset, U.C. Schlotthauer-Voos and X. Tarrago, Phys. Rev. C 9:1113 (1974), 9:1126 (1974).
- Ga 74a J. Galin, B. Gatty, D. Guerreau, U.C. Schlotthauer-Voos and X. Tarrago, Phys. Rev. C 10:638 (1974).
- Ga 79 A. Gamp, H.L. Harvey, J.C. Roynette, E. Plagnol, H. Fuchs, H. Doubre, J.C. Jacmart, and N. Poffe, Z. Phys. A 291:347 (1979).
- Ga 80 A. Gavron, Phys. Rev. C 21:230 (1980).
- Ga 81 A. Gavron, R.L. Ferguson, F.E. Obenshain, F. Plasil, G.R. Young, G.A. Pettit, K. Geoffrey-Young, D.G. Sarantites, and C.F. Maguire, Phys. Rev. Lett. 46:8 (1981).
- Ge 78 K.A. Geoffrey, J.B. Natowitz, R.C. Eggers, and M.N. Namboodiri, Nucl. Phys. A 302:310 (1978).
- Ge 80 H. Gemmeke, P. Netter, Ax. Richter, L. Lassen, S. Lewandowski, W. Lücking, and R. Schreck, Phys. Lett. 97B:213 (1980).
- Gi 65 A. Gilbert and A.G.W. Cameron, Can. J. Phys. 43:1446 (1965).
- Gi 65a A. Gilbert, F.S. Chen, and A.G.W. Cameron, Can. J. Phys. 43:1248 (1965).
- Gi 70 J. Gilat, Phys. Rev. C 1:1432 (1970).
- Gi 73 J.N. Ginocchio, Phys. Rev. Lett. 31:1260 (1973).
- Gi 73a J. Gilat, E.R. Jones, and J.M. Alexander, Phys. Rev. C 7:1973 (1973).
- Gi 75 J.N. Ginocchio and M.M. Yen, Nucl. Phys. A 239:365 (1975).
- Go 74 J. Gomez del Campo, J.L.C. Ford, Jr., R.L. Robinson, and P.H. Stelson, Phys. Rev. C 9:1258 (1974).

- Go 75 J. Gomez del Campo, D.E. Gustafson, R.L. Robinson, P.H. Stelson, P.D. Miller, J.K. Bair, and J.B. McGrory, Phys. Rev. C 12:1247 (1975).
- Go 76 J. Gomez del Campo, M.E. Ortiz, A. Dacal, J.L.C. Ford, Jr., R.L. Robinson, P.H. Stelson, and S.T. Thornton, Nucl. Phys. A 262:125 (1976).
- Go 79 J. Gomez del Campo, R.G. Stokstad, J.A. Biggerstaff, R.A. Dayras, A.H. Snell, and P.H. Stelson, Phys. Rev. C 19:2170 (1979).
- Go 79a J. Gomez del Campo, R.A. Dayras, J.A. Biggerstaff, D. Shapira, A.H. Snell, P.H. Stelson, and R.G. Stokstad, Phys. Rev. Lett. 43:26 (1979).
- Go 79b J. Gomez del Campo, Proc. Symp. on Heavy-Ion Physics from 10 to 200 MeV/AMU, Brookhaven National Laboratory, New York (July 16-20, 1979) BNL-51115 Vol. I, p. 93 (1979).
- Go 80 P. Gonthier, H. Ho, M.N. Namboodiri, L. Adler, J.B. Natowitz, S. Simon, K. Hagel, R. Terry, and A. Khodai, Phys. Rev. Lett. 44:1387 (1980).
- Go 80a J. Gomez del Campo, Notas de Fisica 3:74 (1980).
- Go 80b C.R. Gould, R. Bass, J.V. Czarnecki, V. Hartmann, K. Stelzer, R. Zitzmann, and Y. Eyal, Z. Physik A 294:323 (1980).
- Go 81 J. Gomez del Campo and R.G. Stokstad, ORNL Report TM-7295 (1981).
- Gr 67 J.R. Grover, Phys. Rev. 157:832 (1967).
- Gr 67a J.R. Grover and J. Gilat, Phys. Rev. 157:802 (1967).
- Gr 67b J.R. Grover and J. Gilat, Phys. Rev. 157:814 (1967).
- Gr 67c J.R. Grover and J. Gilat, Phys. Rev. 157:823 (1967).

- Gr 72 S.M. Grimes, J.D. Anderson, A.K. Kerman, and C. Wong, Phys. Rev. C 5:85 (1972).
- Gr 72a L.R. Greenwood, K. Katori, R.E. Malmin, T.H. Braid, J.C. Stoltzfus, and R.H. Siemssen, Phys. Rev. C 6:2112 (1972).
- Gr 75 L.R. Greenwood, R.E. Segal, K. Raghunathan, M.A. Lee, H.T. Fortune, and J.R. Erskine, Phys. Rev. C 12:156 (1975).
- Gr 80 S.M. Grimes in Theory and Applications of Moment Methods in Many Fermion Systems, Plenum Press, New York (1980).
- Ha 52 W. Hauser and H. Feshbach, Phys. Rev. 87:366 (1952);
L. Wolfenstein, Phys. Rev. 82:690 (1951).
- Ha 67 M.L. Halbert, F.E. Durham, and A. Van der Woude, Phys. Rev. 162:899 (1967).
- Ha 71 E.C. Halbert, J.B. McGrory, B.H. Wildenthal, and S.P. Pandya, in Advances in Nuclear Physics, Vol. 4 (M. Baranger and E. Vogt, ed.), Plenum Press, New York (1971), p. 315.
- Ha 74 D.L. Hanson, R.G. Stokstad, K.A. Erb, C. Olmer, and D.A. Bromley, Phys. Rev. C 9:929 (1974).
- Ha 77 H.L. Harney, H.A. Weidenmuller, and A. Richter, Phys. Rev. C 16:1774 (1977).
- Ha 77a H. Hagelund and A.S. Jensen, Physica Scripta 15:226 (1977).
- Ha 79 D.v. Harrach, P. Glässel, Y. Civelekoglu, R. Männer, and H.J. Specht, Phys. Rev. Lett. 42:1728 (1979).
- He 81 B. Heusch, C. Beck, J.P. Coffin, R.M. Freeman, A. Gallmann, F. Haas, F. Rami, P. Wagner, and D.E. Alburger, Phys. Rev. C 23:1527 (1981).
- Hi 69 M. Hillman and J.R. Grover, Phys. Rev. 185:1303 (1969).

- Hi 74 M. Hillman and J.R. Grover, Phys. Rev. C 9:2289 (1974).
- Hi 79 D.L. Hillis, J.D. Garrett, O. Christensen, B. Fernandez, G.B. Hagemann, B. Herskind, B.B. Back, and F. Folkmann, Nucl. Phys. A 325:216 (1979).
- Hi 79a D. Hilscher, J.R. Birkelund, A.D. Hoover, W.U. Schröder, W.W. Wilcke, J.R. Huizenga, A.C. Mignerey, K.L. Wolf, H.F. Breuer, and V.E. Viola, Jr., Phys. Rev. C 20:576 (1979).
- Ho 73 R. Holub, A.F. Zeller, G.R. Choppin, R.J. DeMeijer, and H.S. Plendl, Phys. Lett. 43B:375 (1973).
- Ho 76 J.A. Holmes, unpublished Ph.D. thesis, Kellogg Radiation Lab, California Institute of Technology, Pasadena, California (1976).
- Ho 76a J.A. Holmes, S.E. Woosley, W.A. Fowler, and B.A. Zimmerman, At. Data and Nuc. Data Tables 18:306 (1976).
- Ho 77 H. Ho, R. Albrecht, W. Dünweber, G. Graw, S.G. Steadman, J.P. Wurm, D. Disdier, V. Rauch and F. Scheibling, Z. Phys. A, 283:235 (1977).
- Ho 80 H. Ho, P. Gonthier, M.N. Namboodiri, J.B. Natowitz, L. Adler, S. Simon, K. Hagel, R. Terry, and A. Khodai, Phys. Lett. 96B:51 (1980).
- Hu 69 J.R. Huizenga, H.K. Vonach, A.A. Katsanos, A.J. Gorski, and C.J. Stephan, Phys. Rev. 182:1149 (1969).
- Hu 72 J.R. Huizenga and L.G. Moretto, Ann. Revs. Nucl. Sci. 22:427 (1972).
- Hu 72a J.R. Huizenga, in Statistical Properties of Nuclei (J. Garg, ed.), Plenum, New York (1972).

- Hu 74 J.R. Huizenga, A.N. Behkami, R.W. Atcher, J.S. Sventek, H.C. Britt, and H. Freiesleben, Nucl. Phys. A 223:589 (1974).
- Hu 74a J.R. Huizenga, A.N. Behkami, J.S. Sventek, and R.W. Atcher, Nucl. Phys. A 223:577 (1974).
- In 77 T. Inamura, M. Ishihata, T. Fukuda, T. Shimoda, and H. Hiruta, Phys. Lett. 69B:51 (1977).
- Ka 66 P. Kahn and N. Rosenzweig, Phys. Lett. 22:307 (1966).
- Ka 69 S. Kahana, H.C. Lee, and C.K. Scott, Phys. Rev. 185:1378 (1969).
- Ki 73 M. Kildir and J.R. Huizenga, Phys. Rev. C 8:1965 (1973).
- Kl 74 H.V. Klapdor, H. Reiss, and G. Rosner, Phys. Lett. 53B:147 (1974).
- Kl 75 H.V. Klapdor, H. Reiss, and G. Rosner, Phys. Lett. 58B:279 (1975).
- Kl 75a H.V. Klapdor, G. Rosner, H. Reiss, and M. Schrader, Nucl. Phys. A 244:157 (1975).
- Kl 80 H.V. Klapdor, Nucleonika 25:289 (1980).
- Ko 76 J.J. Kolata, R.M. Freeman, F. Haas, B. Heusch, and A. Gallmann, Phys. Lett. 65B:333 (1976).
- Ko 77 J.J. Kolata, R.C. Fuller, R.M. Freeman, F. Haas, B. Heusch, and A. Gallmann, Phys. Rev. C 16:891 (1977).
- Ko 77a B. Kohlmeyer, W. Pfeffer, and F. Pühlhofer, Nucl. Phys. A 292:288 (1977).
- Ko 80 S. Kox, A.J. Cole, and R. Ost, Phys. Rev. Lett. 44:1204 (1980).
- Kr 74 H.J. Krappe and J.R. Nix, Proc. Third IAEA Symp. on Phys. and Chem. of Fission, Vol. I, IAEA, Vienna (1974) p. 159.
- Ku 68 T.T.S. Kuo and G.E. Brown, Nucl. Phys. A 114:241 (1968).
- Ku 79 T. Kuang-Hsi, T. Døssing, C. Gaarde, and J.S. Larsen, Nucl. Phys. A 316:189 (1979).
- La 54 J.D.W. Lang and K.J. LeCouteur, Proc. Phys. Soc. (London) A67:585 (1954).

- La 63 D.W. Lang, Nucl. Phys. 42:353 (1963).
- La 63a N.O. Lassen and J.S. Olsen, K. Dan. Vidensk. Selsk. Mat. Fys. Medd. 33:1 (1963).
- La 65 D.W. Lang, Nucl. Phys. 77:545 (1965).
- La 81 A. Lazzarini, V. Metag, A.G. Seamster, R. Vandenbosch, and R. Loveman, Phys. Rev. Lett. 46:988 (1981).
- Li 78 R.J. Liotta and R.A. Sorensen, Nucl. Phys. A 297:136 (1978).
- Lo 76 M. Lowry, J.S. Schweitzer, R. Dayras, and R.G. Stokstad, Nucl. Phys. A 259:122 (1976).
- Lo 80 D. Logan, M. Rajagopalan, M.S. Zisman, J.M. Alexander, M. Kaplan, and L. Kowalski, Phys. Rev. C 22:104 (1980).
- Lo 80a D. Logan, H. Delagrange, M.F. Rivet, M. Rajagopalan, J.M. Alexander, M. Kaplan, M.S. Zisman, and E. Duek, Phys. Rev. C 22:1080 (1980).
- Lu 71 C.C. Lu, J.R. Huizenga, C.J. Stephan, and A.J. Gorski, Nucl. Phys. A 164:225 (1971).
- Lu 72 C.C. Lu, L.C. Vay, and J.R. Huizenga, Nucl. Phys. A 197:321 (1972).
- Ma 55 M.G. Mayer and J.H.D. Jensen, Elementary Theory of Nuclear Shell Structure, Wiley, New York (1955).
- Ma 79 C. Mahaux and H.A. Weidenmüller, Ann. Rev. Nucl. Part. Sci. 29:1 (1979).
- Ma 80 M.A. McMahan and J.M. Alexander, Phys. Rev. C 21:1261 (1980).
- Mi 70 R. Middleton, J.D. Garrett, and H.T. Fortune, Phys. Rev. Lett. 24:1436 (1970).
- Mi 72 J.M. Miller in Statistical Properties of Nuclei (J.B. Garg, ed.), Plenum, New York (1972), p. 505.

- Mi 78 J.M. Miller, D. Logan, G.L. Catchen, M. Rajagopalan, J.M. Alexander, M. Kaplan, J.W. Ball, M.S. Zisman, and L. Kowalski, Phys. Rev. Lett. 40:1074 (1978).
- Mi 79 R. Middleton, R.R. Betts, H.T. Fortune, and R.G. Stokstad, Phys. Rev. C 19:100 (1979).
- Mi 80 G.E. Mitchell in Theory and Applications of Moment Methods in Many Fermion Systems, Plenum Press, New York (1980).
- Mo 64 S.A. Moszkowski in Alpha-, Beta-, and Gamma-Ray Spectroscopy (K. Siegbahn, ed.), North-Holland, Amsterdam (1964), p. 881.
- Mo 64a P.A. Moldauer, Phys. Rev. 135:B642 (1964)
- Mo 70 L.G. Moretto and R. Stella, Phys. Lett. 32B:558 (1970).
- Mo 71 U. Mosel and H.W. Schmitt, Phys. Lett. 37B:335 (1971).
- Mo 72 L.G. Moretto, Nucl. Phys. A 185:145 (1972).
- Mo 72a L.G. Moretto, Nucl. Phys. A 182:641 (1972).
- Mo 72b L.G. Moretto, Phys. Lett. 40B:185 (1972).
- Mo 72c L.G. Moretto, S.G. Thompson, J. Routti and R.C. Gatti, Phys. Lett. 38B:471 (1972).
- Mo 74 U. Mosel, P.G. Zint, and K.H. Passler, Nucl. Phys. A 236:252 (1974).
- Mo 74a L.G. Moretto, Proc. Third IAEA Symp. on Phys. and Chem. of Fission, Vol. I, IAEA, Vienna (1974) p. 329.
- Mo 75 L.G. Moretto, Nucl. Phys. A 247:211 (1975).
- Mo 75a P.A. Moldauer, Phys. Rev. C 11:426 (1975).
- Mo 80 L.G. Moretto and R.P. Schmitt, Phys. Rev. C 21:204 (1980).
- Mo 80a L.G. Moretto, S. Blau, and A. Pacheco, Lawrence Berkeley Laboratory report LBL-10805.
- Na 81 M.N. Namboodiri, P. Gonthier, H. Ho, J.B. Natowitz, R. Eggers, L. Adler, P. Kasiraj, C. Cessreti, A. Chevarier, N. Chevarier, and A. Demeyer, Nucl. Phys. A, in press.

- 01 74 C. Olmer, R.G. Stokstad, D.L. Hanson, K.A. Erb, M.N. Sachs, and D.A. Bromley, Phys. Rev. C 10:1722 (1974).
- Os 80 R. Ost, A.J. Cole, M.R. Clover, B.R. Fulton, and B. Sikora, Nucl. Phys. A 342:185 (1980).
- Pe 81 D. Pelte, V. Winkler, R. Novotny, and H. Gräf, Preprint MPIH-1981-V5
- P1 75 F. Plasil and M. Blann, Phys. Rev. C 11:508 (1975).
- P1 78 F. Plasil, Phys. Rev. C 17:823 (1978).
- P1 80 F. Plasil, R.L. Ferguson, R.L. Hahn, F.E. Obenshain, F. Pleasonton, and G.R. Young, Phys. Rev. Lett. 45:333 (1980).
- Pu 77 F. Pühlhofer, Nucl. Phys. A 280:267 (1977).
- Pu 79 R.J. Puigh, P. Dyer, R. Vandenbosch, J.D. Thomas, L. Nunnolley, and M.S. Zisman, Phys. Lett. 86B:24 (1979).
- Pu 79a H. Puchta, W. Dünneweber, W. Hering, C. Lauterbach, and W. Trautmann, Phys. Rev. Lett. 43:623 (1979).
- Pu 80 R.J. Puigh, H. Doubre, A. Lazzarini, A. Seamster, R. Vandenbosch, M.S. Zisman, and T.D. Thomas, Nucl. Phys. A 336:279 (1980).
- Ra 70 V.S. Ramamurthy, S.S. Kopow, and S.K. Kataria, Phys. Rev. Lett. 25:386 (1970).
- Ra 79 M. Rajagopalan, L. Kowalski, D. Logan, M. Kaplan, J.M. Alexander, M.S. Zisman, and J.M. Miller, Phys. Rev. C 19:54 (1979).
- Re 69 R.C. Reedy, M.J. Fluss, G.F. Herzog, L. Kowalski, and J.M. Miller, Phys. Rev. 188:1771 (1969).
- Re 80 G. Reffo in Theory and Applications of Moment Methods in Many Fermion Systems, Plenum Press, New York (1980).
- Ro 73 D. Robson, A. Richter, and H.L. Harney, Phys. Rev. C 8:153 (1973).

- Ro 75 D. Robson, A. Richter, and H.L. Harney, Phys. Rev. C 11:1867 (1975).
- Ru 69 F.H. Ruddy, B.D. Pate, and E.W. Vogt, Nucl. Phys. A 127:323 (1969).
- Ru 72 C. Rudy, R. Vandenbosch, P. Russo, and W.J. Braithwaite, Nucl. Phys. A 188:430 (1972).
- Sa 67 D.G. Sarantites and B.D. Pake, Nucl. Phys. A 93:545 (1967).
- Sa 67a D.G. Sarantites, Nucl. Phys. A 93:567 (1967).
- Sa 67b D.G. Sarantites, Nucl. Phys. A 93:576 (1967).
- Sa 72 D.G. Sarantites and E.J. Hoffman, Nucl. Phys. A 180:177 (1972).
- Sa 78 A.M. Sandorfi and A.M. Nathan, Phys. Rev. Lett. 40:1252 (1978).
- Sa 78a D.G. Sarantites, L. Westerberg, R.A. Dayras, M.L. Halbert, D.C. Hensley, and J.H. Barker, Phys. Rev. C 17:601 (1978).
- Sa 78b D.G. Sarantites, L. Westerberg, M.L. Halbert, R.A. Dayras, D.C. Hensley, and J.H. Barker, Phys. Rev. C 18:774 (1978).
- Sc 79 M. Schrader, A. Szanto de Toledo, and H.V. Klapdor, Z. Phys. A 289:193 (1979).
- Sc 81 R.P. Schmitt, G.J. Wozniak, G.V. Rattazzi, G.J. Mathews, R. Regimbart, and L.G. Moretto, Phys. Rev. Lett. 46:522 (1981).
- Se 57 P.A. Seeger and R.C. Perisho, Los Alamos Scientific Laboratory report LA-3751 (1957).
- Sh 69 R.W. Shaw, J.C. Norman, R. Vandenbosch, and C.J. Bishop, Phys. Rev. 184:1040 (1969).
- Sh 74 D. Shapira, R.G. Stokstad, and D.A. Bromley, Phys. Rev. C 10:1063 (1974).
- Si 77 R.S. Simon, M.V. Banaschik, R.M. Diamond, J.O. Newton, and F.S. Stephens, Nucl. Phys. A 290:253 (1977).

- Si 77a J.J. Simpson, P.O. Tjøm, I. Espe, G.B. Hagemann, B. Herskind, and M. Neiman, Nucl. Phys. A 287:362 (1977).
- Si 79 K. Siwek-Wilczynska, E.H. Du Marchie van Voorthuysen, J. Van Popta, R.H. Siemssen, and J. Wilczynski, Phys. Rev. Lett. 42:1599 (1979).
- Si 81 S.H. Sie, J.O. Newton, J.R. Leigh, and R.M. Diamond, Phys. Rev. Lett. 46:405 (1981).
- Sk 66 S.J. Skorka, J. Hertel, and T.W. Retz-Schmidt, Nucl. Data A 2:347 (1966).
- So 81 L.G. Sobotka, C.C. Hsu, G.J. Wozniak, G.V. Rattazzi, R.J. McDonald, A.J. Pacheco, and L.G. Moretto, Phys. Rev. Lett. 46:887 (1981).
- Sp 74 H. Spinka and H. Winkler, Nucl. Phys. A 233:456 (1974).
- St 71 R.M. Steffen, Los Alamos National Laboratory report LA-4565-MS (1971).
- St 74 R.G. Stokstad, Proceedings of the International Conference on Reactions between Complex Nuclei, Nashville, Tennessee (10-14 June 1974), ed. R.L. Robinson, F.K. McGowan, J.B. Ball, and J.H. Hamilton, North-Holland, Amsterdam/American Elsevier, New York (1974) Vol. 2, p. 327.
- St 76 R. G. Stokstad, J. Gomez del Campo, J.A. Biggerstaff, A.H. Snell, and P.H. Stelson, Phys. Rev. Lett. 36:1529 (1976).
- St 77 R. G. Stokstad, M.N. Namboodiri, E.T. Chulick, J.B. Natowitz, and D.L. Hanson, Phys. Rev. C 16:2249 (1977).

- St 78 R. G. Stokstad, Y. Eisen, S. Kaplanis, G. Pelte, U. Smilansky, and I. Tserruya, Phys. Rev. Lett. 41:465 (1978);
Phys. Rev. C 21:2427 (1980).
- St 81 R. G. Stokstad and E.E. Gross, Phys. Rev. C 23:281 (1981).
- Sw 76 Z.E. Switkowski, R.G. Stokstad, and R.M. Wieland, Nucl. Phys. A 261:478 (1976); 274:202 (1976).
- Sw 77 Z.E. Switkowski, R.G. Stokstad, and R.M. Wieland, Nucl. Phys. A 279:502 (1977).
- Sw 80 W. Swiatecki, Lawrence Berkeley Laboratory preprint 11403 (1980).
- Sz 78 A. Szanto de Toledo, M. Schrader, G. Rosner, E.M. Szanto, and H.V. Klapdor, Phys. Lett. 78B:58 (1978).
- Sz 79 E.M. Szanto, A. Szanto de Toledo, H.V. Klapdor, M. Diebel, J. Fleckner, and U. Mosel, Phys. Rev. Lett. 42:622 (1979).
- Ta 79 B. Tamain, R. Chechik, H. Fuchs, F. Hanappe, M. Morjean, M. Dakowski, B. Lucas, C. Mazur, M. Ribray, and C. Signarbieux, Nucl. Phys. A 330:253 (1979).
- Th 64 T.D. Thomas, Nucl. Phys. 53:558 (1964).
- Th 68 T.D. Thomas, Ann. Revs. Nucl. Sci. 18:343 (1968).
- Tj 78 P.O. Tjøm, I. Espe, G.B. Hagemann, B. Herskind, and D.L. Hillis, Phys. Lett. 72B:439 (1978).
- Ts 78 I. Tserruya, Y. Eisen, D. Pelte, A. Gavron, H. Oeschler, D. Berndt, and H.L. Harney, Phys. Rev. C 18:1688 (1978).
- Va 67 R. Vandenbosch, J.C. Norman, and C.J. Bishop, Phys. Rev. 158:887 (1967).
- Va 72 R. Vandenbosch and U. Mosel, Phys. Rev. Lett. 28:1726 (1972).
- Va 72a L.C. Vaz, C C. Lu, and J.R. Huizenga, Phys. Rev. C 5:463 (1972).

- Va 73 R. Vandenbosch and J.R. Huizenga, Nuclear Fission, Academic Press, New York (1973).
- Vi 77 F. Videbaeck, R.B. Goldstein, L. Grodzins, S.G. Steadman, T.A. Belote, and J.D. Garrett, Phys. Rev. C 15:954 (1977).
- Vi 79 J.B. Viano, A.J. Cole, N. Longequeue, J.J. Lucas, J. Menet, J.C. Saulnier, and J.W. Sunier, Phys. Rev. C 20:551 (1979).
- Vi 80 S.E. Vigdor, Proc. XIIIth Masurian Summer School on Nuclear Physics, Mikolajki, Poland (September 1980), to be published in Nukleonika.
- Vo 68 E. Vogt, in Advances in Nuclear Physics, Volume I (M. Baranger and E. Vogt, ed.), Plenum, New York (1968), p. 261.
- Wa 78 M. Wakai and A. Faessler, Nucl. Phys. A 307:349 (1978).
- We 40 V.F. Weisskopf and D.H. Ewing, Phys. Rev. 57:472,935 (1940)
- We 76 A. Weidinger, F. Busch, G. Gaul, W. Trautmann, and W. Zipper, Nucl. Phys. A 263:511 (1976).
- We 78 L. Westerberg, D.G. Sarantites, D.C. Hensley, R.A. Dayras, M.L. Halbert, and J.H. Barberg, Phys. Rev. C 18:796 (1978).
- Wi 72 F.C. Williams, Jr., G. Chan, and J.R. Huizenga, Nucl. Phys. A 187:225 (1972).
- Wi 74 R. Wieland, R. Stokstad, A. Gobbi, D. Shapira, L. Chua, M.W. Sachs, and D.A. Bromley, Phys. Rev. C 9:1474 (1974).
- Wo 78 G.J. Wozniak, R.P. Schmitt, P. Glässel, R.C. Jared, G. Bizzard, and L.G. Moretto, Phys. Rev. Lett. 40:1436 (1978).
- Wo 80 S.E. Woosley in Theory and Applications of Moment Methods in Many Fermion Systems, Plenum Press, New York (1980).

- Wo 80a G.J. Wozniak, R.J. McDonald, A.J. Pacheco, C.C. Hsu, D.J. Morrissey, L.G. Sobotka, L.G. Moretto, S. Shih, C. Schück, R.M. Diamond, H. Kluge, and F.S. Stephens, Phys. Rev. Lett. 45:1081 (1980)
- Yo 80 G.R. Young, R.L. Ferguson, A. Gavron, D.C. Hensley, F.E. Obershain, F. Plasil, A.H. Snell, M.P. Webb, C.F. Maguire, and G.A. Pettit, Phys. Rev. Lett. 45:1389 (1980).
- Zo 78 D.R. Zolnowski, H. Yamada, S.E. Cala, A.C. Kahler, and T.T. Sugihara, Phys. Rev. Lett. 41:92 (1978).

Table 1

Statistical properties of a Fermi gas with $A = 50$ and a uniform single-particle level density $g = 3.8 \text{ MeV}^{-1}$ ($a = A/8 \text{ MeV}^{-1}$).

$E(\text{MeV})$	$E(\text{MeV})$	$T(\text{MeV})$	n_{ex}	$\omega(E)(\text{MeV}^{-1})$
3	0.69	1.0	4	1.4×10^2
10	1.3	1.5	6	3.9×10^4
30	2.2	2.4	9	4.8×10^9
100	4.0	4.2	16	1.5×10^{18}

Table 2
Statistical Model Computer Codes

Name of Code	Type	γ Emission	n,p, α Evap.	Fission	Angular Distributions	Author(s)	References
ALICE	MSGR	no	W.E.*	yes	no	M. Blann and F. Plasil	Bl 66, Bl 72, Pl 78
CASCADE	MSGR	yes	H.F.	no	no	F. Pühlhofer	Pu 77
DFF	MSMC	no	W.E.	no	no	I. Dostrovsky, Z. Fraenkel and G. Friedlander	Do 59
GROGI	MSGR	yes	H.F.	no	no	J.R. Grover and J. Gilat	Gr 67a
HELGA	SS	no	H.F.	no	yes	S.K. Penney	Go 74
ICARUS [†]	MSMC	yes	H.F.	no	no	M. Wakai and A. Faessler	Wa 78
JULIAN	MSMC	yes	H.F.	no	yes	M. Hillman and Y. Eyal	Ei 77
LANCELOT	MSMC	yes	H.F.	no	yes	A.J. Cole	Co 80, Ko 80
LILITA	MSMC	no**	H.F.	no	yes	J. Gomez del Campo and R.G. Stokstad	St 76, Go 79, Go 81
MB-II ^{††}	MSGR	no	H.F.	yes	no	M. Beckerman and M. Blann	Be 78
PACE ^{†††}	MSMC	yes	H.F.	yes	yes	A. Gavron	Ga 80
ROULETTE	MSMC	yes	H.F.	no	no	D.G. Sarantites and B.D. Pate	Sa 67, Wa 78
STATIS ^{††††}	SS	no	H.F.	no	yes	R.G. Stokstad	Ha 74, OI 74, Da 76

*Although the use of the Weisskopf-Ewing formulation precludes a proper treatment of angular momentum, provision is made in ALICE to assign predetermined and fixed amounts of angular momentum removed with the evaporation of a proton and neutron or alpha particle.

**Gamma-ray competition is not included in the manner described in Sect. 3.2.1. Provision is made for an effective γ -ray competition at the last stage of the evaporation sequence.

†Based on the code ROULETTE

††A subsequent version of MBII, called ALERT, includes γ -ray emission and particle angular distributions (M. Blann, private communication).

†††A version of JULIAN, modified to include fission competition and a quantum mechanical coupling of angular momentum.

††††A later version of this code, STAT-II (Da 76) has been extended to calculate the number of effective channels contributing to a fluctuating cross section.

Table 3
Non-equilibrium Emission of Light Particles

Projectile	Target	E_{lab} (MeV/A)	$E-B^a)$ (MeV/A)	Heavy ion Detected	Coincident Particle	Deduction of Nonequilibrium Component	Reference
^{12}C	^{158}Gd	12.7	8.2	ER(γ)	n, α	YES	We 78
^{12}C	^{160}Gd	8-17	3.5	TLF(γ)	α	yes	Si 79
^{14}N	^{159}Tb	6.8	2.3	TLF(γ)	α	yes	In 77
^{10}B - ^{20}Ne	$^{152}Sm, ^{159}Tb$	6-9	1.6-4.5	TLF(γ)	α	yes	Zo 78
^{16}O	Ti	19.4	17.0	TLF	α	yes	Go 80
^{16}O	Ti	19.4	17.0	PLF	α	yes	Ho 80
^{16}O	^{58}Ni	6	3.2	PLF	n	yes	Ge 80
^{16}O	^{93}Nb	12.8	9.4	PLF	α	no	Yo 80
^{16}O	^{93}Nb	12.8	9.4	PLF	n	yes	Ga 81
^{20}Ne	^{63}Cu	8.4	5.5	PLF	α	yes	Go 79b
^{20}Ne	^{63}Cu	12.6	9.7	PLF	p	no	Sc 81
^{20}Ne	^{150}Nd	8.8	4.5	ER(γ)	n, α	no	We 78
^{32}S	^{27}Al	4.2,5.9	1.9,3.6	TLF	PLF	no	Pe 81

^{32}S	Au	11.7	6.6	PLF	α	yes	Ga 79
^{40}Ar	^{58}Ni	7	4	PLF	p, α	no	Ba 80b
^{40}Ar	Sn-Au	5.5-8.5	0.9-4.8	ER,FF	p, α	yes	De 79, Lo 80, Lo 80a
^{56}Fe	^{165}Ho	8.5	4.0	PLF	n	no	Hi 79a
^{63}Cu	Au	6.3	1.4	PLF	n	no	Ta 79
^{84}Kr	Ag	7.9	4.0	PLF	α	no	So 81
^{86}Kr	^{166}Er	7.0	2.6	PLF	n	no	Ey 80
^{132}Se	Au	7.5	2.5	PLF	n	no	Go 80b

a) $r_0 = 1.44$ fm

ER = Evaporation Residue
 TLF = Target-Like Fragment
 PLF = Projectile-Like Fragment
 FF = Fission Fragment

ER(γ) = indirect observation of residue by characteristic
 γ -ray emission
 TLF(γ) = indirect observation of TLF by characteristic
 γ -ray emission

FIGURE CAPTIONS

1. a) A uniform spacing of single particle levels. The occupation of levels up to the Fermi energy ϵ_F for zero and for finite temperatures is indicated.
b) Single-particle levels in the harmonic oscillator shell model without (left) and with (right) a spin-orbit interaction (Ma 55). The figure is taken from M.G. Mayer and J.H.D. Jensen, Elementary Theory of Nuclear Shell Structure, Wiley, N.Y. (1955).
c) Single-particle spectrum for axially symmetric harmonic oscillator potentials (Bo 75). The eigenvalues are measured in units of $\bar{\omega} = (2\omega_{\perp} + \omega_3)/3$, which is the deformation parameter δ_{osc} . The arrows mark the deformations corresponding to the indicated rational ratios of oscillator frequencies $\omega_{\perp}:\omega_3$. The figure is taken from A. Bohr and B. Mottelson, Nuclear Structure, Vol. II, Benjamin, NY (1975).
2. The total number of levels and the level density as a function of excitation energy in ^{20}Ne . The constant temperature formula is shown as the straight line. The Fermi-gas expression is the curved line (Bo 63).
3. Differential cross sections at 160° for elastic scattering of protons from three isotopes of Ca. There are 5 resonances for ^{40}Ca , 120 resonances for ^{42}Ca , and 429 resonances for ^{44}Ca . The line through the data is a fit with a multilevel R-matrix program (Mi 80).
4. The level density parameter "a" defined in Eq. (2.1) plotted as a function of atomic mass number for 265 nuclei as given by Holmes (Ho 76). Note marked local decreases in "a" in the vicinity of shell closures. There is a rough systematic trend of "a" to increase linearly with atomic mass and is given by the line $a = A/9$ (Wo 80).

5. The density of $M = 1/2$ states in ^{63}Cu . The dots are the numbers of exact shell model eigenvalues counted in 1 MeV intervals. The dashed curve is the Gaussian approximation. The solid curve includes the third and fourth moments (Gi 75).
6. a) Level density of ^{56}Fe ; the jagged curve is the level density calculated with a combinatorial method (Hi 69); the circles are the experimental points.
b) Comparison of the experimental level density of ^{56}Fe with a microscopic theory including the pairing interaction (Be 73). The theoretical calculations were performed with the single particle levels of Seeger et al. (Se 57) and Nix et al. (Bo 72).
7. Spin cutoff factors (Ay 74). The spin-cutoff factors for the nuclei ^{23}Na - ^{23}Mg , ^{24}Mg , ^{26}Al and ^{28}S are presented up to 30 MeV excitation. Curves B are the results of calculations in the (s, d, $f_{7/2}$) shell with the KLS interaction, whereas curves C are the results of the calculations in the s-d shell with the Kuo interaction. The spin-cutoff factors, which correspond to the Fermi distribution, are also plotted. The two Fermi-gas curves correspond to two different rigid-body radii, $r_0 = 1.4$ and 1.5 fm.
8. Schematic illustration of the dependence of shell effects and pairing on excitation energy and angular momentum. The energy of rotation for the ground-state (Yrast) and saddle point configurations are indicated (Vi 80).
9. The angular momentum coupling scheme for emission of a spinless particle in the direction $\vec{\Omega}$ with orbital angular momentum $\vec{\ell}$ leaving the residual nucleus with angular momentum \vec{j} .

10. The spectrum of intrinsic states at the equilibrium and at the fission saddle-point deformations for an even-odd nucleus, and in the residual nucleus following neutron emission. (The figure is taken from R. Vandenbosch and J.R. Huizenga, Nuclear Fission, Academic Press, NY (1973) and is used with permission of the North Holland Publishing Co.)
11. The angular momentum coupling scheme for fission of an axially symmetric nucleus with total angular momentum \vec{J}_i , projection K on the axis of symmetry and projection M on the axis of quantization.
12. Angular distributions for excited states in ^{25}Mg from the $^{12}\text{C}(^{14}\text{N}, p)^{25}\text{Mg}$ reaction at bombarding energies of 20 and 25 MeV. The solid lines are Hauser-Feshbach predictions (Ol 74).
13. Total α angular distributions for $E_x = 13.5-17.5$ MeV in ^{24}Mg for incident energies of 48, 49, and 49.5 MeV. The dashed lines are least-squares fits to the function $1/\sin\theta$ (Gr 72a).
14. Absolute Hauser-Feshbach statistical model calculations compared with experimental angular distributions from (Be 73a) for low-lying states in ^{20}Ne populated by the $^{12}\text{C}(^{14}\text{N}, ^6\text{Li})^{20}\text{Ne}$ reaction at $E_{\text{c.m.}} = 36$ MeV (Ha 74).
15. Absolute statistical model calculations (Ha 74) compared with experimental integrated yields for various $^{12}\text{C} + ^{14}\text{N}$ reaction products (Ho 73). The abscissa is the energy of the ^{14}N beam. The ^{24}Na yield has been calculated assuming the successive emission of two protons.

16. Comparison of the $^{20}\text{Ne}(\alpha, ^{12}\text{C})^{12}\text{C}$ reaction at $\theta_{\text{c.m.}} = 90^\circ$ from (La 63a) and the predictions of the Hauser-Feshbach statistical theory (Wi 74). The calculations, performed at 1-MeV intervals, are connected by a full-drawn line. The energy average of the experimental cross section is given by the dotted line.
17. A typical $^{10}\text{B}(^{16}\text{O}, \alpha)^{22}\text{Na}$ spectrum measured at a bombarding energy of 44 MeV and a laboratory angle of 7° (Go 74).
18. Angular distributions for some of the excited states in ^{22}Na measured at a bombarding energy of 46 MeV. The solid lines are the results of Hauser-Feshbach calculations (Go 74).
19. A plot of the $K = 3^+$, $K = 0^+$, and $K = 1^-$, rotational bands in ^{22}Na (Go 74). The dots represent the experimentally observed states and the crosses are the result of the large basis shell-model calculations of McGrory (see Ha 71).
20. Dominant decay modes (partial width $> 50\%$) for the nucleus ^{44}Sc (Pu 77). In the right-hand part of the figure, the most likely decay chains in the reaction 76 MeV $^{19}\text{F} + ^{27}\text{Al}$ are indicated for different angular momenta of the compound nucleus ^{46}Ti . Heavy arrows are for α emission, thin ones are for nucleons.
21. Decomposition of the calculated evaporation residue mass distribution into contributions from different compound nucleus spins formed in the reaction of 76 MeV ^{19}F with ^{27}Al (normalized to 1000 mb) (Pu 77). The sum of these distributions weighted by the partial formation cross sections ($\propto 2l + 1$) gives the result shown at the bottom.

22. Energy spectra for evaporation residues for the reaction $^{20}\text{Ne} + ^{12}\text{C}$ at $E(^{20}\text{Ne}) = 66.5$ MeV. The histograms represent the experimental data and the smooth curve is the result of a Monte Carlo statistical model calculation (Co 80).
23. Angular distributions (cross section per unit radian) for the reactions $^{16}\text{O} + ^{16}\text{O}$ and $^{12}\text{C} + ^{20}\text{Ne}$ at bombarding energies leading to the compound nucleus ^{32}S at $E_{\text{X}} \sim 44$ MeV. The theoretical curves are each independently normalized to the data. Absolute normalizations agree with experiment to within $\sim 15\%$ for the strongest yields (Co 80).
24. a) ΔE vs. E array for the reaction products of $^{14}\text{N} + ^{12}\text{C}$ at $E_{^{14}\text{N}} = 43.9$ MeV and $\theta_{\text{lab}} = 10^\circ$. The curves around the contours of constant Z are used to obtain projections along the E axis.
- b) ΔE vs. E array for the reaction products of $^{14}\text{N} + ^{12}\text{C}$ at $E_{^{14}\text{N}} = 178.1$ MeV and $\theta_{\text{lab}} = 6^\circ$. Note the increased yield for lighter elements relative to the data shown in (a) (Go 79).
25. Energy and angular distributions for reaction products from 0 to C for the reaction $^{14}\text{N} + ^{12}\text{C}$ at $E(^{14}\text{N}) = 145.5$ MeV (Go 79). The energy distributions for carbon ions, plotted on the right side, show components characteristic of evaporation residues (the lower energy component) and of direct reactions (the higher energy component). The dashed lines indicate the way these two components were unfolded. The histograms are the results of Monte Carlo Hauser-Feshbach calculations.
26. Angular correlations for protons and α particles following the reaction $^{16}\text{O} + ^{27}\text{Al}$ at $E(^{16}\text{O}) = 50$ MeV. The detector telescopes are placed in the plane perpendicular to the beam. The error bars are statistical only and the curves are drawn to guide the eye (Ku 79).

27. Calculated angular correlations for $\alpha\alpha$ decay from ^{43}Sc are given for different limiting angular momenta. Here $J_0(\text{max}) = 47/2 \hbar$ corresponds to the measured fusion cross section. The experimental correlation from Fig. 26 is given for comparison (Ku 79).
28. Energy spectra of α particles measured in coincidence with evaporation residues ($Z = 14-21$) formed in the reaction of 120 MeV $^{20}\text{Ne} + ^{27}\text{Al}$. The solid lines are the result of a Monte Carlo statistical model calculation (Na 81).
29. In-plane α -particle angular correlations measured in coincidence with specified evaporation residues from $^{20}\text{Ne} + ^{27}\text{Al}$. A negative angle means the α -particle detector was on the opposite side of the beam from the heavy-ion detector. The ordinate is the differential multiplicity integrated over the energies of both the evaporation residues and the detected α particles (Na 81). The solid curves are from the same statistical model calculation shown in Fig. 28.
30. a) Linear contour plot of the cross section $d^3\sigma/dv_\alpha^3$ as a function of the velocity of α particles in coincidence with fusion residues at 20° . The numbers on the contours represent the cross section in units of $\text{mb}/(\text{cm/ns})^3$. The vectors \vec{v}_{CM} and \vec{v}_{FR} represent the mean velocities of the center of mass and of the fusion residues, respectively. The velocity of the beam is indicated by v_{BEAM} and the straight lines indicate the angles at which α particles were detected.
- b) Statistical model calculation of the quantities shown in (a) (Na 81).

31. Calculated spectra of γ rays, neutrons, protons and alpha particles emitted in the fusion of 90 MeV ^{16}O with ^{140}Ce (Gr 67a).
32. Experimental (solid lines) and calculated (dashed lines) results for the reactions $^{140}\text{Ce} (^{16}\text{O}, xn) ^{156-x}\text{Dy}$. Product cross sections relative to σ_{fus} and the average total photon energy T_γ are shown as a function of the center-of-mass bombarding energy. Calculated values of T_γ at various energies are indicated by points. In (a) and (b), the normalizations of the dipole strength are a factor of 100 and a factor of $2J + 1$ times the strength deduced from neutron radiative capture experiments (Gi 73a).
33. The locations of the γ -cascade band and the α band in ^{150}Dy for two values of the dipole strength factor. The reaction is the same as in Fig. 32. In (b), this factor is 100 times larger than in (a). The dotted line in (b) corresponds to a $(2J + 1)$ normalization factor. The solid lines are the boundaries at which the indicated probability of emission is 0.5 (Gi 73a).
34. Statistical model predictions for the decay of the ^{164}Er compound system formed at an excitation energy of 54 MeV with 147 MeV ^{40}Ar ions incident on ^{124}Sn (Hi 79). The assumed population of the ^{164}Er compound system is given as a function of angular momentum in the top portion of the figure. The calculated populations $\sigma(\ell, E^*)$ are indicated as a function of the excitation energy and angular momentum for the system after the emission of 1-5 neutrons. The shaded region of 3n-5n population shows the portion in which γ -ray emission competes. The entry populations for the 3n-5n evaporation residues are indicated as a function of angular momentum and excitation energy

at the bottom and to the left side of the figure. The predicted entry line (Tj 74) is shown for each γ -ray emitting region.

35. Comparison of the deduced multiplicity distributions (solid curves) with statistical model predictions (broken curves) for the $^{124}\text{Sn}(^{40}\text{Ar}, xn)^{164-x}\text{Er}$ reaction at $E(^{40}\text{Ar}) = 161, 182, 190, 209$ and 236 MeV. The M_γ scale (bottom of figure) for the multiplicity distributions and the ℓ scale (top of figure) for the predicted distributions are related by $\ell = 2(M - 4)$. The predicted distribution for the 6n channel at 236 MeV has been increased a factor of 10.
36. Comparison of experimental and unfolded 12.7 x 15.2 cm NaI γ -ray energy spectra for the $^{124}\text{Sn}(^{40}\text{Ar}, 4n)^{160}\text{Er}$ reaction at $E(\text{Ar}) = 161$ MeV (Hi 79). Above $E_\gamma \sim 1.5$ MeV, only the statistical E1 gamma rays appear. Between 0.5 and 1.5 MeV, collective quadrupole transitions form a bump.
37. Liquid drop energies for ^{149}Tb nuclei according to the rotating drop model. The ordinate is energy in MeV versus angular momentum on the abscissa. The liquid drop fission barrier (B_f) is shown as the difference between the saddle-point energy of the rotating drop (E_r^{sad}) and the rotational energy of the rotating drop at equilibrium deformation (E_r^{min}). For comparison, the rotational energy of a spherical rigid rotor (E_r^0) is also shown (P1 75).
38. Excitation functions for the fission of the ^{153}Tb compound nucleus produced in reactions of ^{12}C with ^{141}Pr and ^{20}Ne with ^{133}Cs . The circles indicate experimental results. The curves are statistical-model fits to both sets of data with $a_f/a_n = 1.08$ and $E_B(0) = 28.5$ MeV (P1 80).

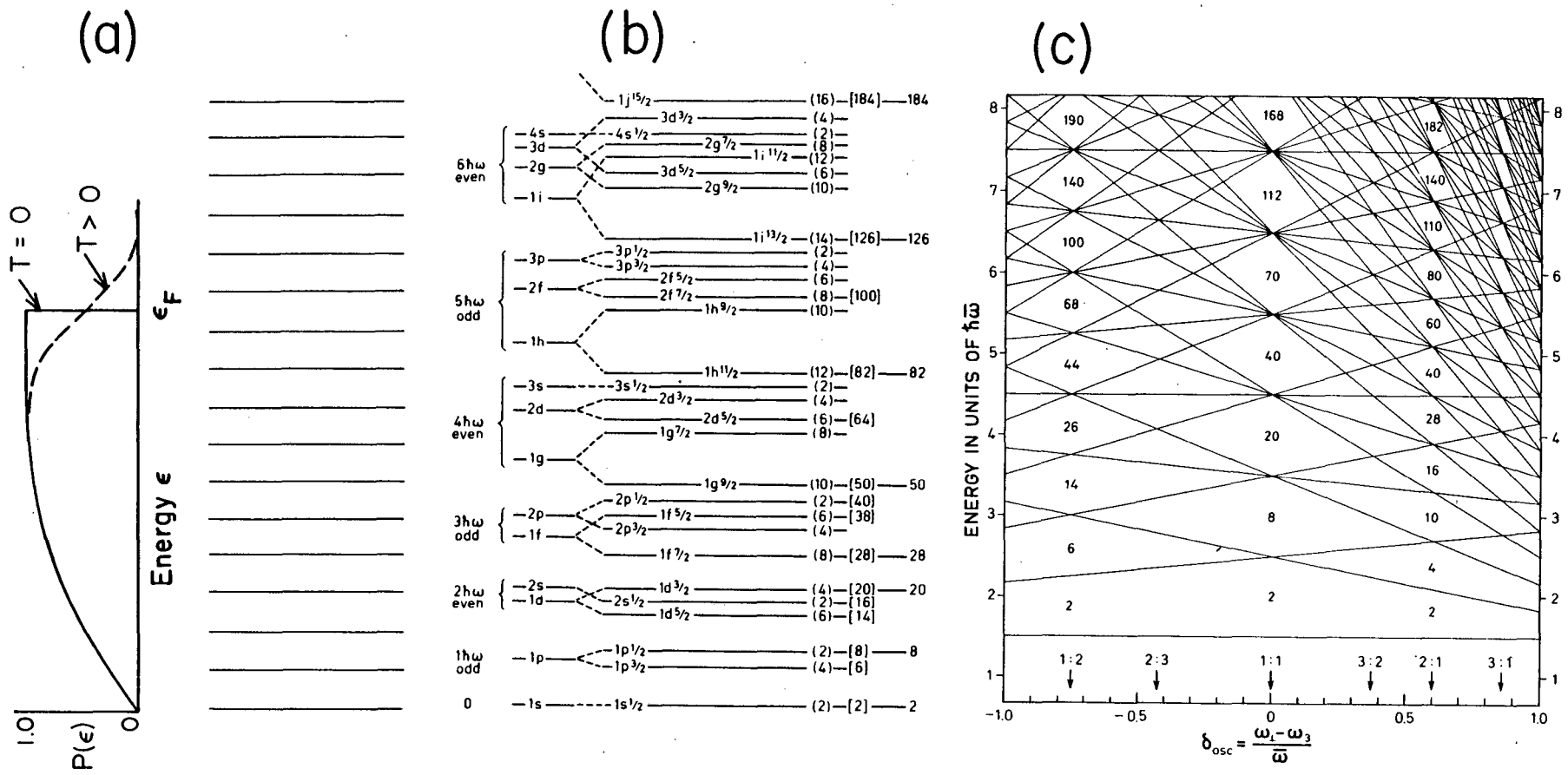
39. The effect of varying the fission barrier height on statistical model fits to the fission excitation function for the $^{12}\text{C} + ^{141}\text{Pr}$ reaction. The numbers for each curve give the value of the scaling parameter k defined by $E_B(\text{J}) = kE_B(\text{RLDM})$. The corresponding values of a_f/a_n vary from 0.985 for $k = 0.7$ to 1.245 for $k = 1.0$ (P1 80).
40. The components of the fission cross section for ^6Li induced reactions on five targets (Vi 80). The larger (dashed) error bars include an additional systematic uncertainty associated with the measurement of σ_{xn} by an x-ray technique. The indicated values of the total reaction cross section are from optical model calculations.
41. The angular momentum distributions for the total cross sections for the various types of reactions (Vi 80). The magnitude and shape of the curve for σ_{reac} are given by optical model calculations. In the case of σ_{fus} the shape is assumed and the area underneath the curve is fixed by the measured value of σ_{fus} . The shape and area of the curve for σ_{fiss} are given by a statistical model calculation.
42. Representative fission fragment angular distributions. The solid curves are a fit of the indicated formula which is empirical only. For comparison a curve corresponding to $(\sin\theta)^{-1}$ is also shown (Vi 80).
43. A comparison of measured and calculated anisotropies and fission cross sections (Vi 80). The calculations are based solely on the liquid drop and Fermi gas models and thus contain no shell effects. The error bars on the calculated values arise from uncertainties in the measured fusion cross sections. The dashed lines connect the calculated values and are to guide the eye.

44. Calculated (Ma 80) and measured (Mi 78) evaporation spectra for particles and protons from ^{194}Hg ($E^* = 98$ MeV, $\ell_{\text{max}} = 46$). Each calculated curve is arbitrarily normalized. Solid line, transmission coefficients from fusion measurements; dashed line, optical model; solid points and dash-dot curve, experimental data for α particles and protons, respectively (Ma 80).
45. Calculated branching ratios for the deexcitation of ^{149}Tb at 120 MeV of excitation versus initial angular momentum. The open circles near the abscissa represent the values of compound nucleus angular momenta for which results were calculated. Smooth curves were drawn through these points. Fission curves (f) represent total fission, whereas n, p, and α curves represent only first chance emission. Curves are for spherical (solid lines) and deformed nuclei (dashed lines) (B1 80).
46. Angle-integrated Z distributions for the deep inelastic (DI) components of $^{20}\text{Ne} + ^{63}\text{Cu}$ at $E(^{20}\text{Ne}) = 168$ MeV. The dotted histogram represents the primary fragment distribution while the solid one corresponds to the secondary distributions predicted by the Monte Carlo evaporation calculations. The solid rectangles are the experimental DI yields integrated from $\theta_{\text{lab}} = 20^\circ - 45^\circ$ (Go 79b).
47. Singles experimental energy spectra (dots) of projectile-like fragments from $Z = 6-8$ observed at $\theta_{\text{lab}} = 20^\circ$ for the reaction 168 MeV $^{20}\text{Ne} + ^{63}\text{Cu}$. The histograms are the secondary energy spectra predicted by the Monte Carlo calculations. The dashed curve drawn for $Z = 6$ (multiplied by a factor 10 for plotting purposes) is the primary distribution for $Z = 6$ (Go 79b, Da 81).

48. Fission angular correlations for the target-like fragment measured in and out of the reaction plane in the collision of 610 MeV Kr with ^{209}Bi . The family of solid curves are calculated for the out-of-plane case with $M = J$, $K_0^2 = 132$. The dashed curve is with $J_{\min} = 18$, $J_{\max} = 58$, and with contributions from $M \neq J$ (Dy 77).
49. Out-of-plane α -carbon correlation for the reaction 168 MeV $^{20}\text{Ne} + ^{63}\text{Cu}$. The solid and dotted histograms are Monte Carlo calculations for two values of the ratio ($R = I_f/I_0$) of fluctuating to aligned components of the transferred angular momentum. The value of 0.9 is favored by comparing to the experimental correlation (dots). This result, calculated using the quantum mechanical expression (eq. 3.11), has also been compared to a classical treatment (eq. 3.14) and they were found to agree to within $\sim 20\%$ (Go 79b).
50. Alpha-particle angular distributions as a function of out-of-plane angle for several Z-bins in the reaction of 664 MeV ^{84}Kr with Ag. Each bin is three Z-units wide and is labeled by the median Z value and the value of $W(0^\circ)/W(90^\circ)$. The distributions without any coincident γ -ray requirement, (a), are expressed in units of differential multiplicity. The distributions with two or more coincident γ rays, (b), are normalized to those in (a) at 90° for the same Z-bin (So 81).

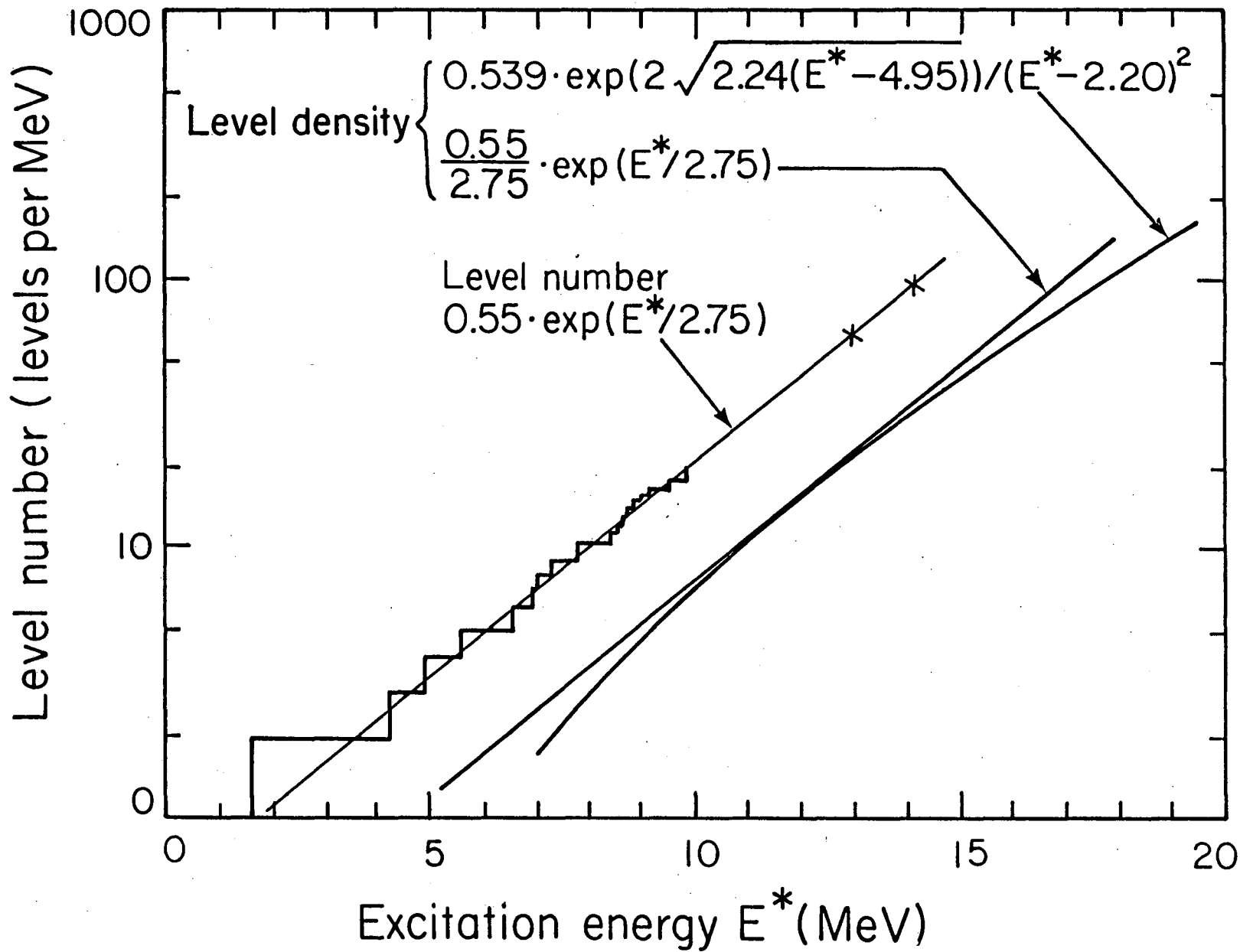
51. Neutron spectra in detectors A, B, C, D, F, and H in coincidence with the heavy-ion telescope. The reaction is 204 MeV $^{16}\text{O} + ^{93}\text{Nb}$. The deployment of detectors is indicated in the insert, and the letters used to indicate individual data points denote the detector from which they originate. Spectra from detectors E and G were omitted to maintain the clarity of the figure. The neutron spectra have had the calculated contribution of neutrons evaporated from the target-like fragment subtracted. The lines (labeled with script letters) are results of simulation calculations assuming the residual spectra to result from evaporation by the projectile-like fragment. There is a correspondence between the script letters labeling the calculated curves and the capital letters depicting the data points (for example, the curve labeled c should be compared with data points C). Above 10 MeV, some data points have been redistributed in larger bins to facilitate the comparison (Ga 81).
52. Same as Fig. 51. The simulation calculation contains an additional source of neutrons which is moving along the beam axis with a velocity of 3.3 cm/ns and having a temperature of 1.5 MeV (Ga 81).
53. Proton energy spectra detected in a colinear geometry with projectile-like fragments of $Z = 6-7$ (circles) and $Z = 8-9$ (squares). The reaction is 12.6 MeV/A $^{20}\text{Ne} + \text{Cu}$. The curves are the spectra predicted by a simple evaporation model with (solid lines) and without (dashed lines) thermal fluctuations in the division of the excitation energy between the two fragments (Sc 81).

54. Energy spectra of α particles detected in coincidence with products having $Z \geq 16$. The reaction is 310 MeV $^{16}\text{O} + \text{Ti}$. Experimental spectra are indicated by solid lines; calculated spectra by dashed lines. Heavy products were detected at (a) $+20^\circ$ and (b) $+40^\circ$ (Go 80).
55. Contour plots of the cross section, $d^3\sigma/dv_\alpha^3$, as a function of the velocity of α particles in coincidence with C ions detected at $+20^\circ$. The reaction is 310 MeV $^{16}\text{O} + \text{Ti}$. The contours are expressed in units of $2 \mu\text{b}/(\text{cm/ns})^3$. The velocity vectors are indicated for the primary beam, the center of mass, mean velocity and the variance of the mean velocity of the detected C ions. (a) For quasi-elastic C ions ($Q > -170$ MeV). (b) For deep-inelastic C ions ($-170 \geq Q \geq -230$ MeV). The solid circles represent the thresholds of the alpha detectors. The dashed circles indicate the ridges corresponding to the most probable emission from the target-like and projectile-like fragments (Ho 80).



XBL 814-8985A

Fig. 1



XBL 813-495

Fig. 2

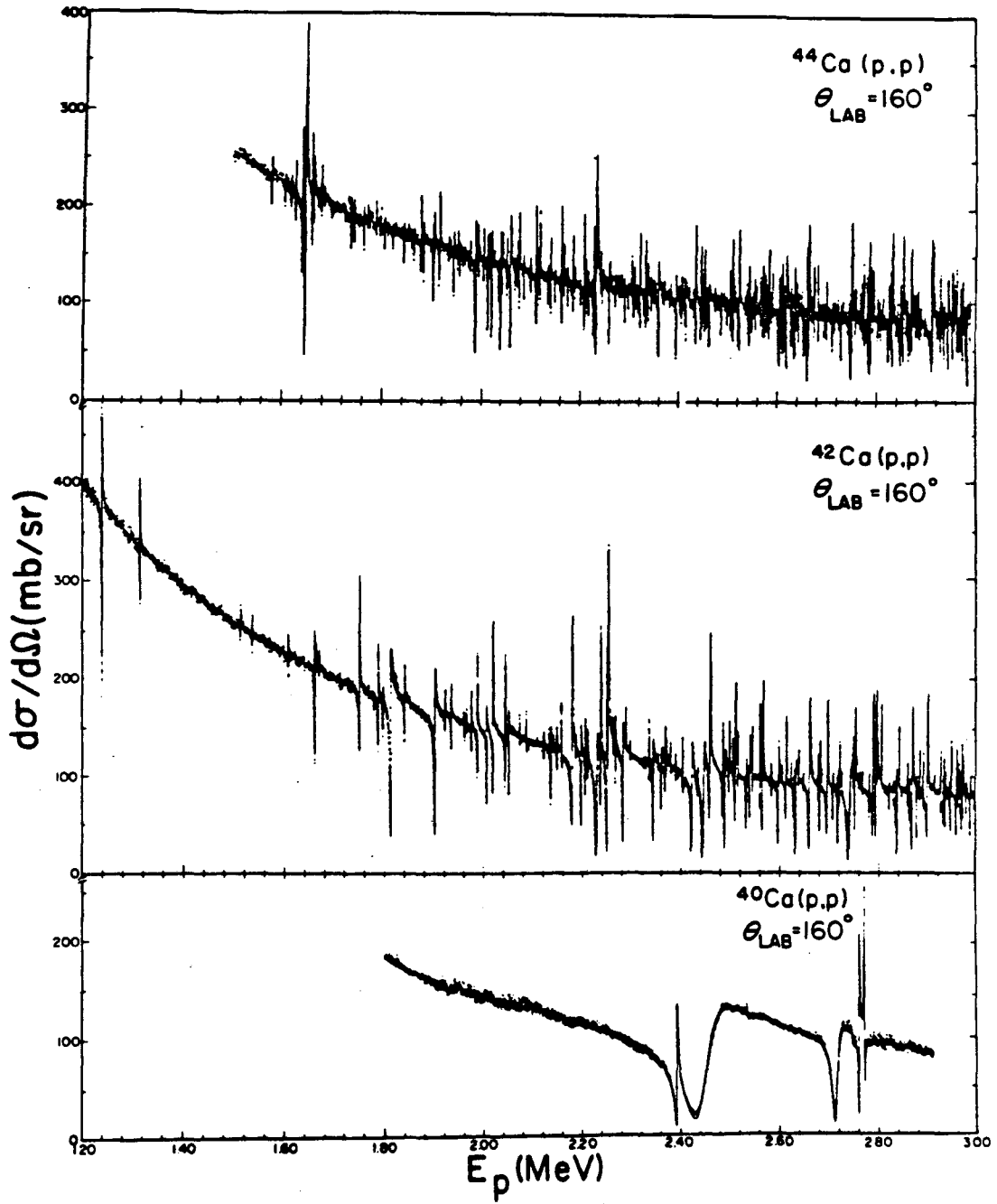


Fig. 3

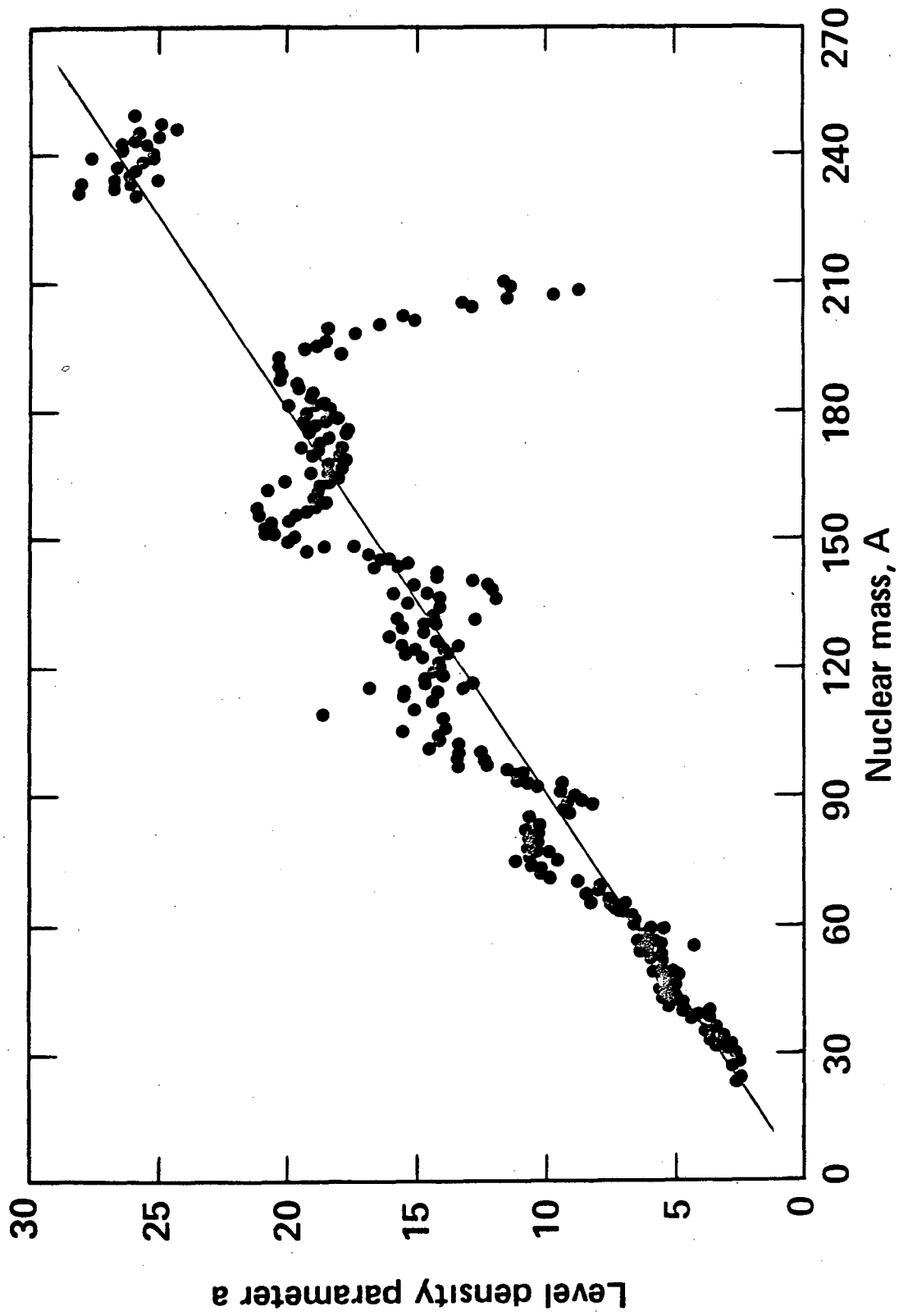
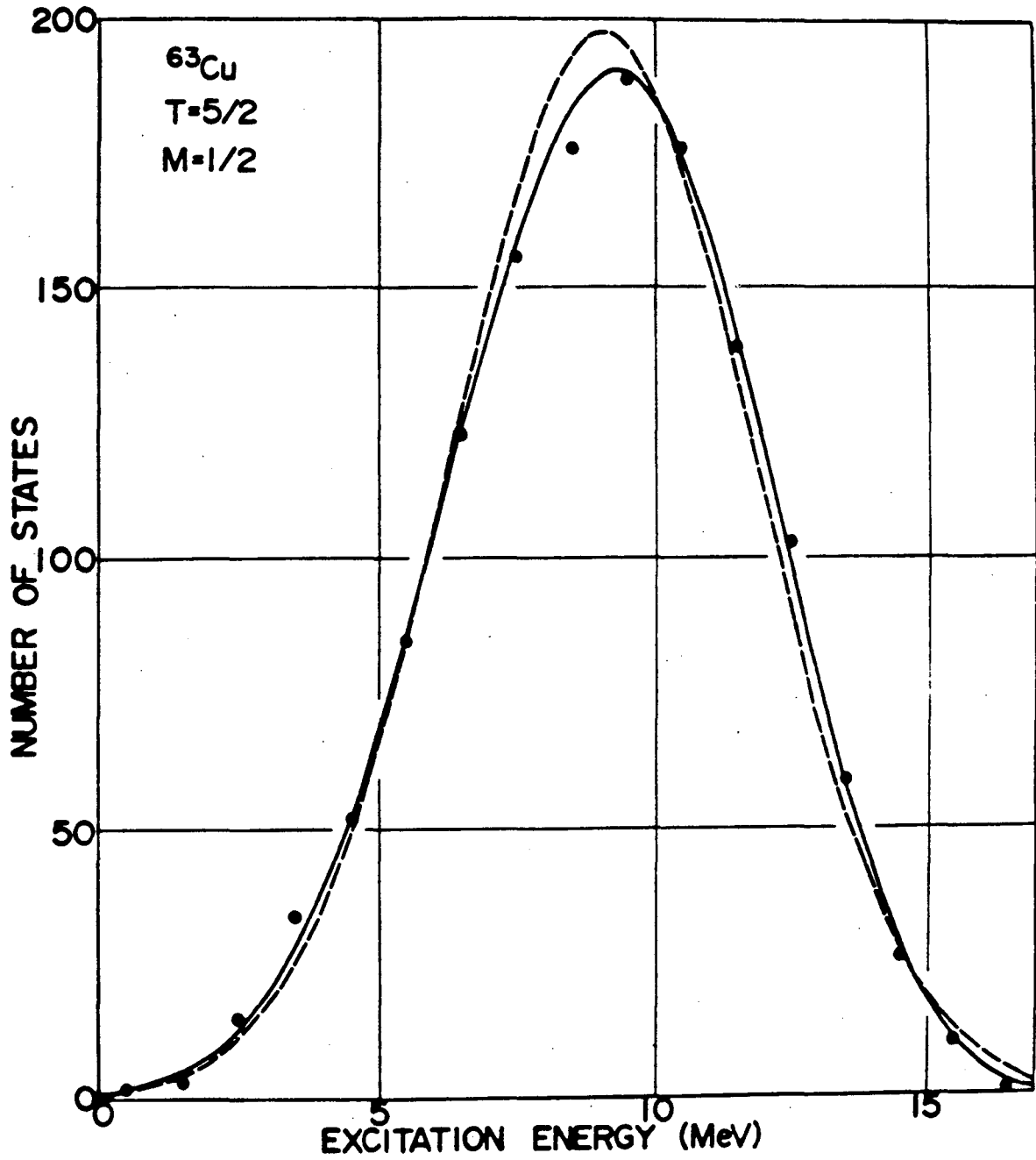
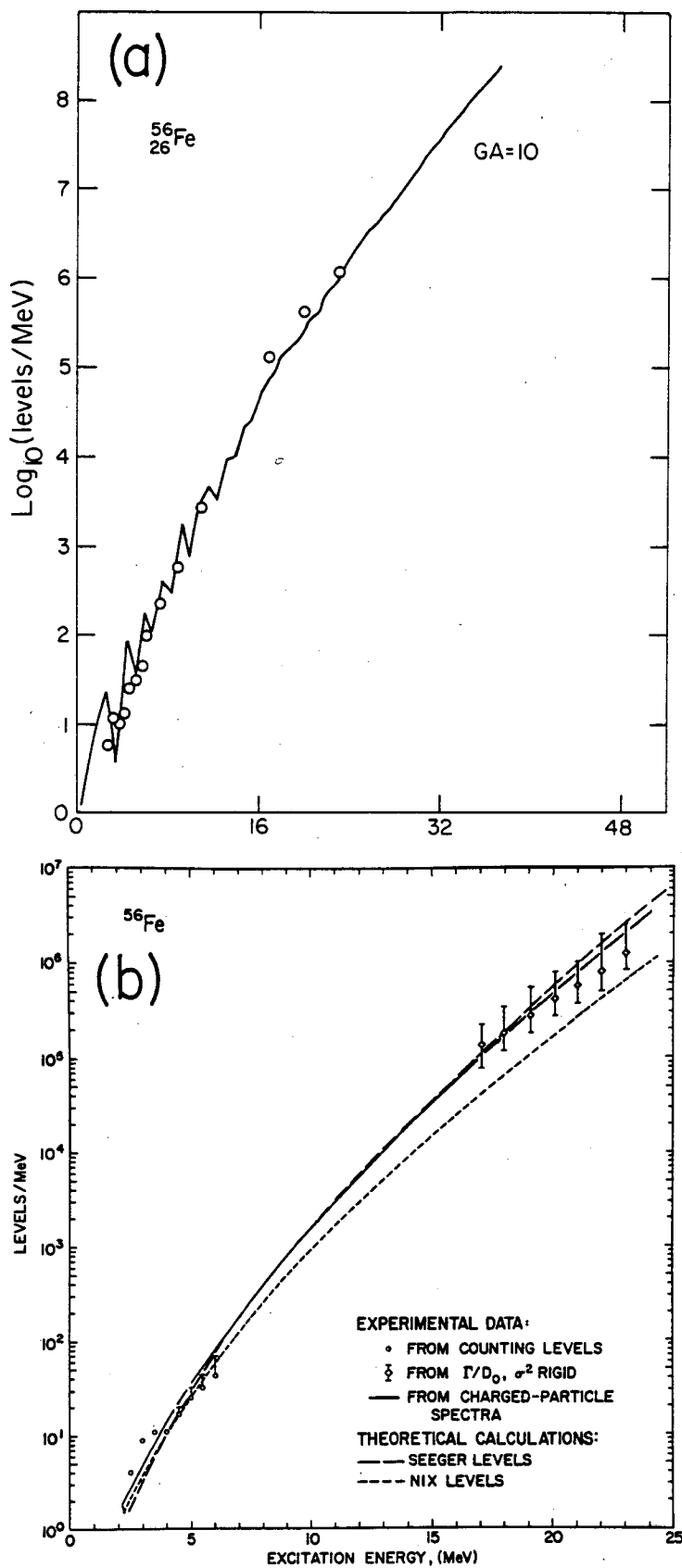


Fig. 4



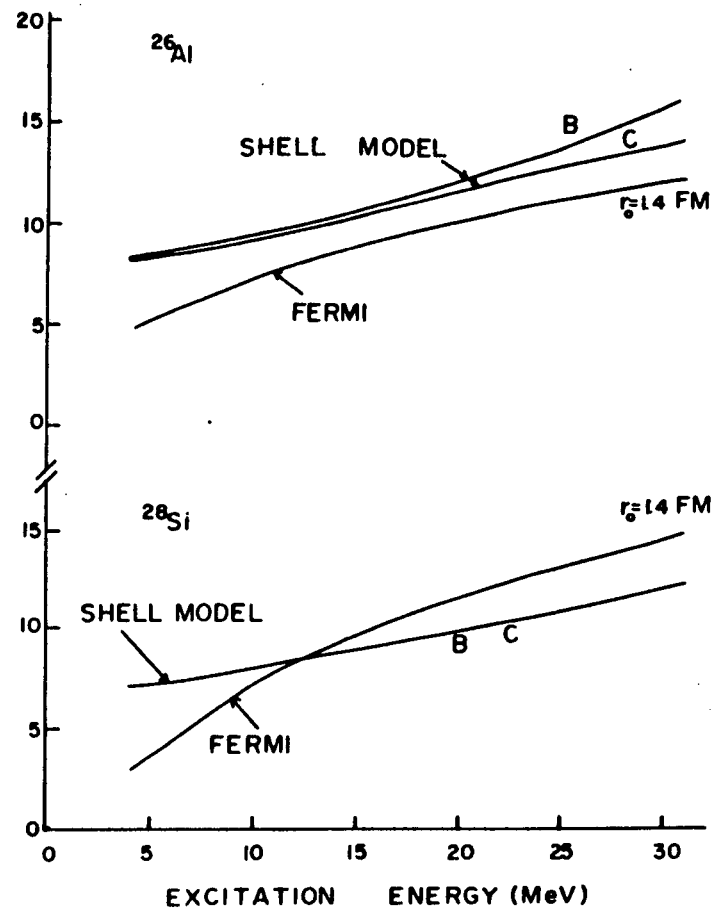
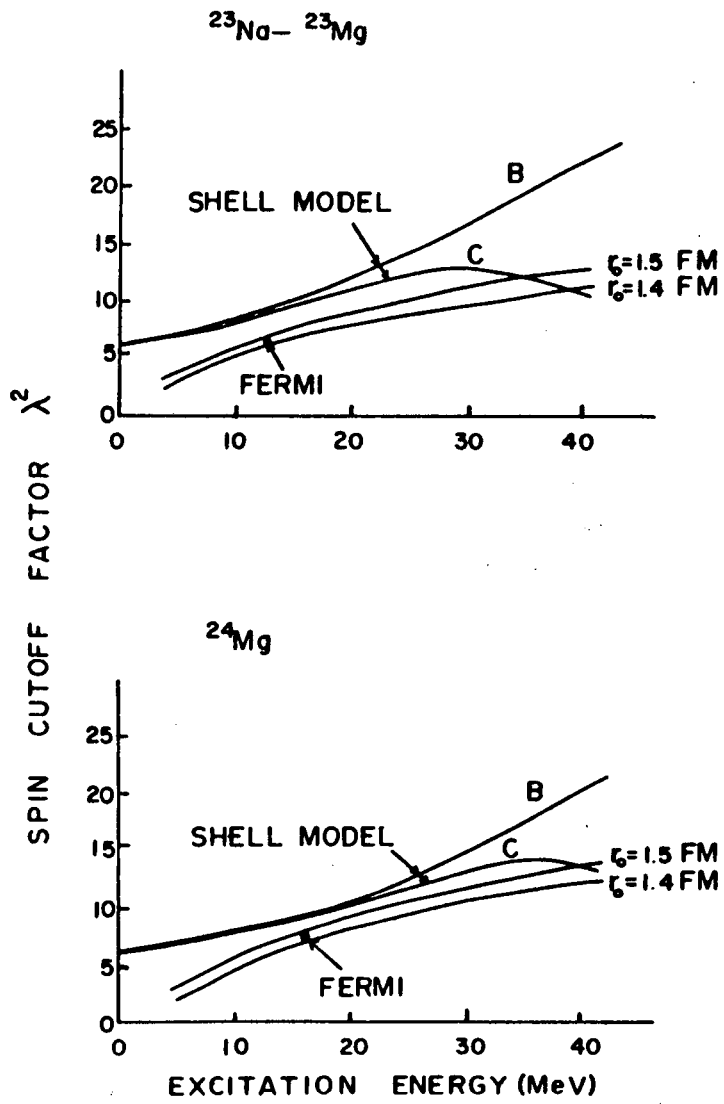
XBL 814-8983

Fig. 5



XBL 814-9307

Fig. 6



XBL 814-8984

Fig. 7

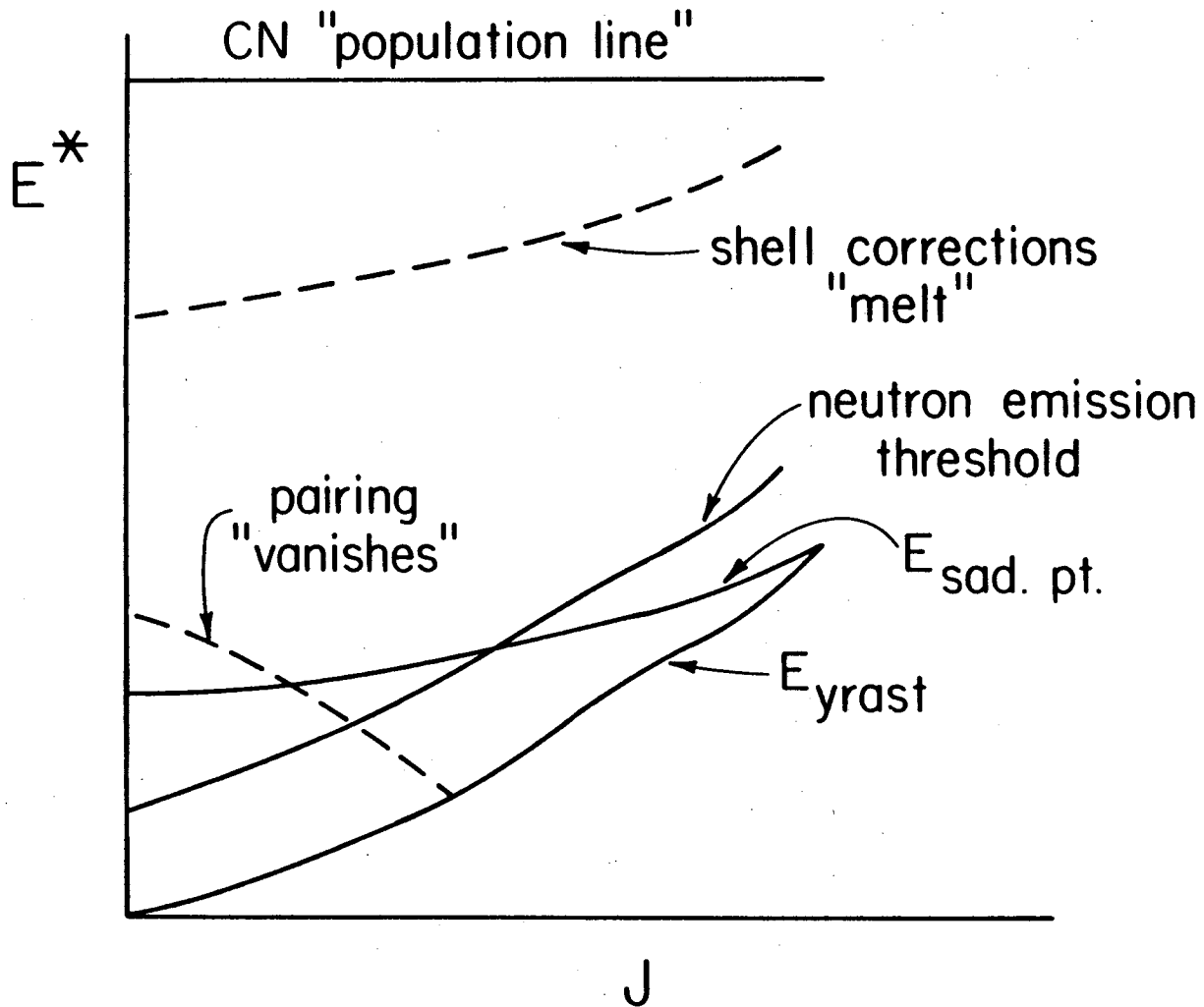
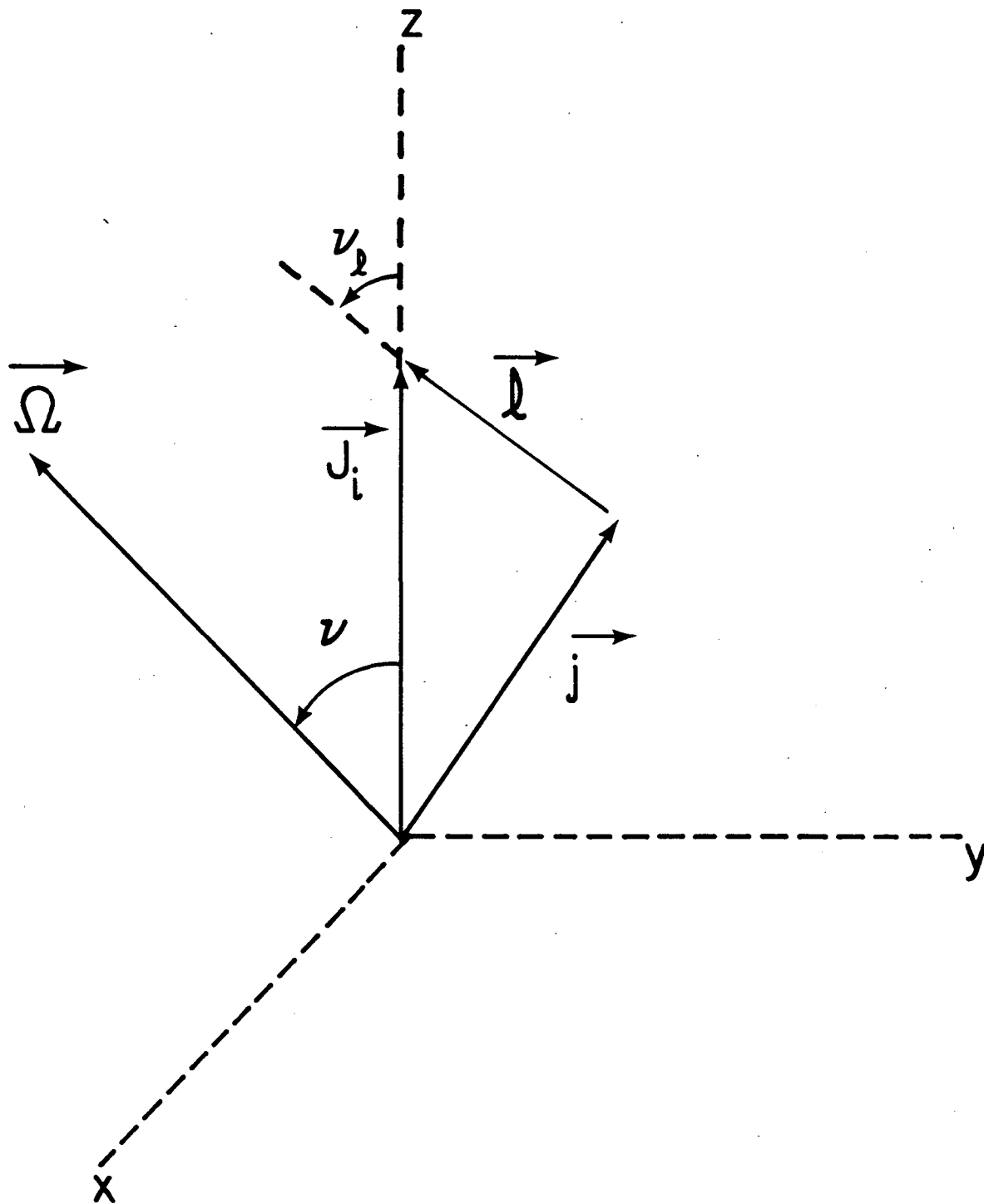
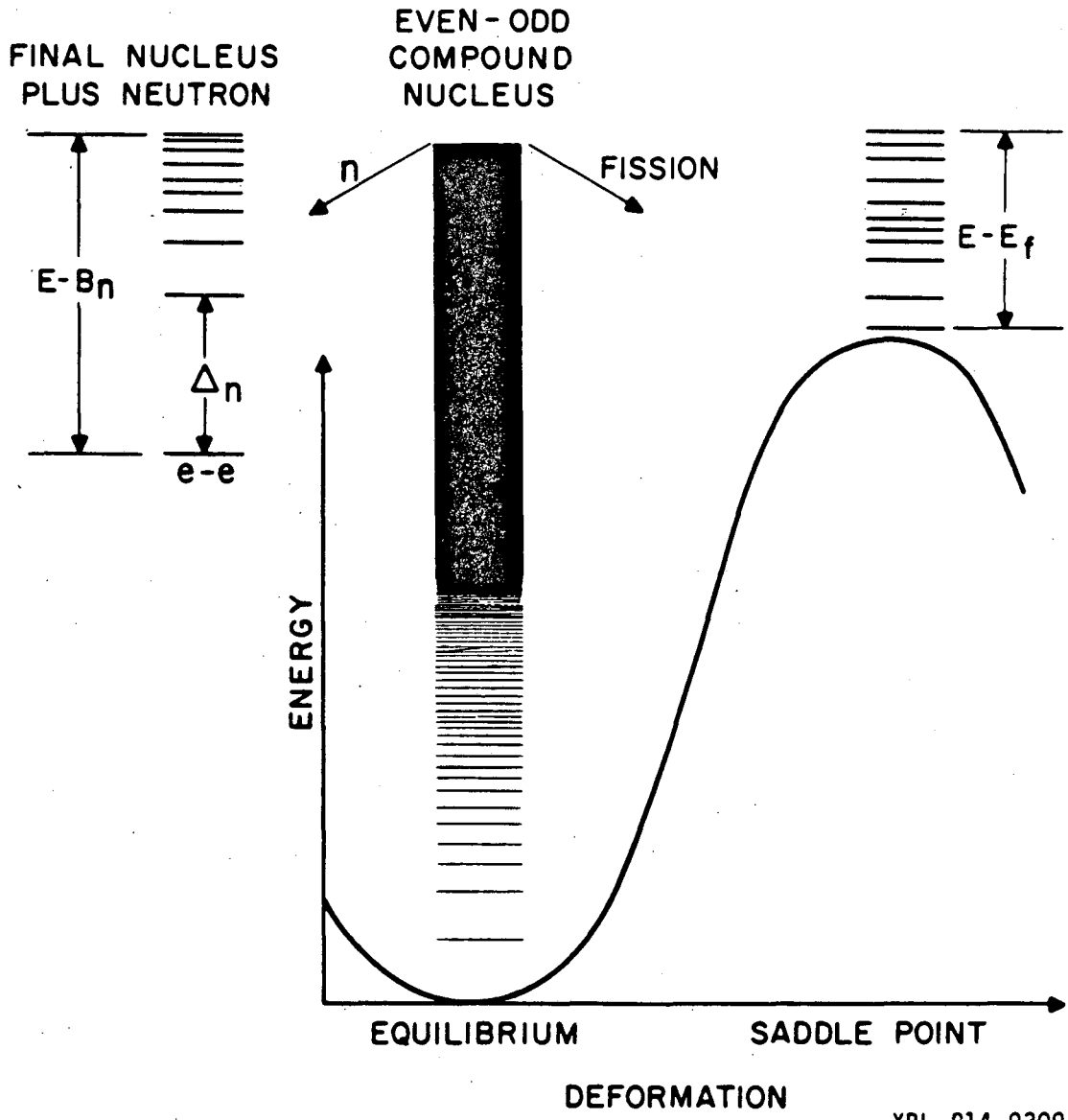


Fig. 8



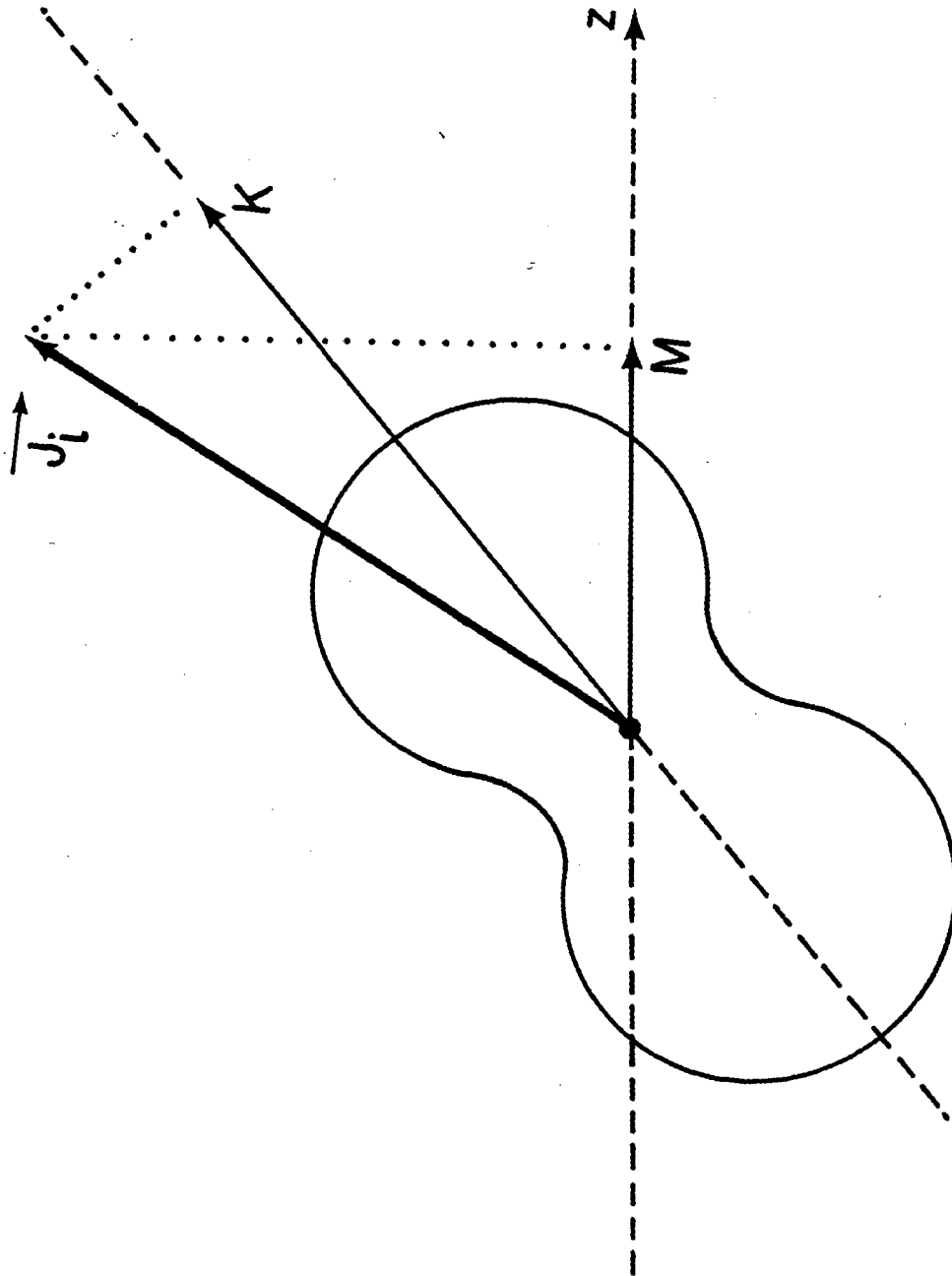
XBL813-489

Fig. 9



XBL 814-9309

Fig. 10



XBL813-488

Fig. 11

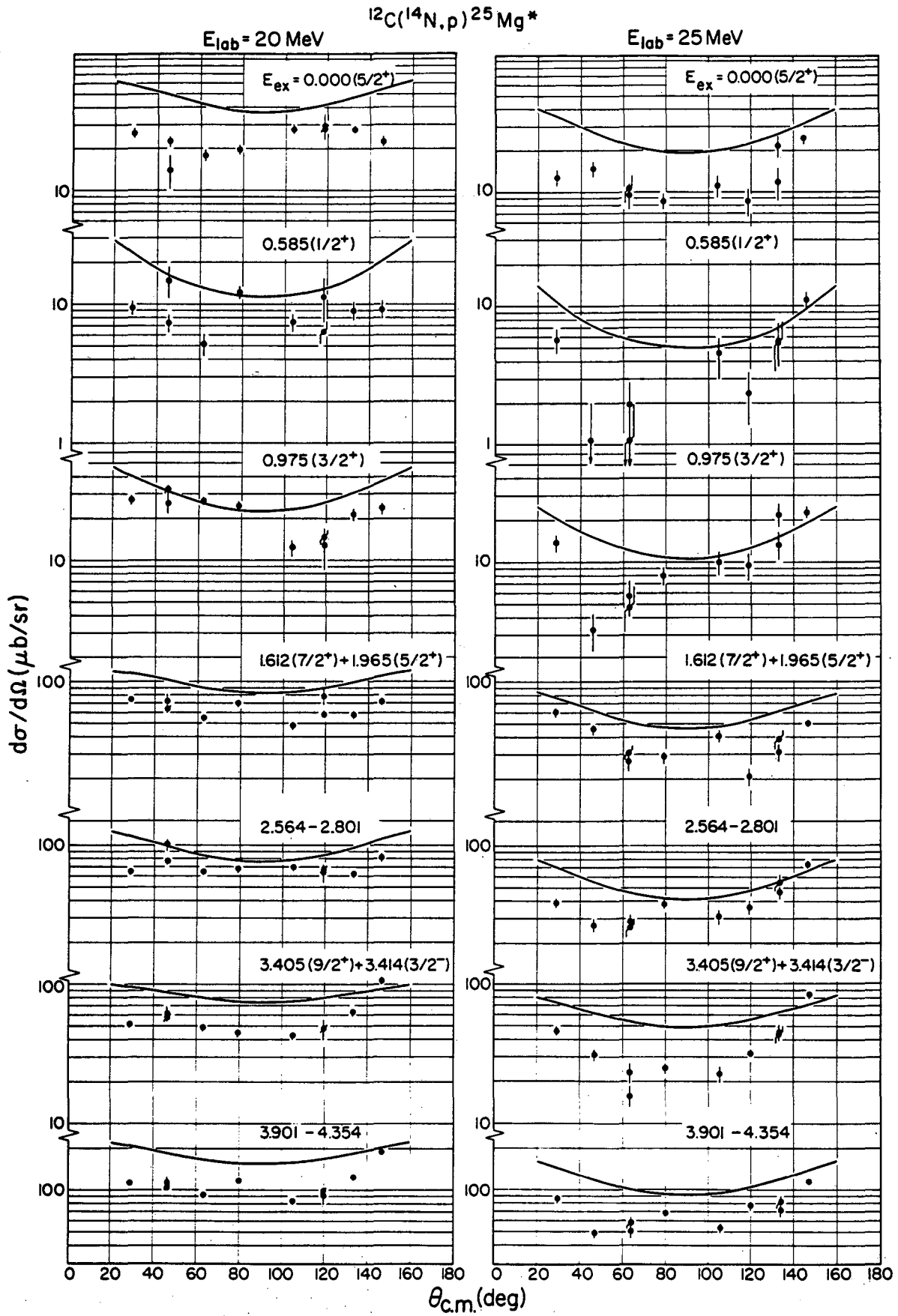
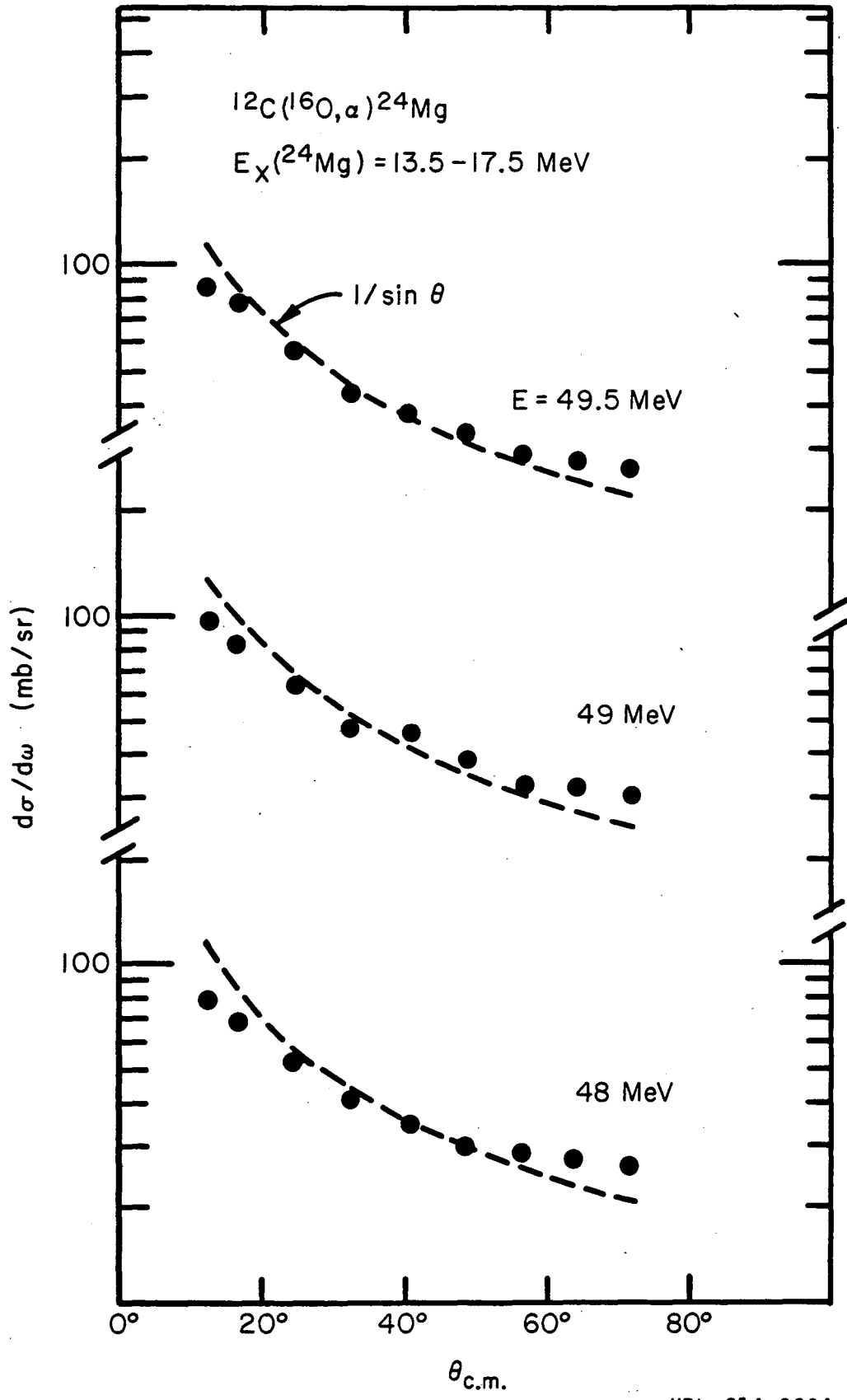


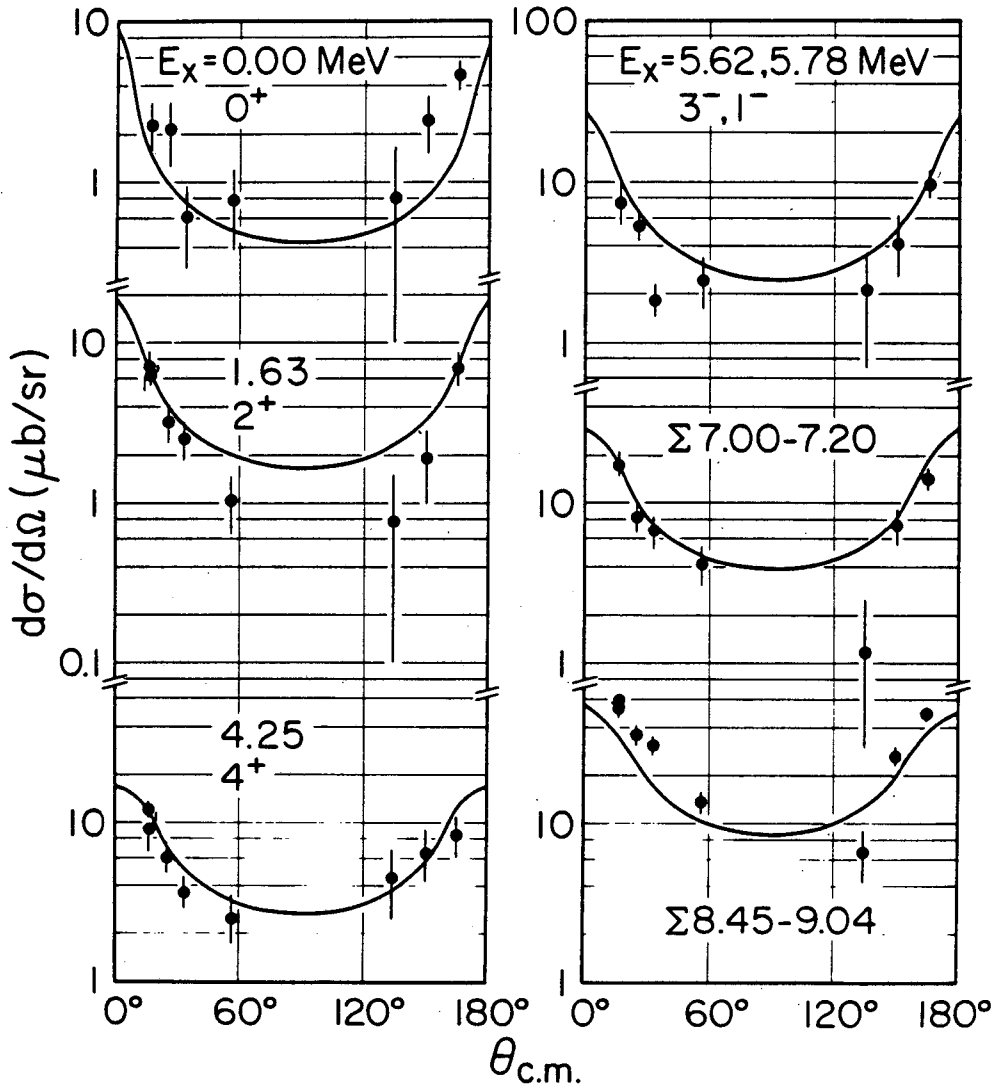
Fig. 12



XBL 814-9304

Fig. 13

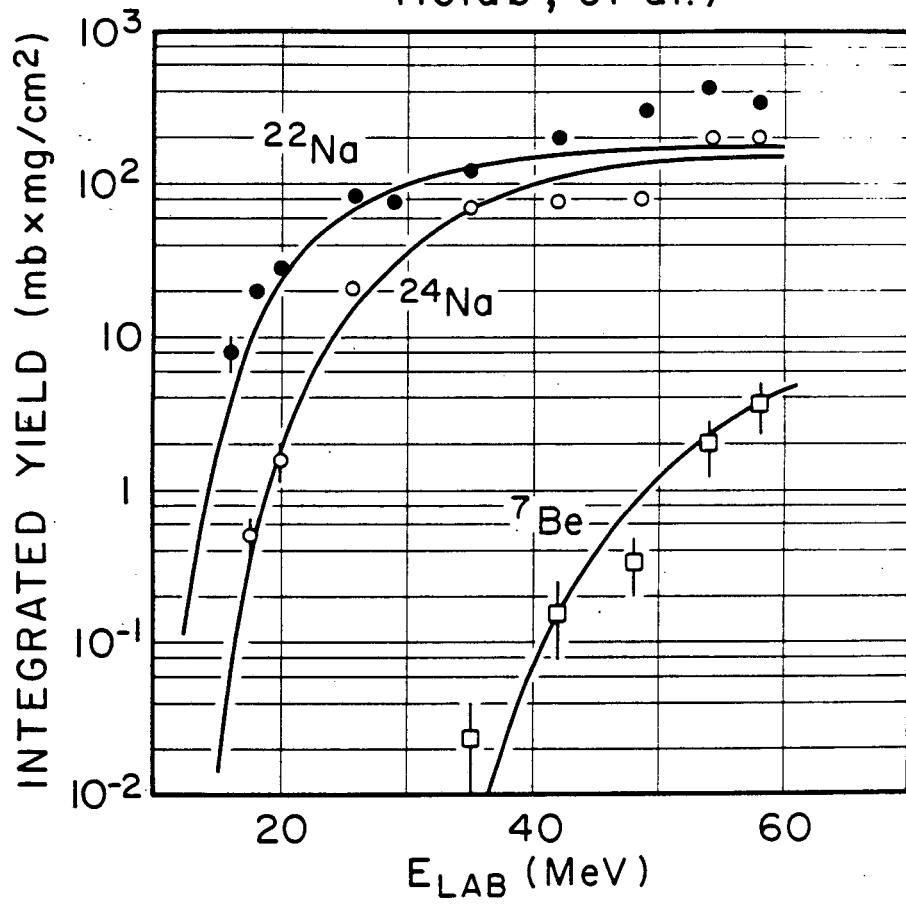
$^{12}\text{C}(^{14}\text{N}, ^6\text{Li})^{20}\text{Ne}$ $E_{\text{c.m.}} = 36 \text{ MeV}$
(Belote, et al.)



XBL 814-9105

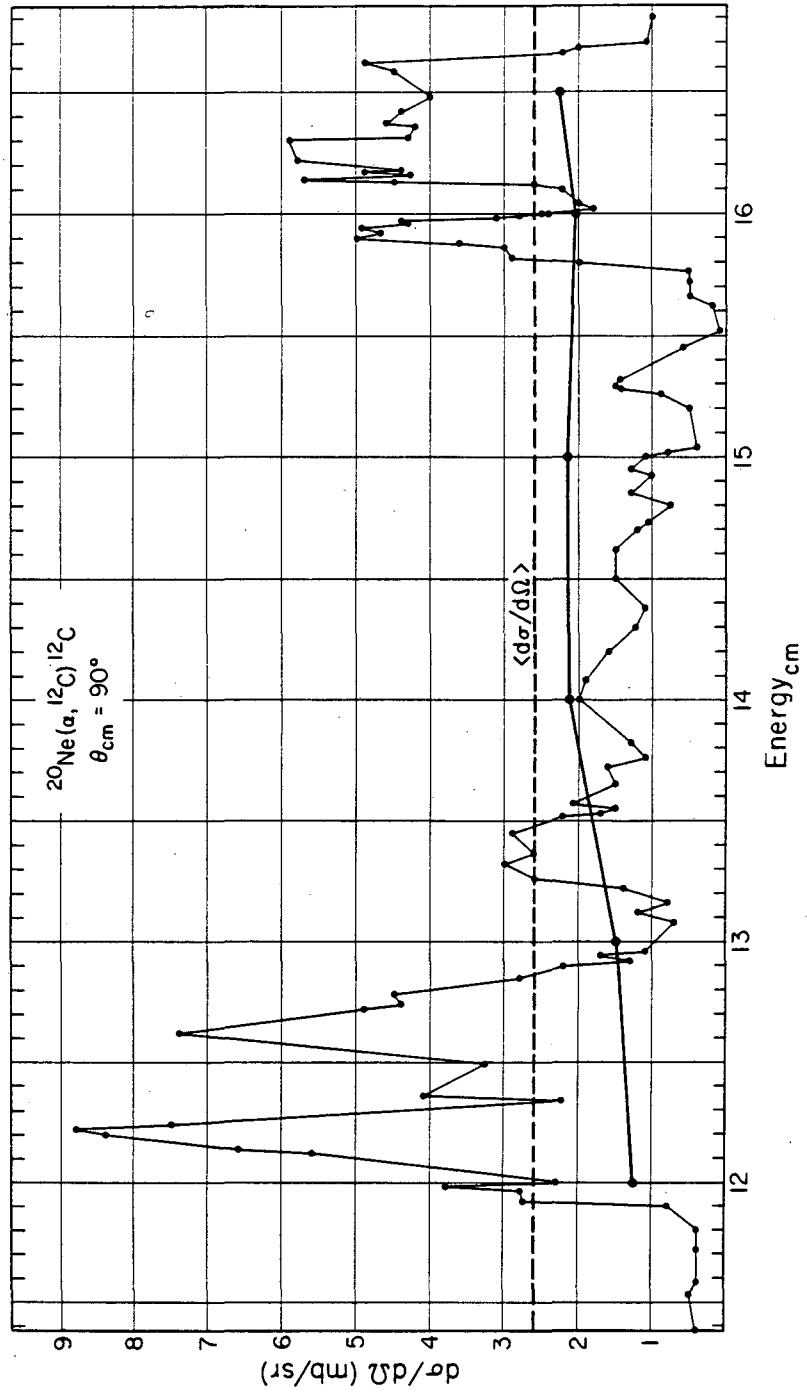
Fig. 14

$^{12}\text{C} + ^{14}\text{N}$ Delayed Activities
Holub, et al.)



XBL 814-9104

Fig. 15

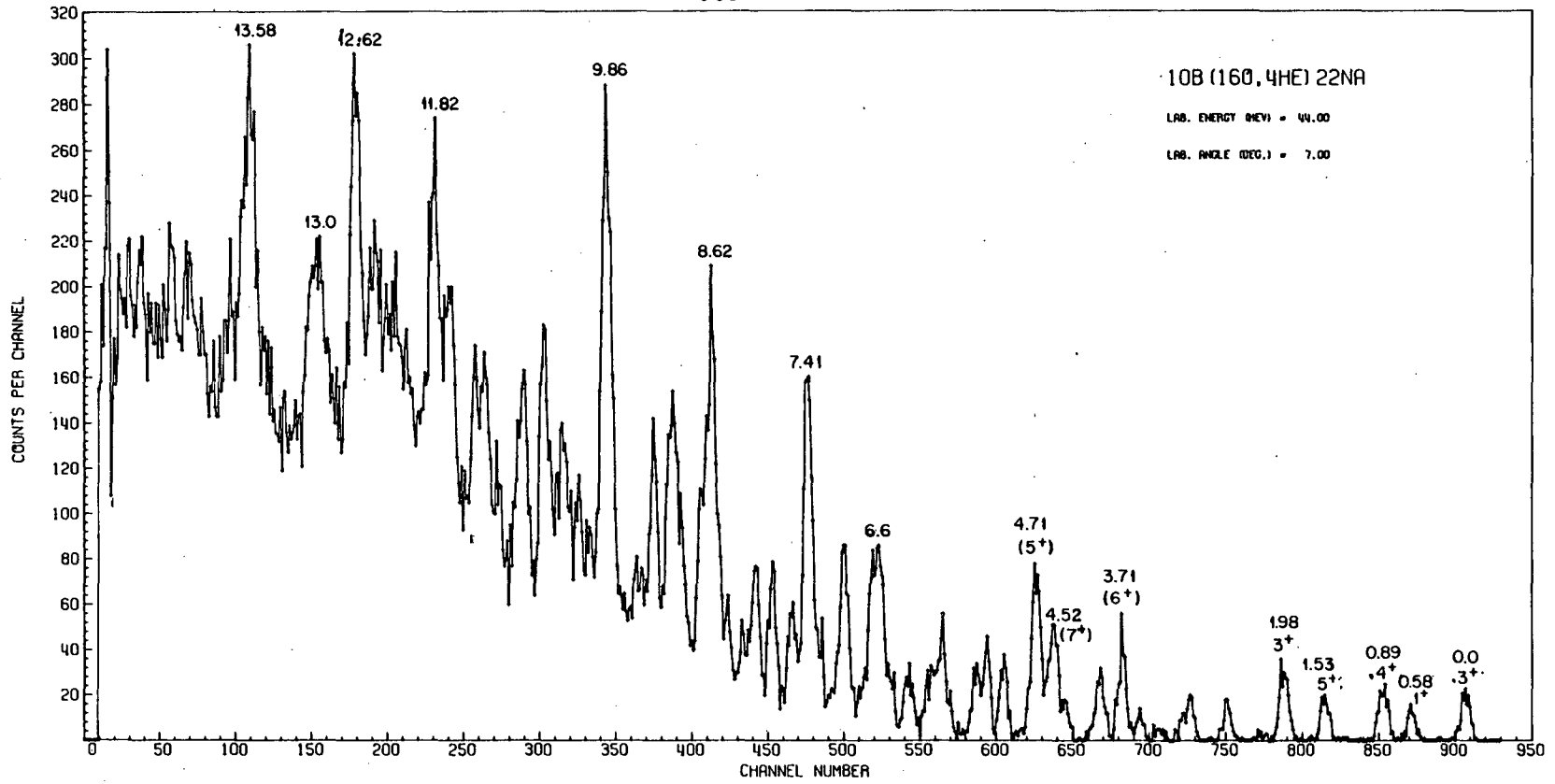


XBL 814-9106

Fig. 16

4499

ORNL - DWG 72-12092A



-154-

Fig. 17

$^{10}\text{B}(^{16}\text{O}, \alpha)^{22}\text{Na}$
 $E_{\text{lab}} = 46 \text{ MeV}$

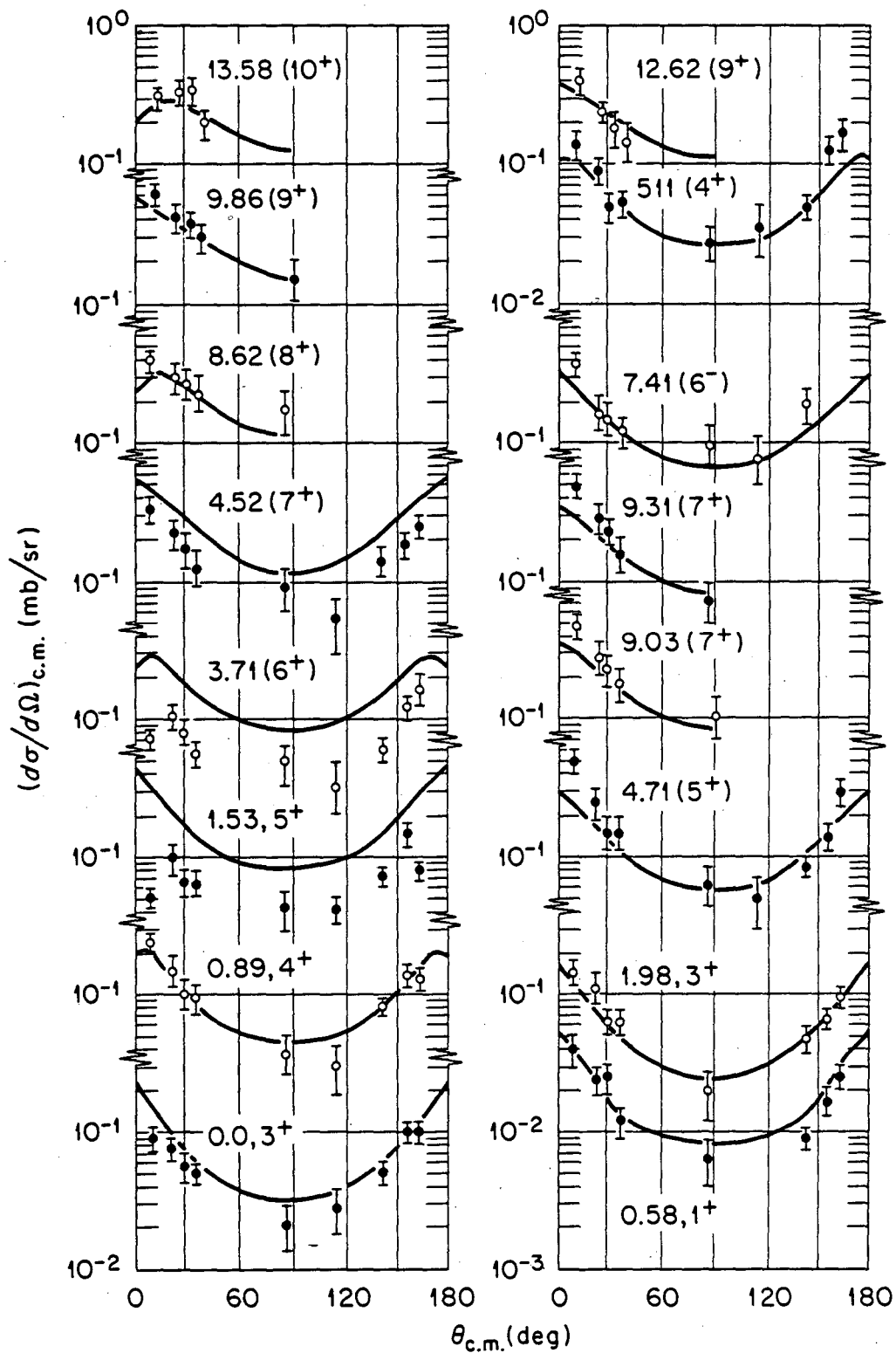


Fig. 18

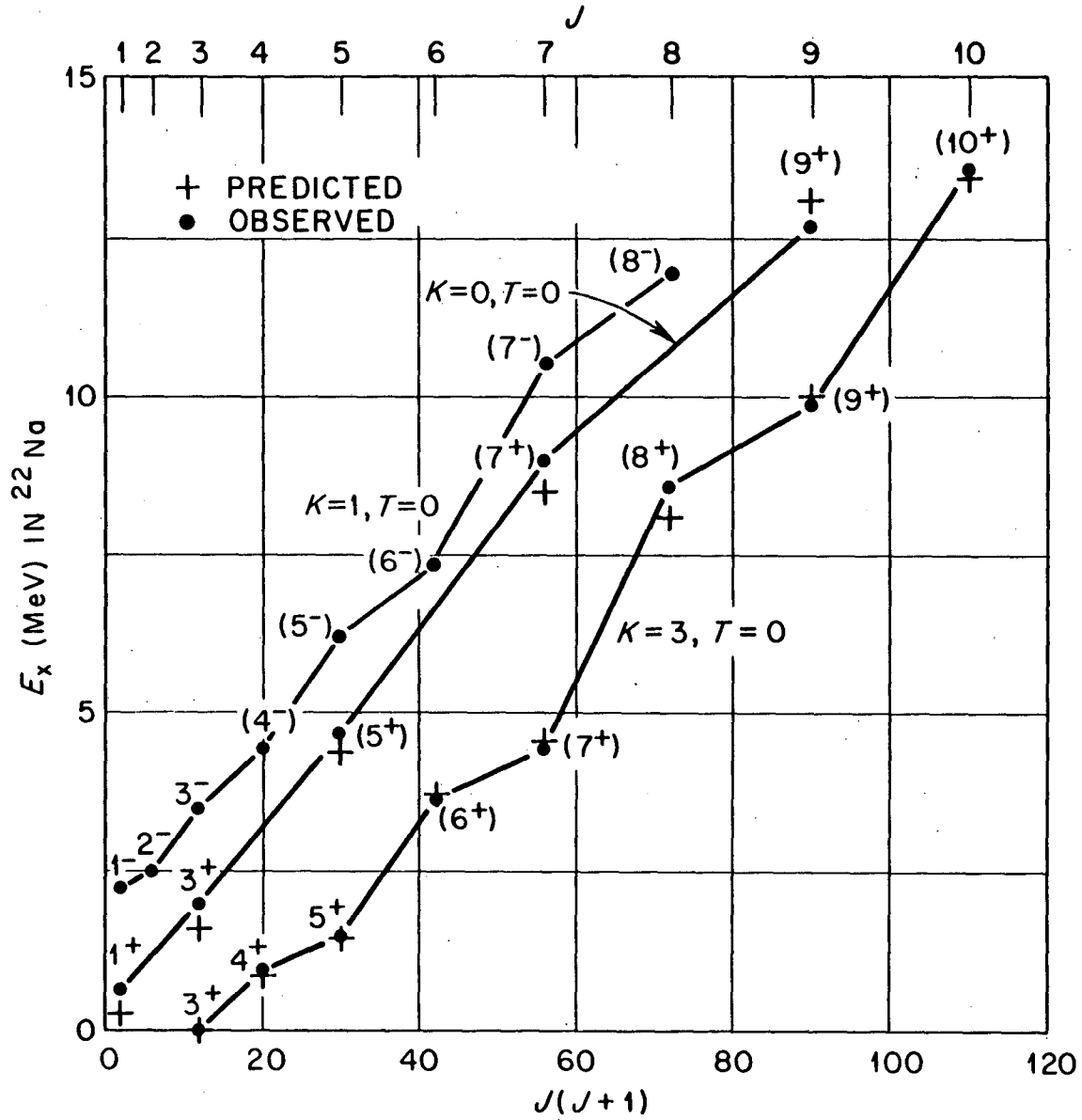


Fig. 19

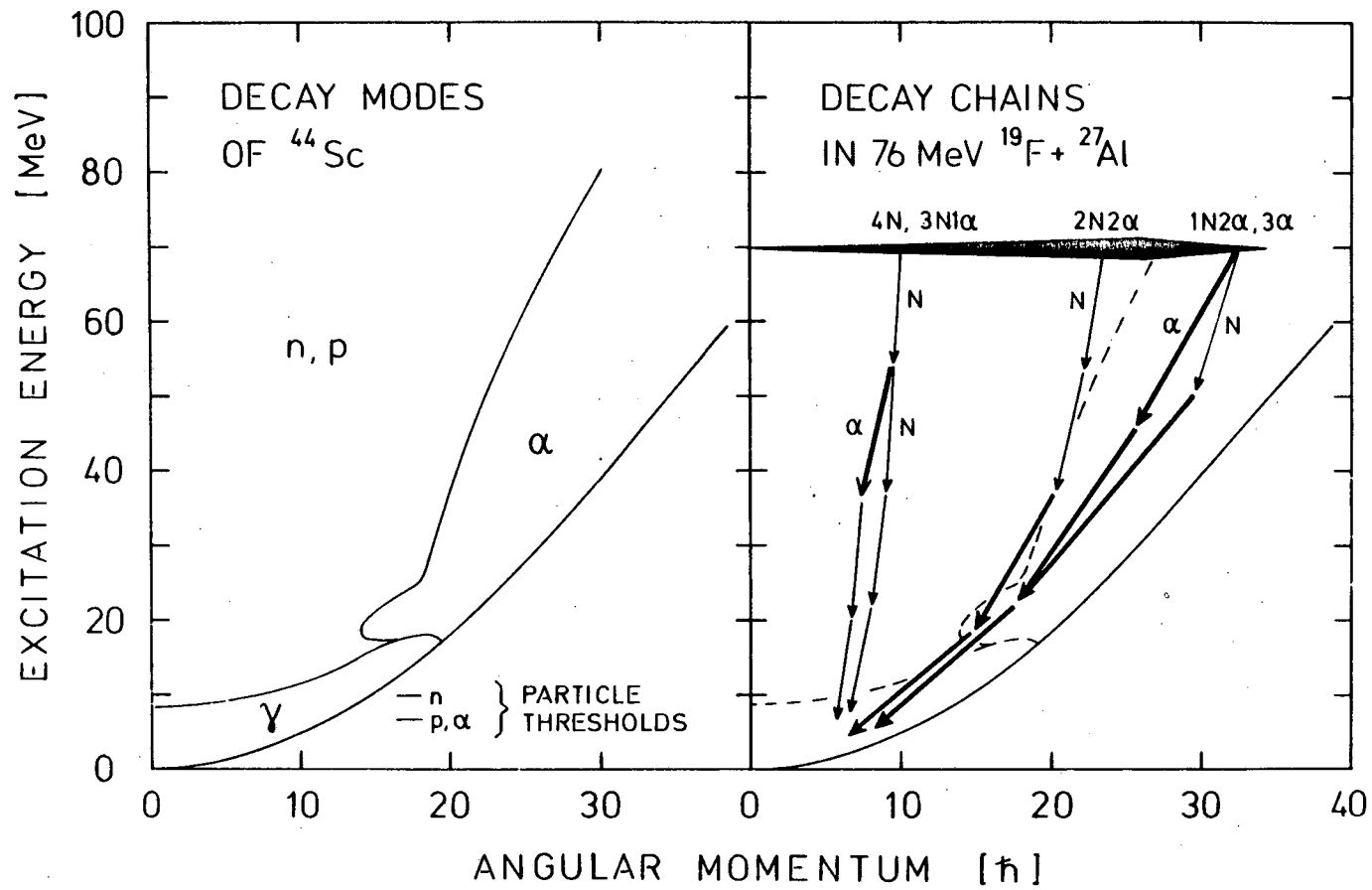


Fig. 20

ORNL-DWG 77-10247

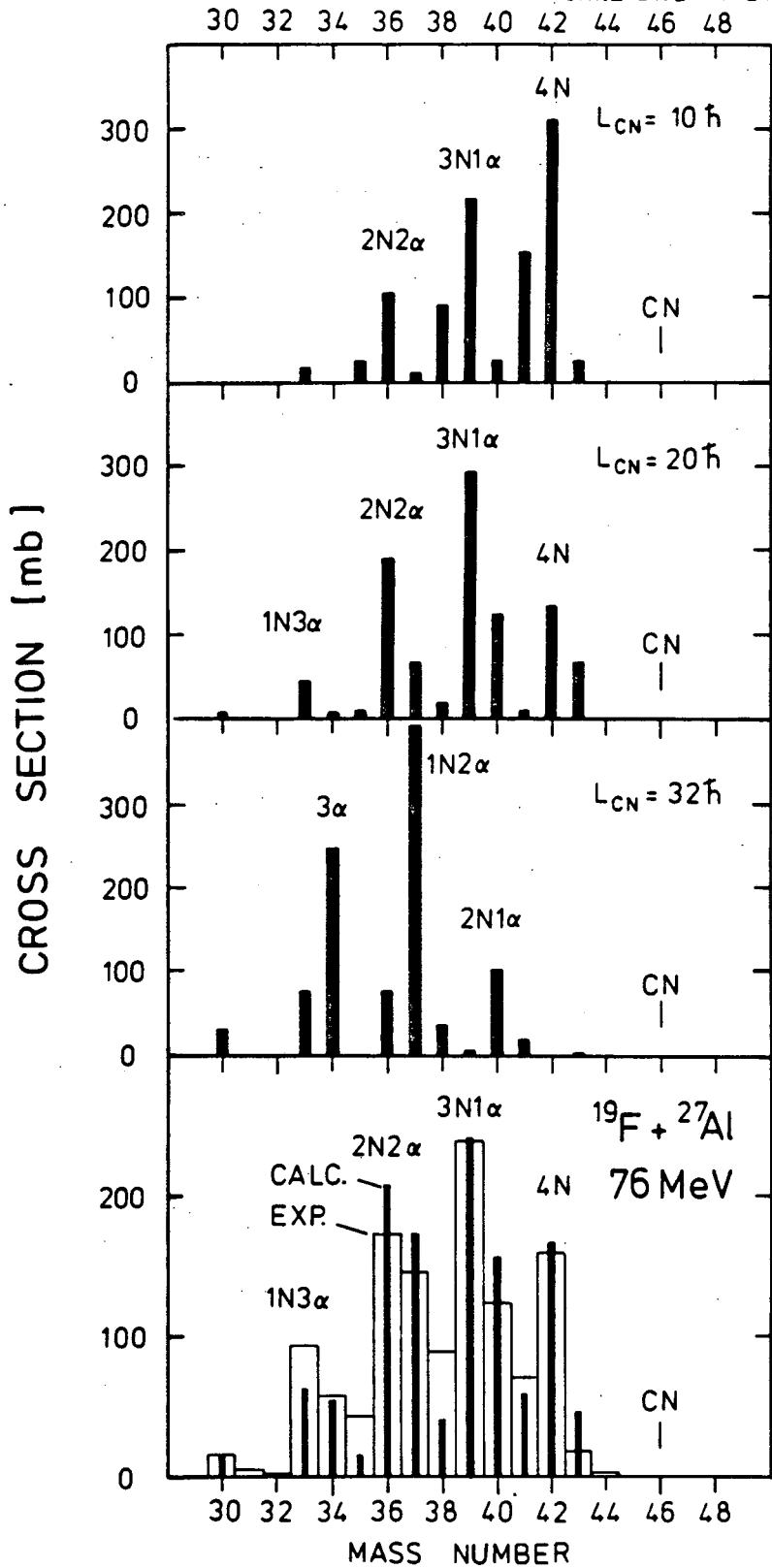
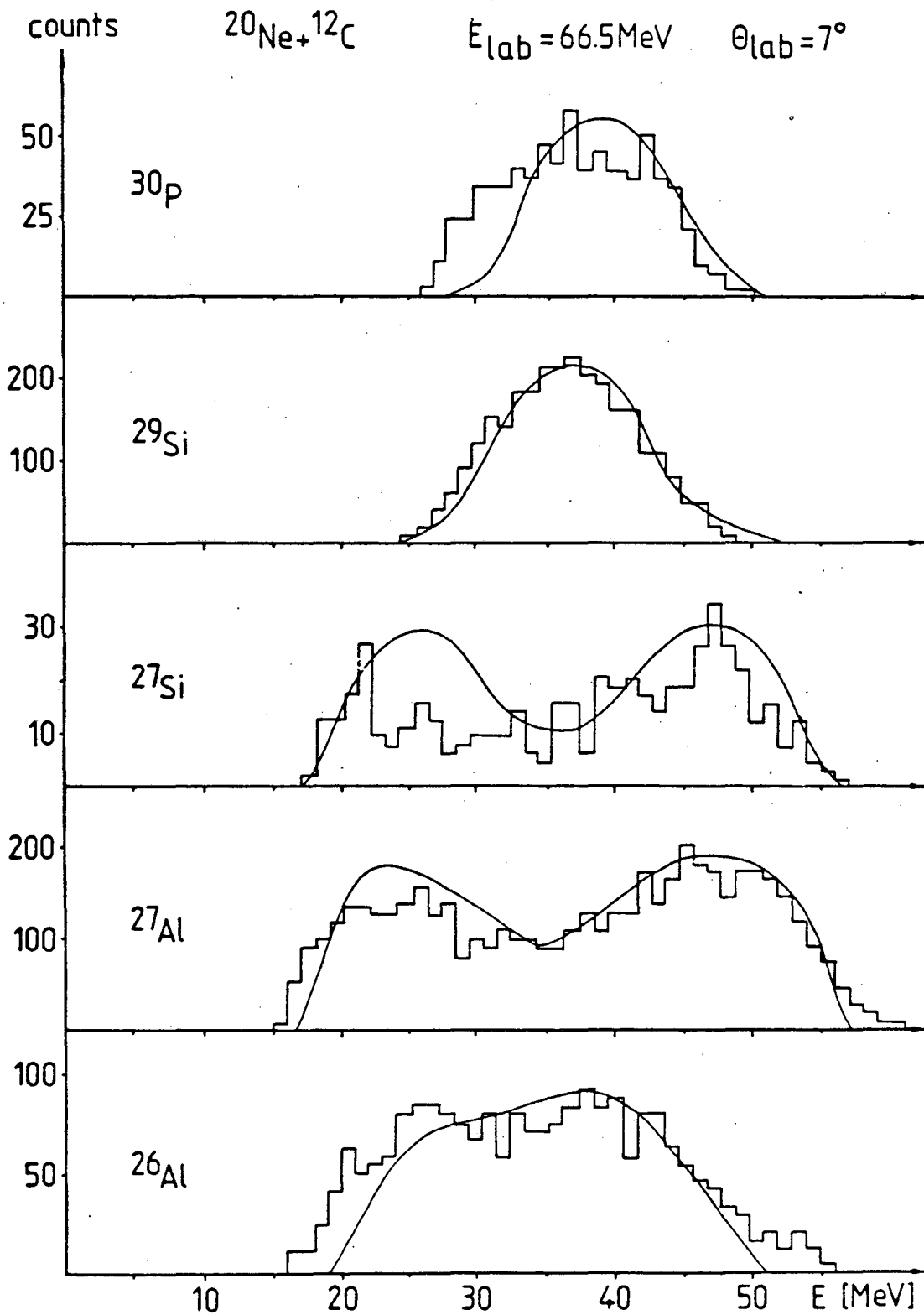


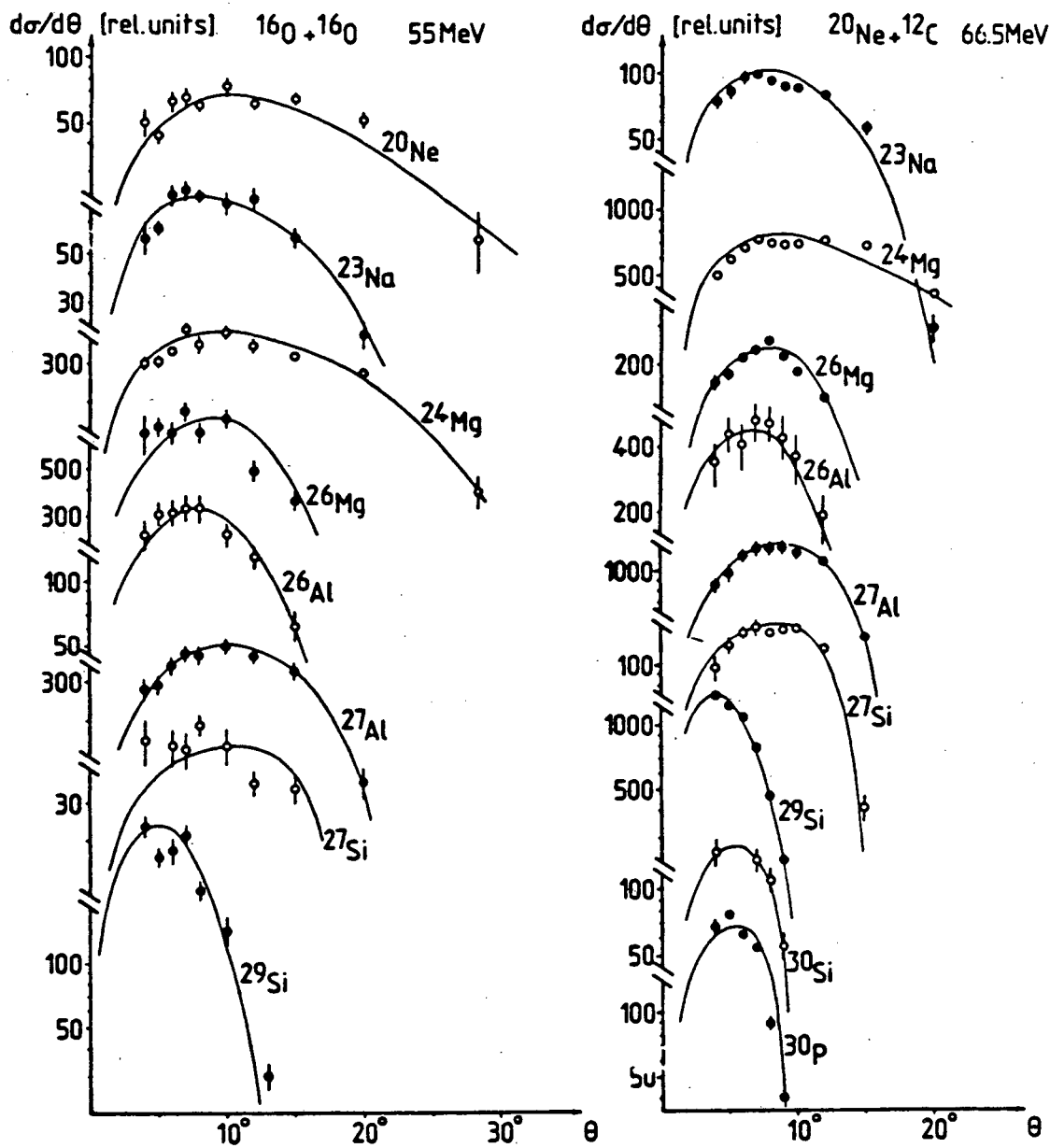
Fig. 21

XBL 814-9108



XBL 814-9295

Fig. 22

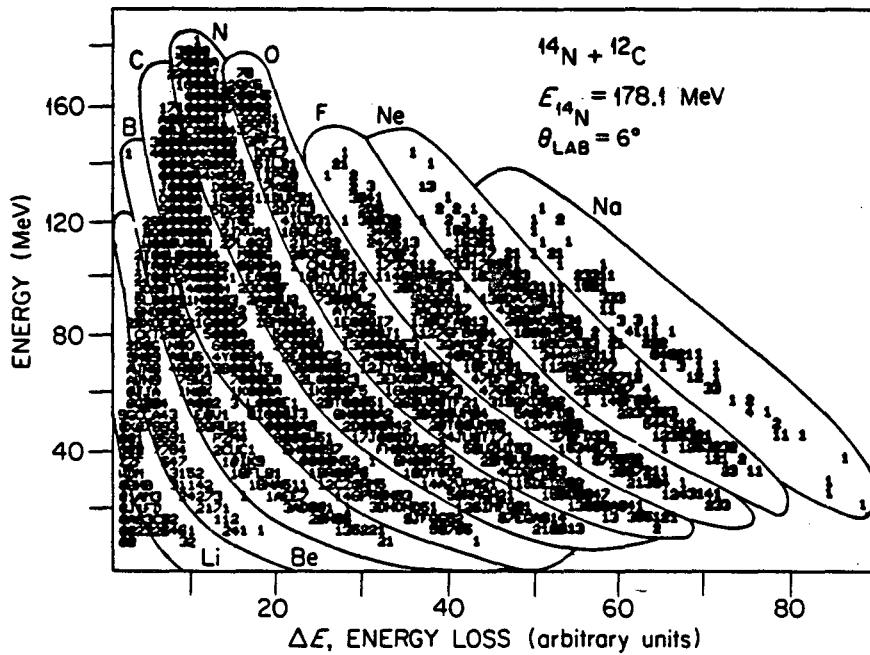
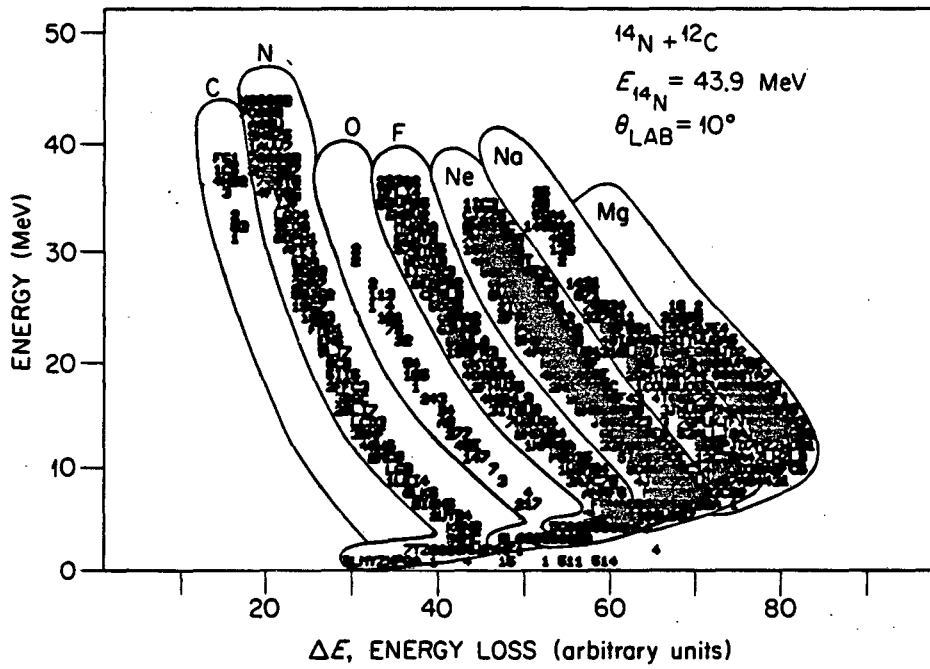


XBL 814-9294

Fig. 23

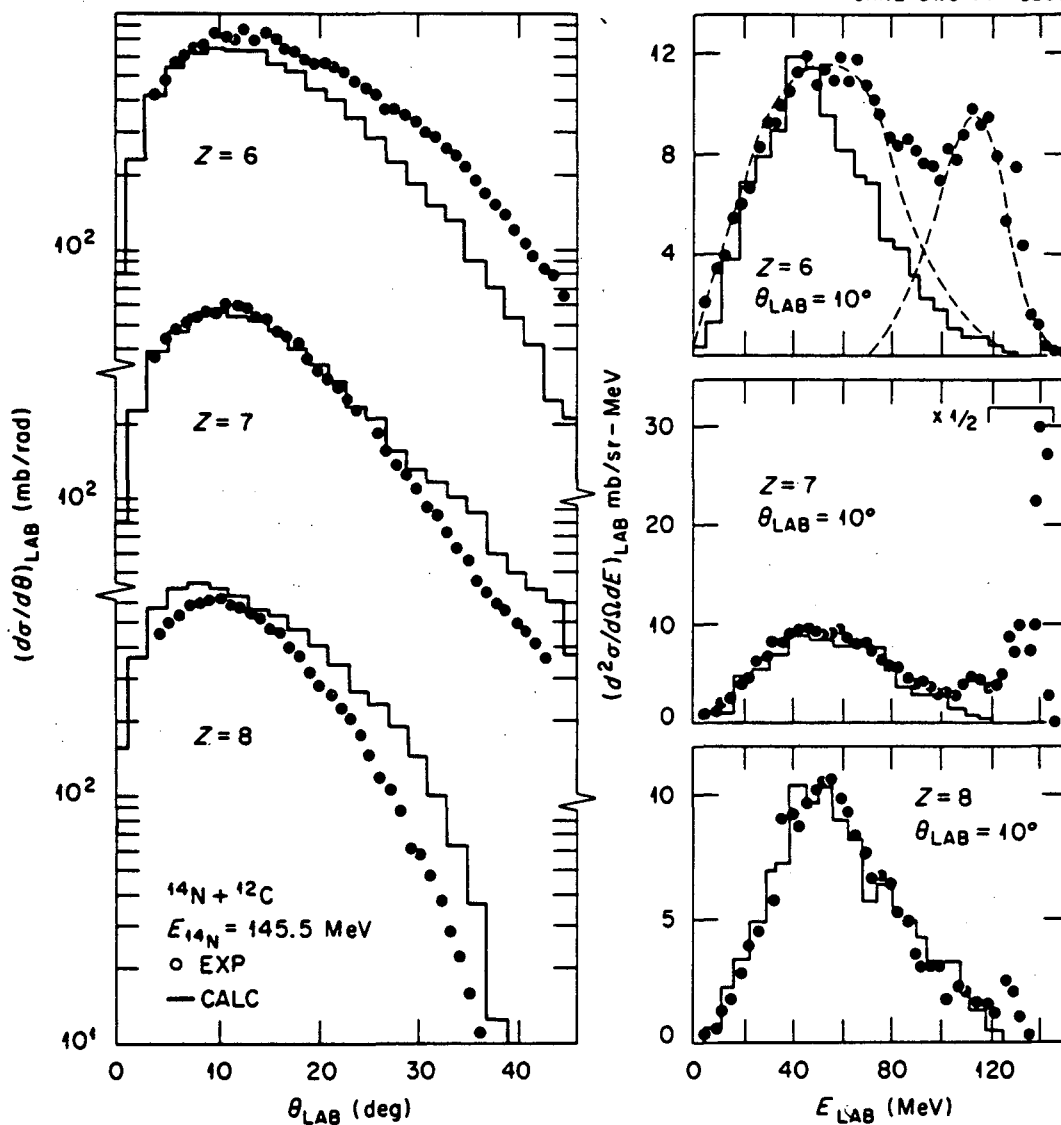
ORNL-DWG 79-19936

TYPICAL E- ΔE DATA
 ΔE (IONIZATION CHAMBER) E (SOLID STATE PSD)



XBL 814-9109

Fig. 24



XBL 814-9107

Fig. 25

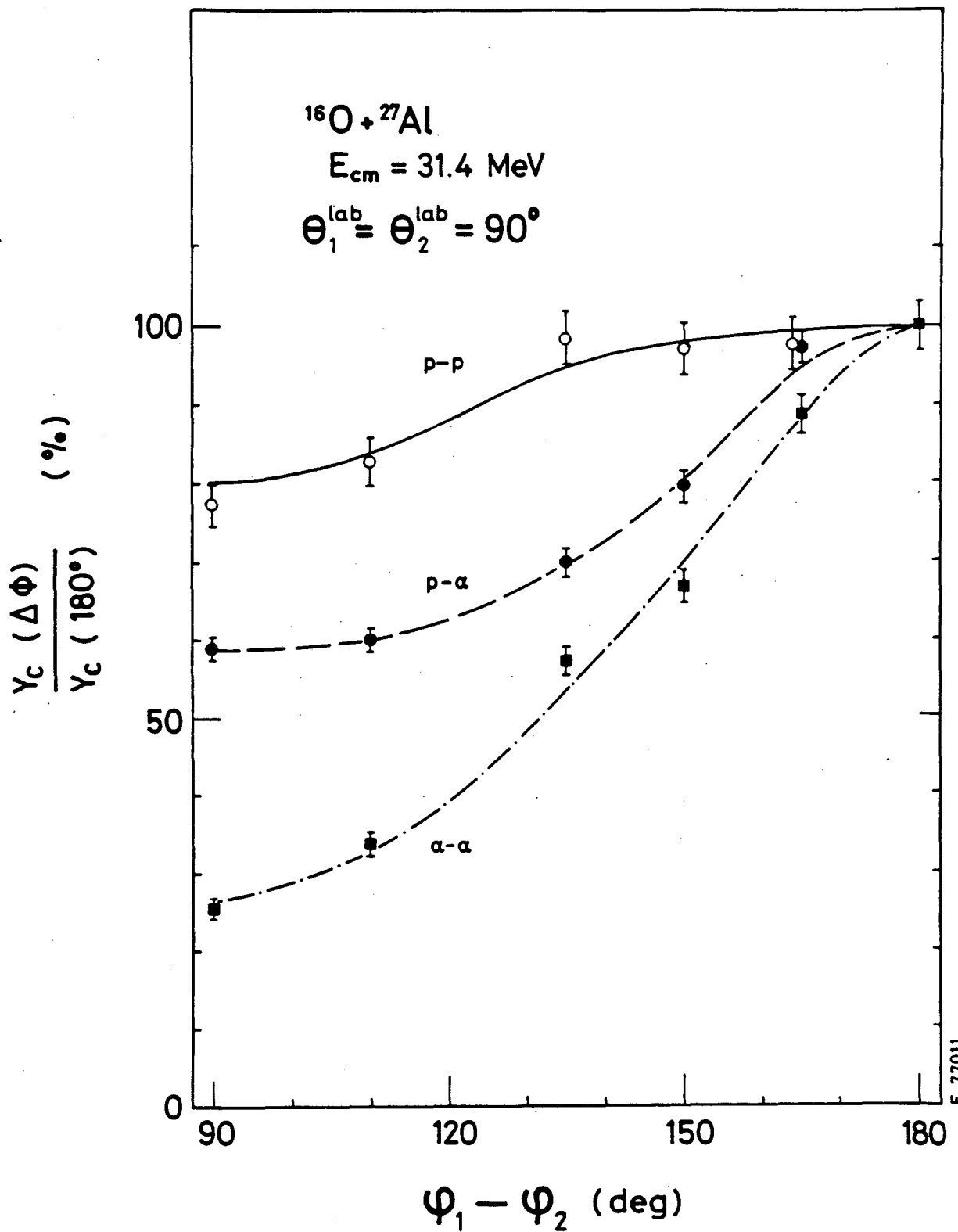


Fig. 26

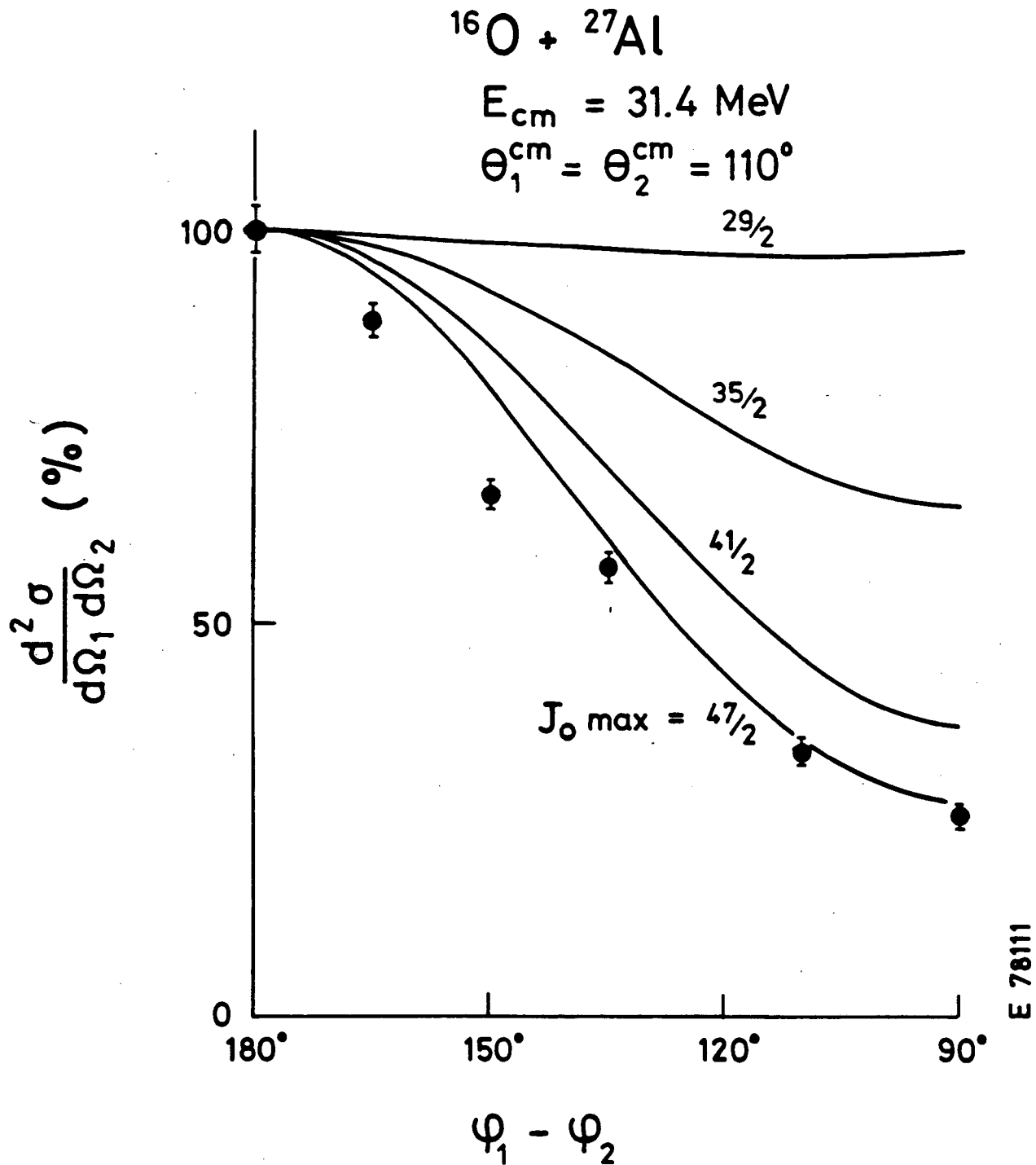


Fig. 27

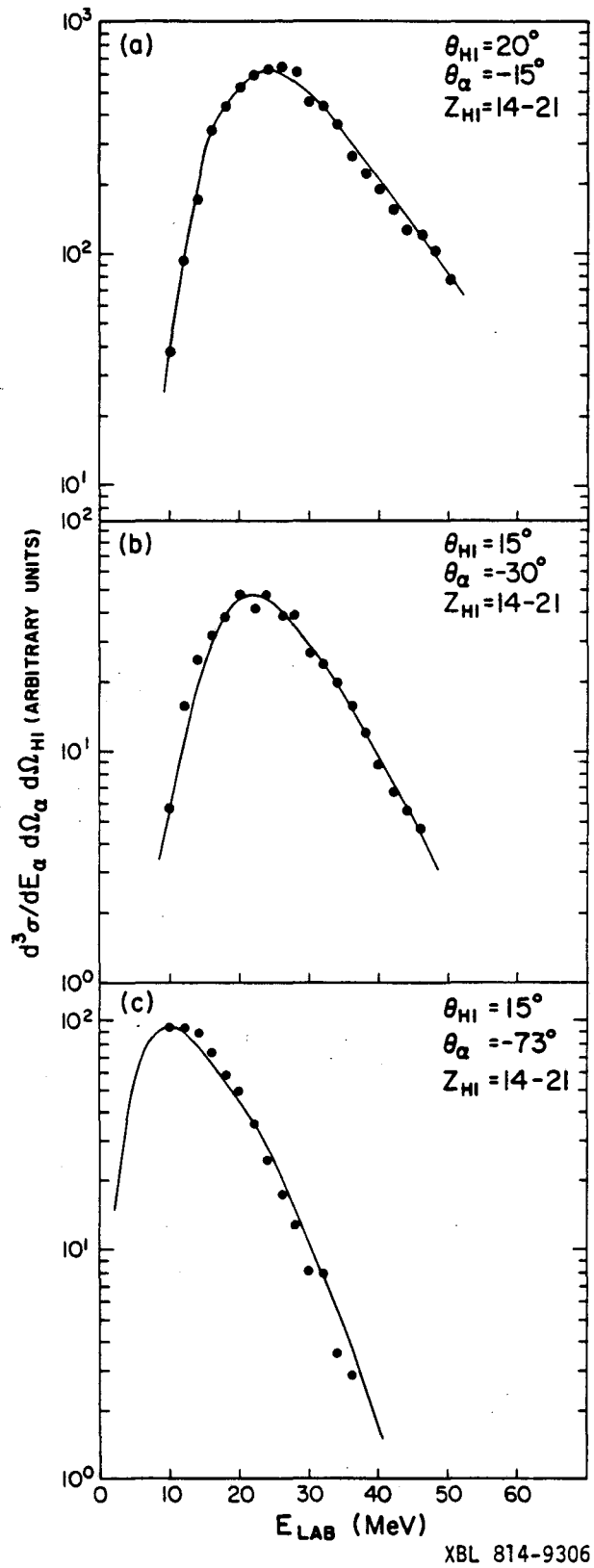


Fig. 28

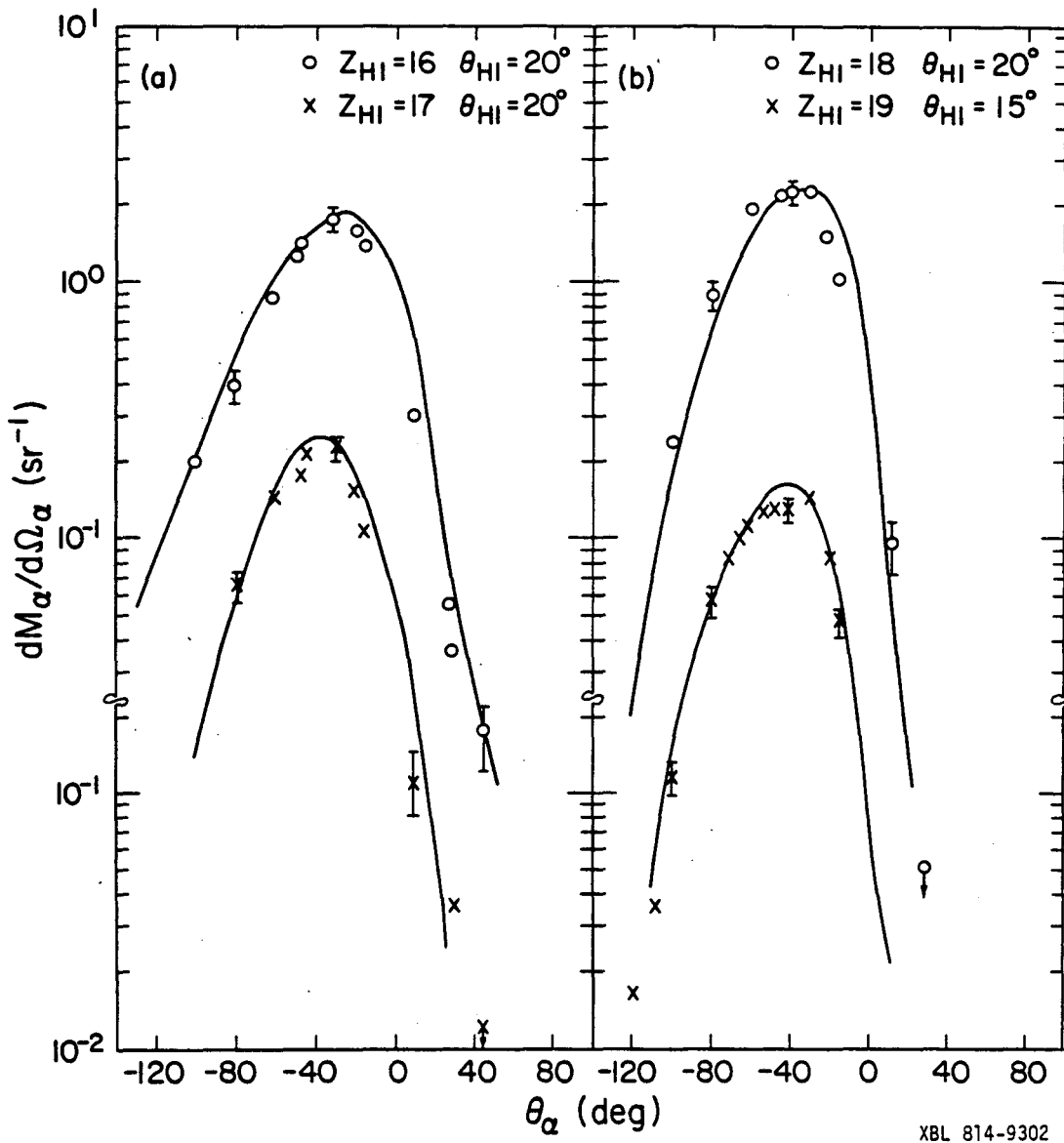


Fig. 29

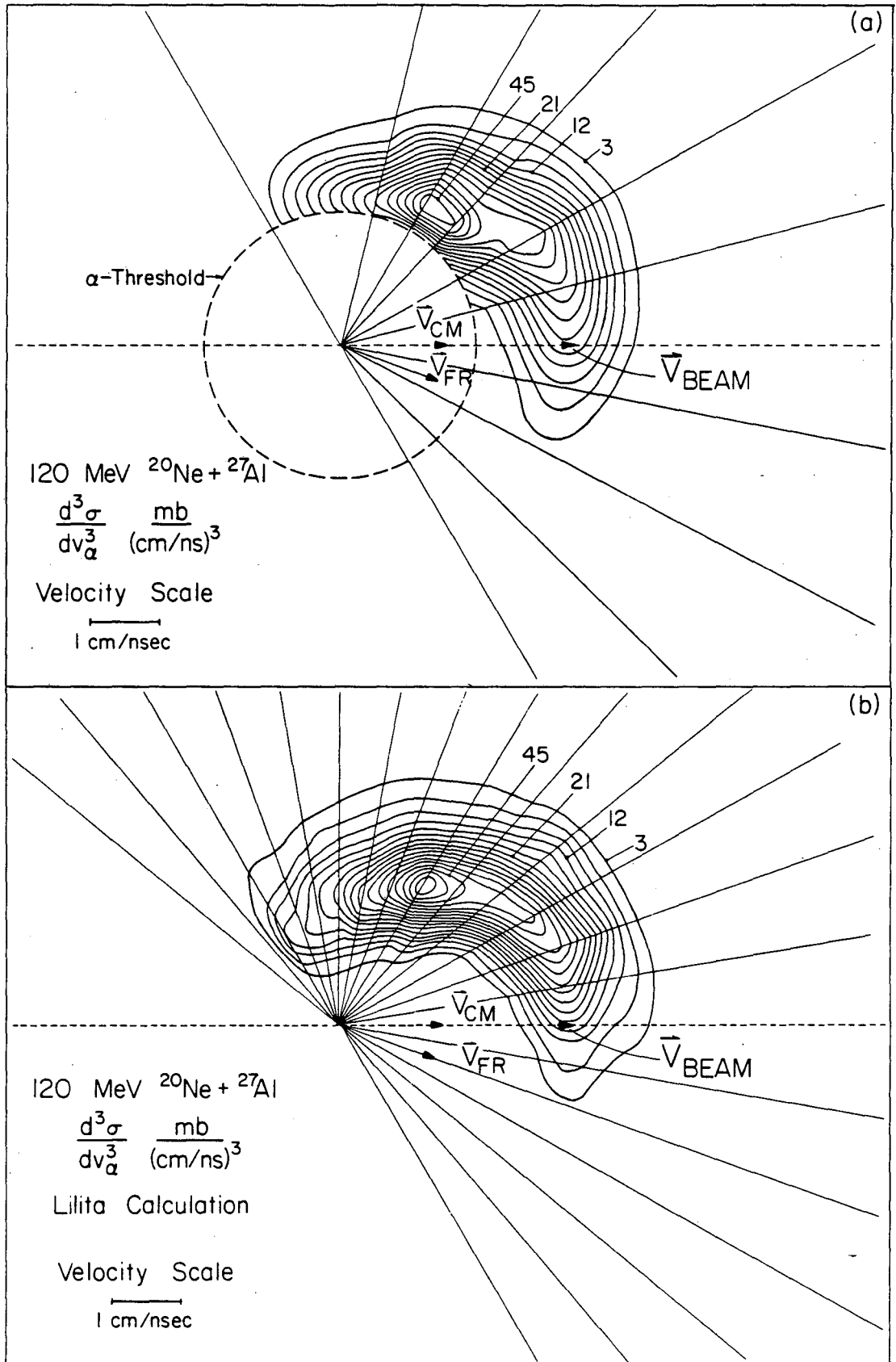
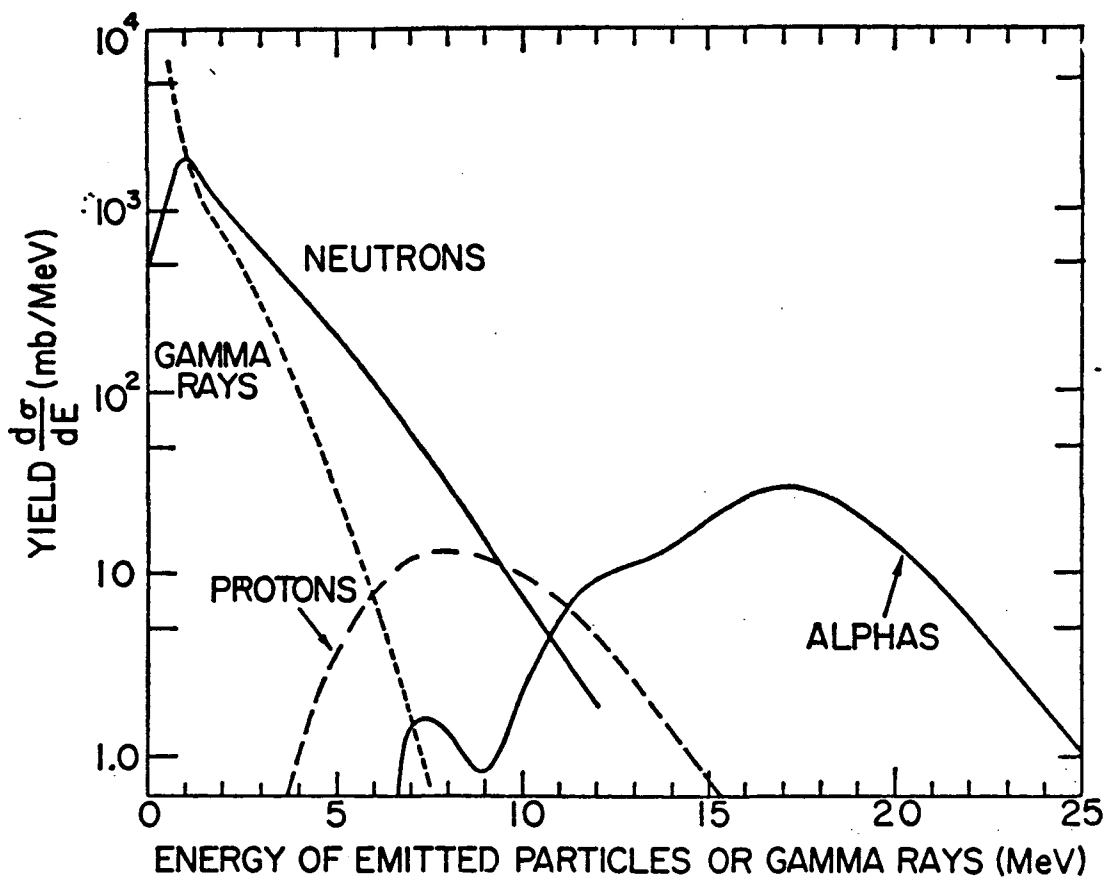


Fig. 30

XBL 814-9303



XBL 814-9164

Fig. 31

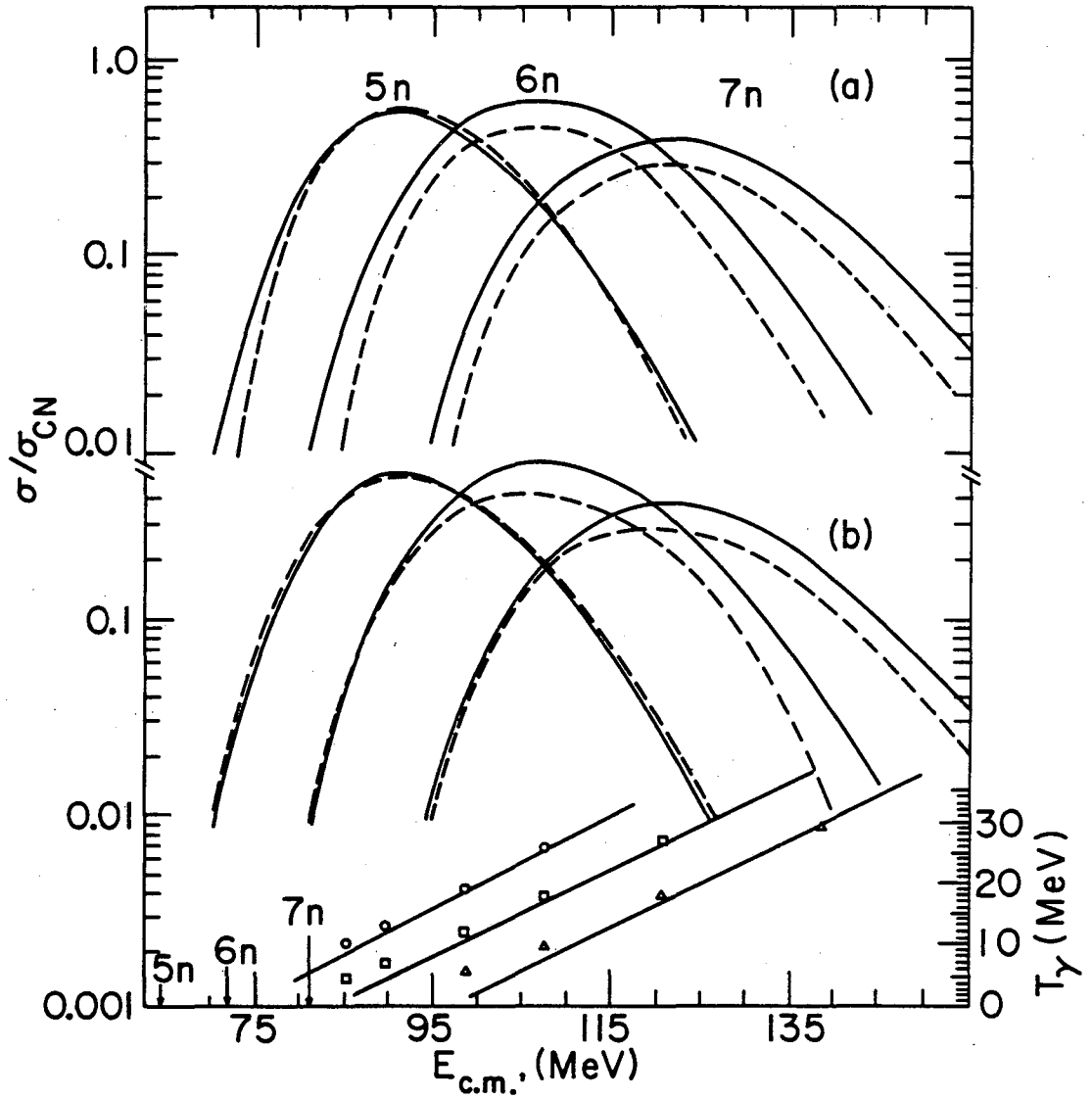


Fig. 32

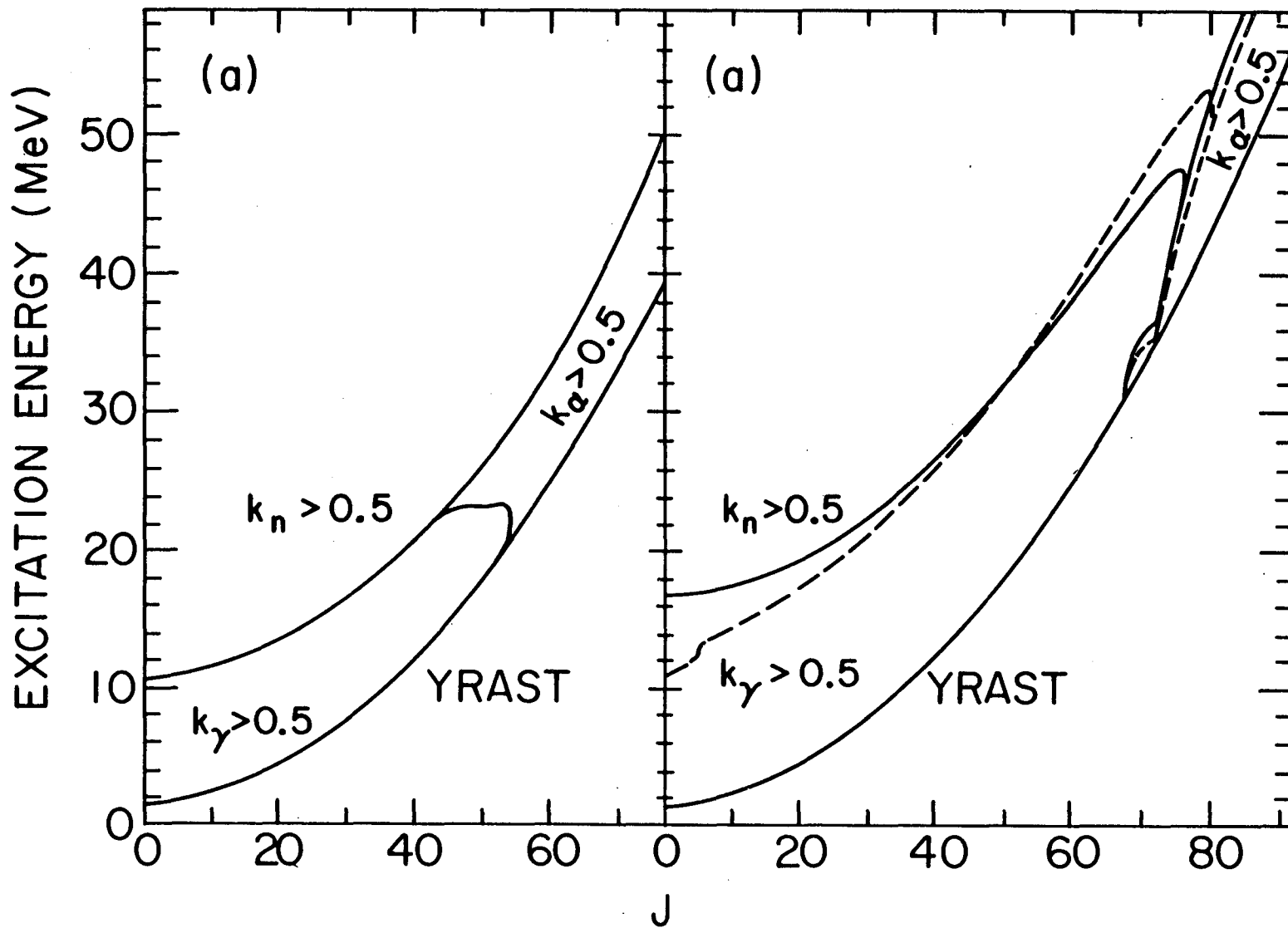
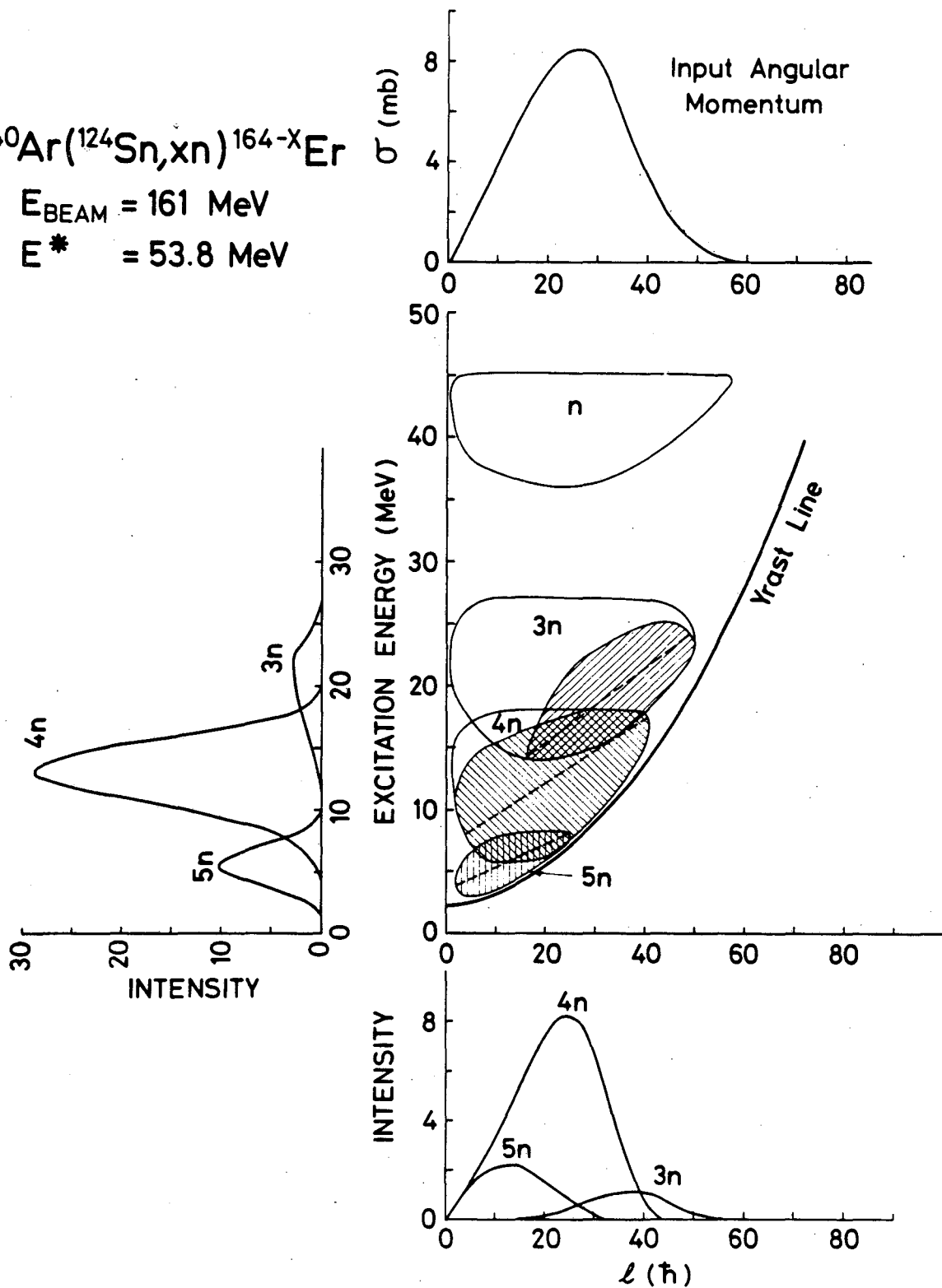


Fig. 33

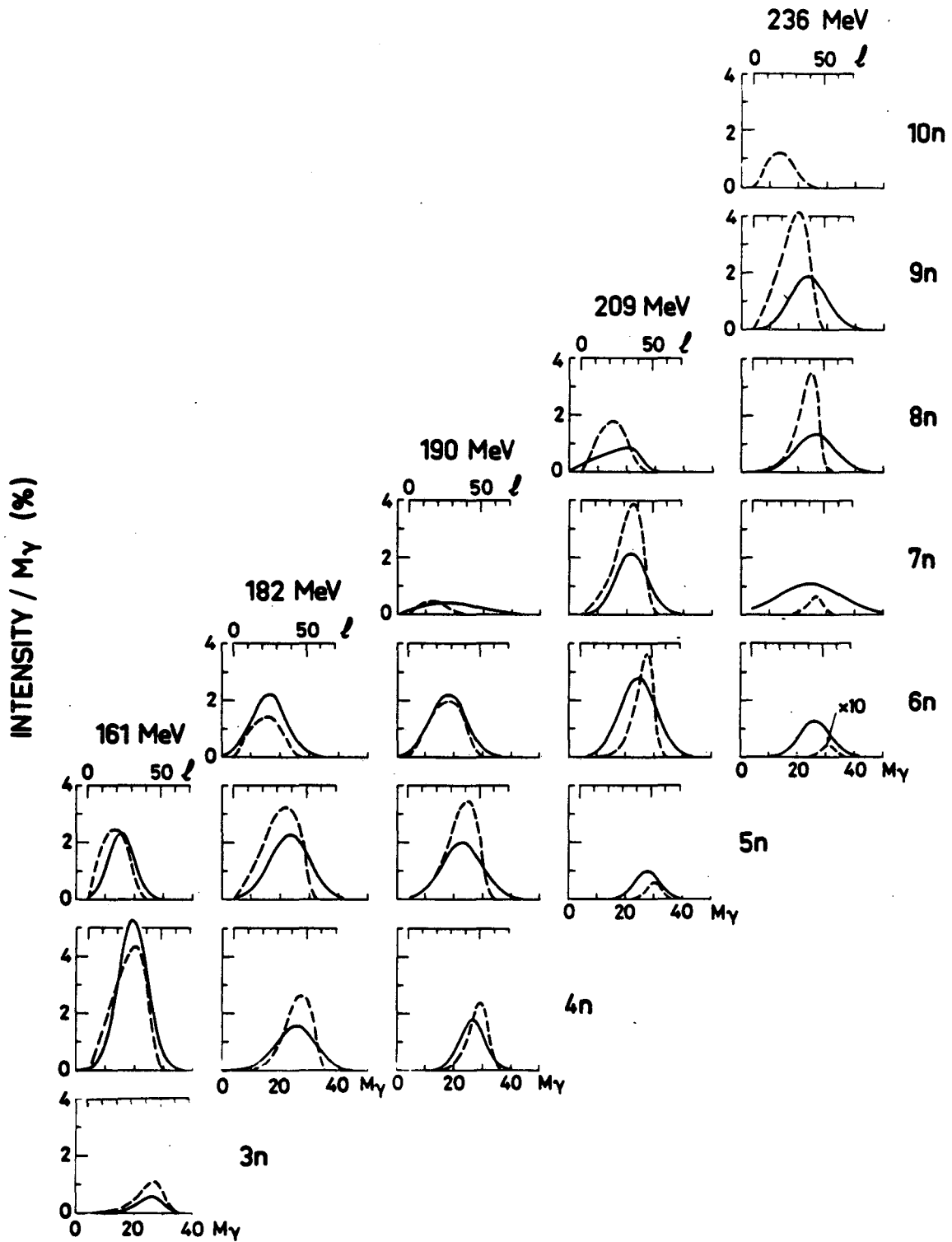
STATISTICAL MODEL CALCULATIONS

$^{40}\text{Ar}(^{124}\text{Sn}, xn)^{164-X}\text{Er}$
 $E_{\text{BEAM}} = 161 \text{ MeV}$
 $E^* = 53.8 \text{ MeV}$



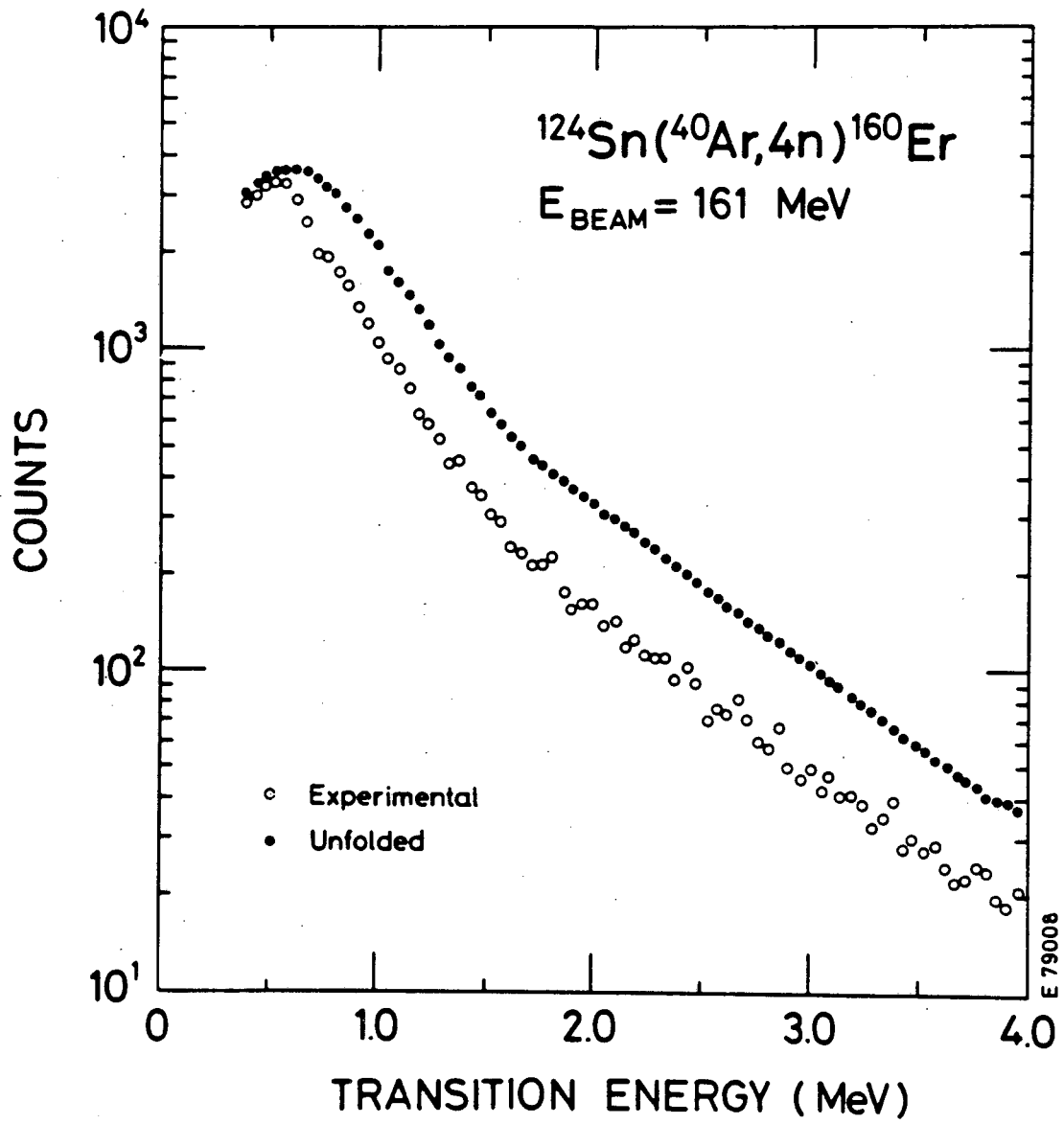
XBL 814-9305

Fig. 34



XBL 814-9300

Fig. 35



XBL 814-9301

Fig. 36

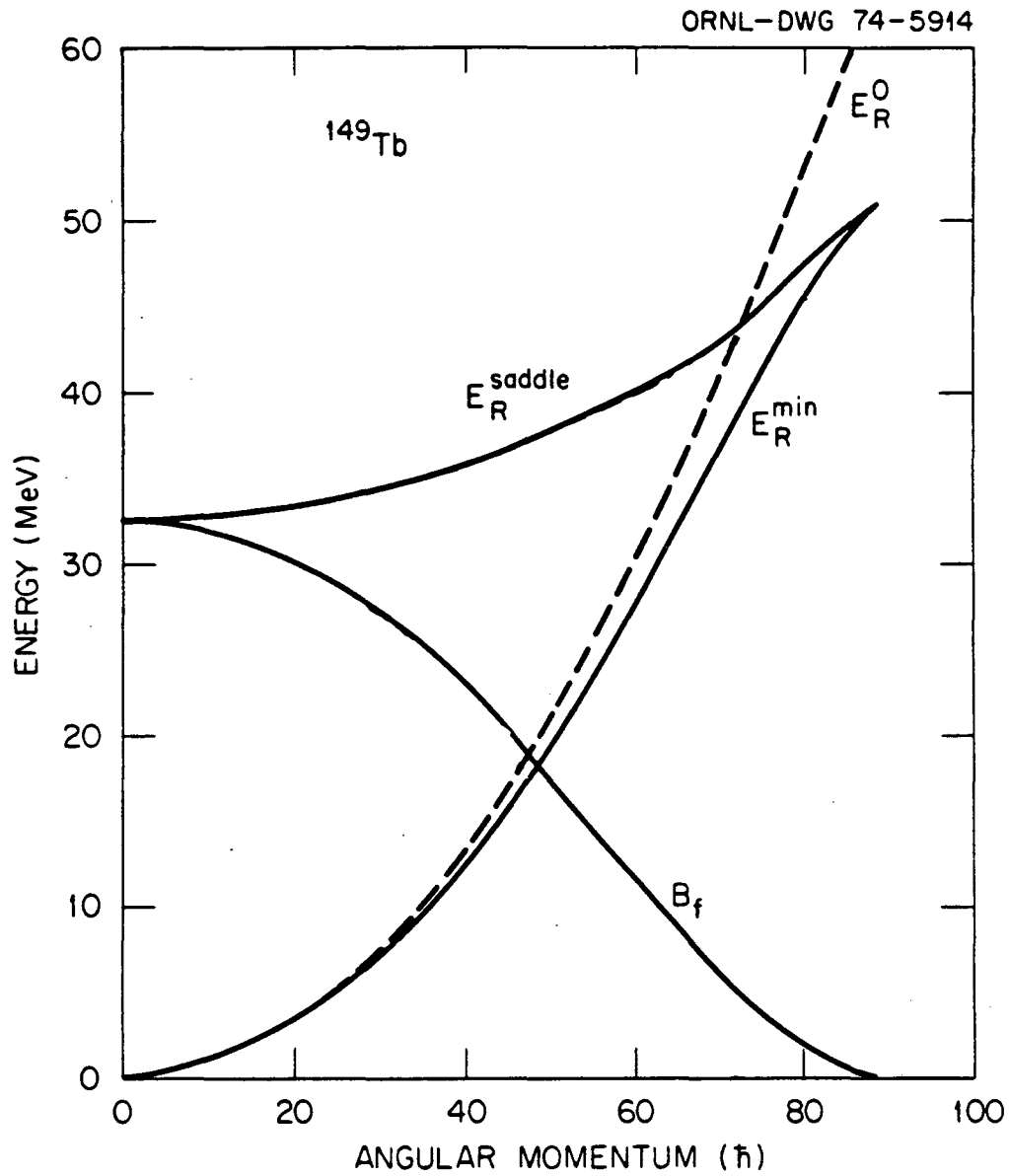


Fig. 37

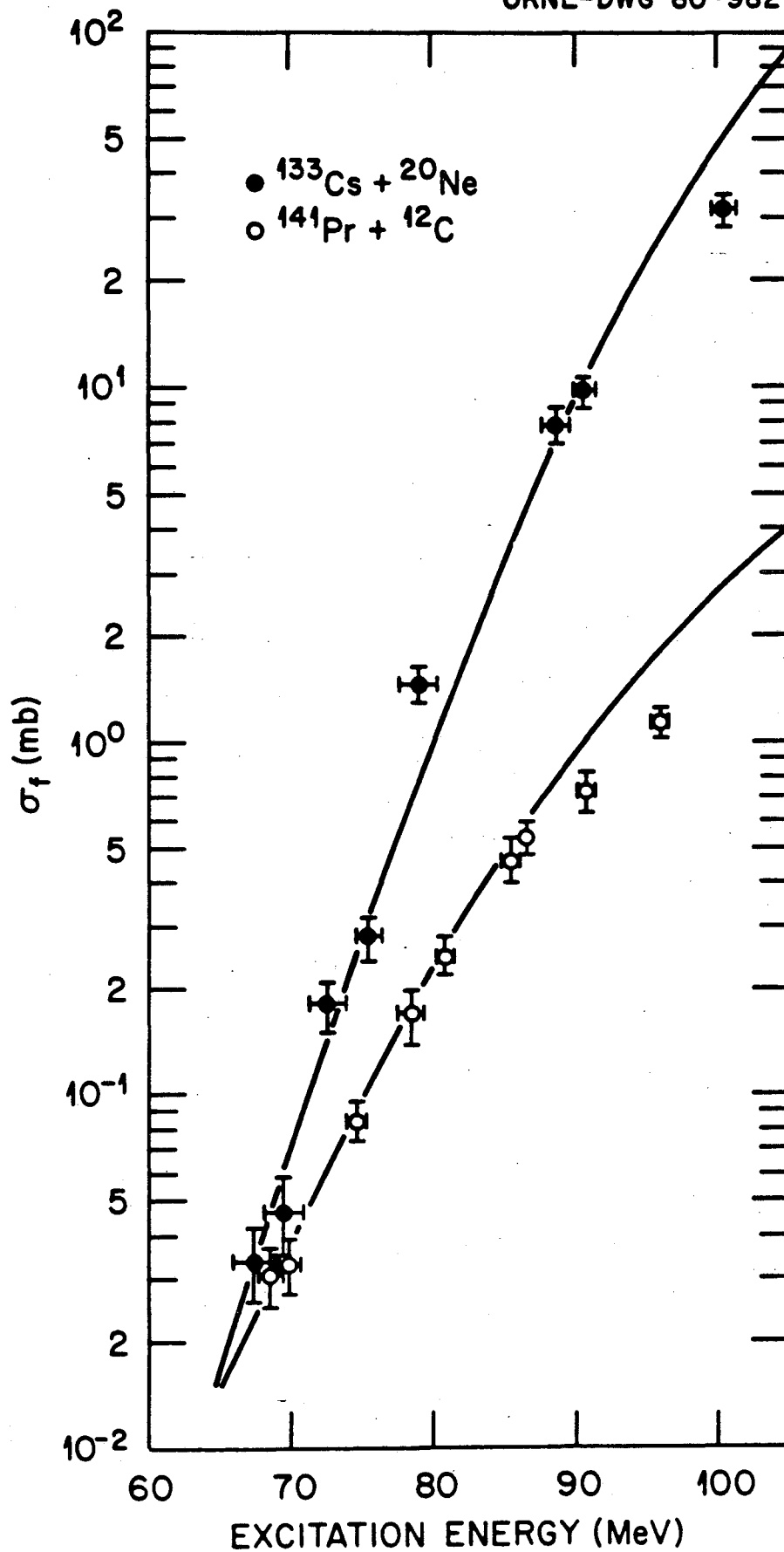


Fig. 38

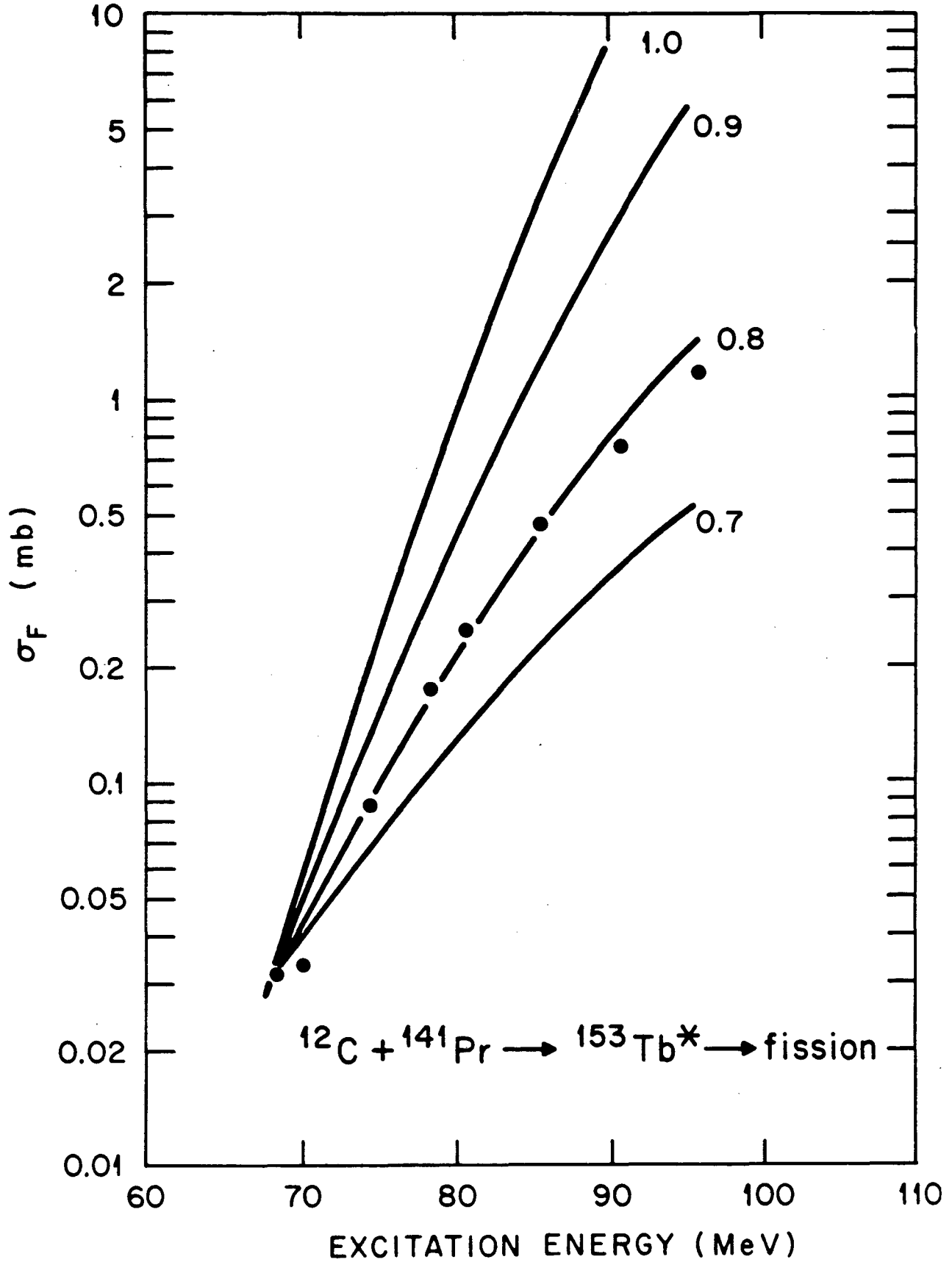
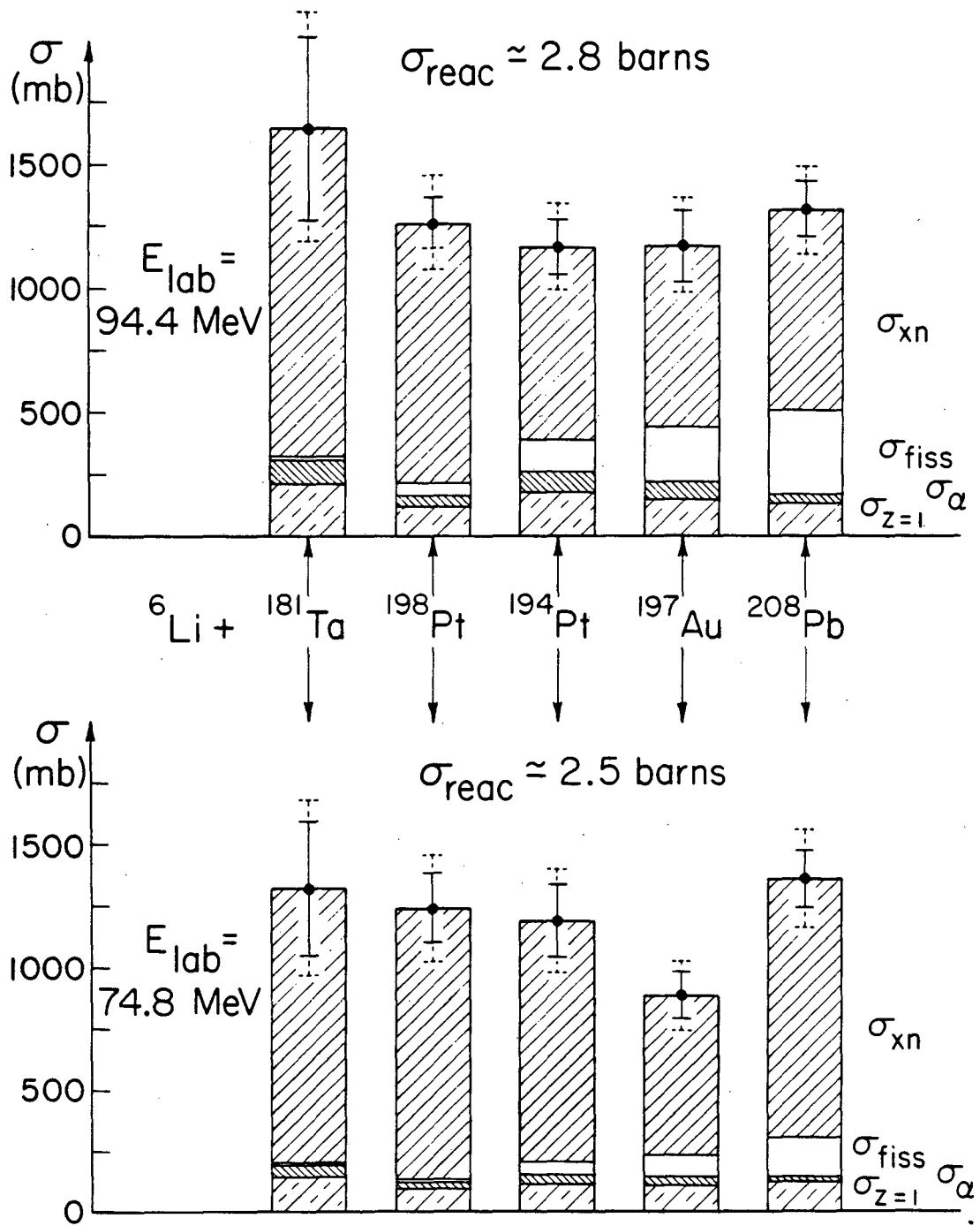


Fig. 39



XBL 814-9298

Fig. 40

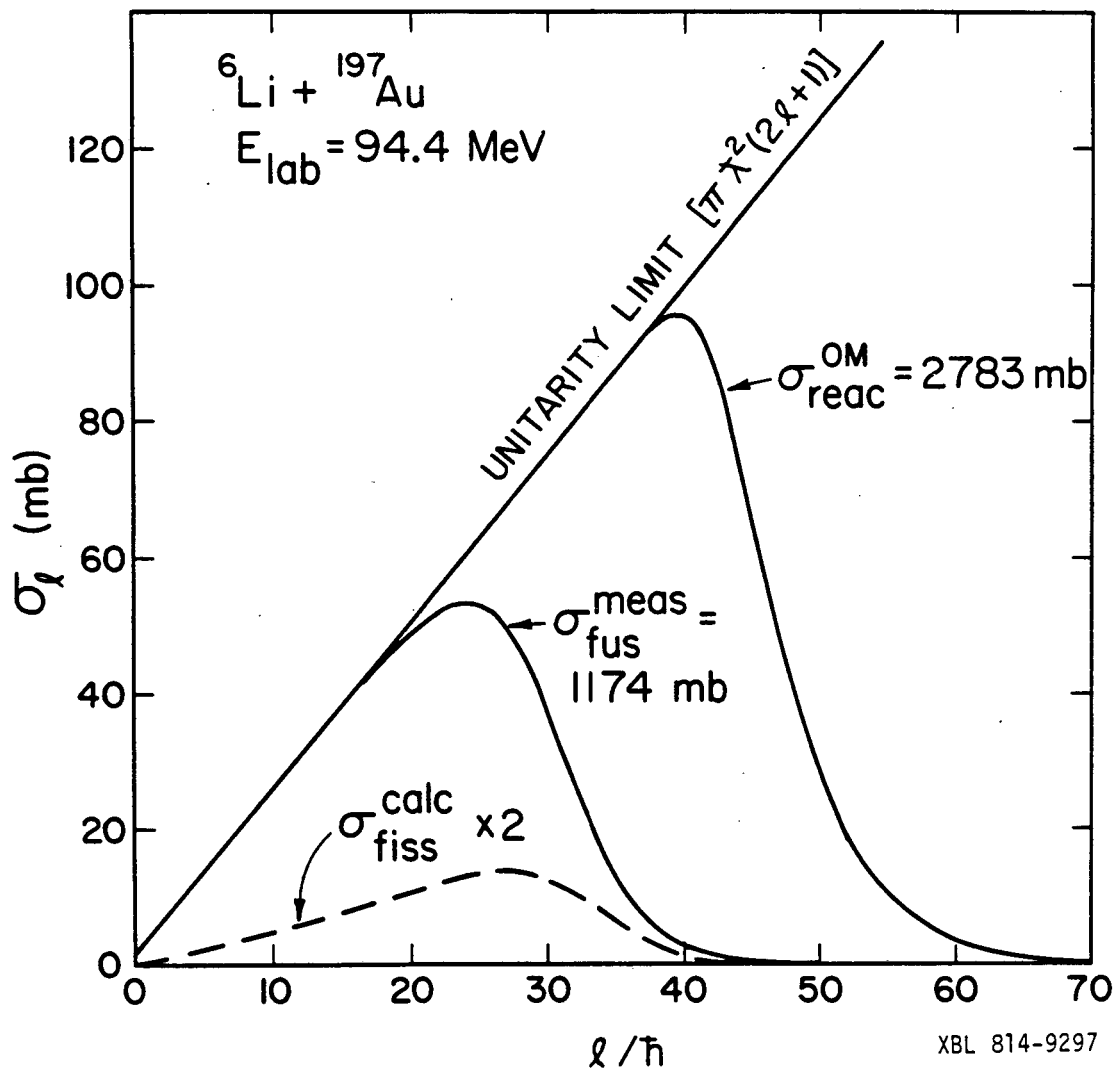


Fig. 41

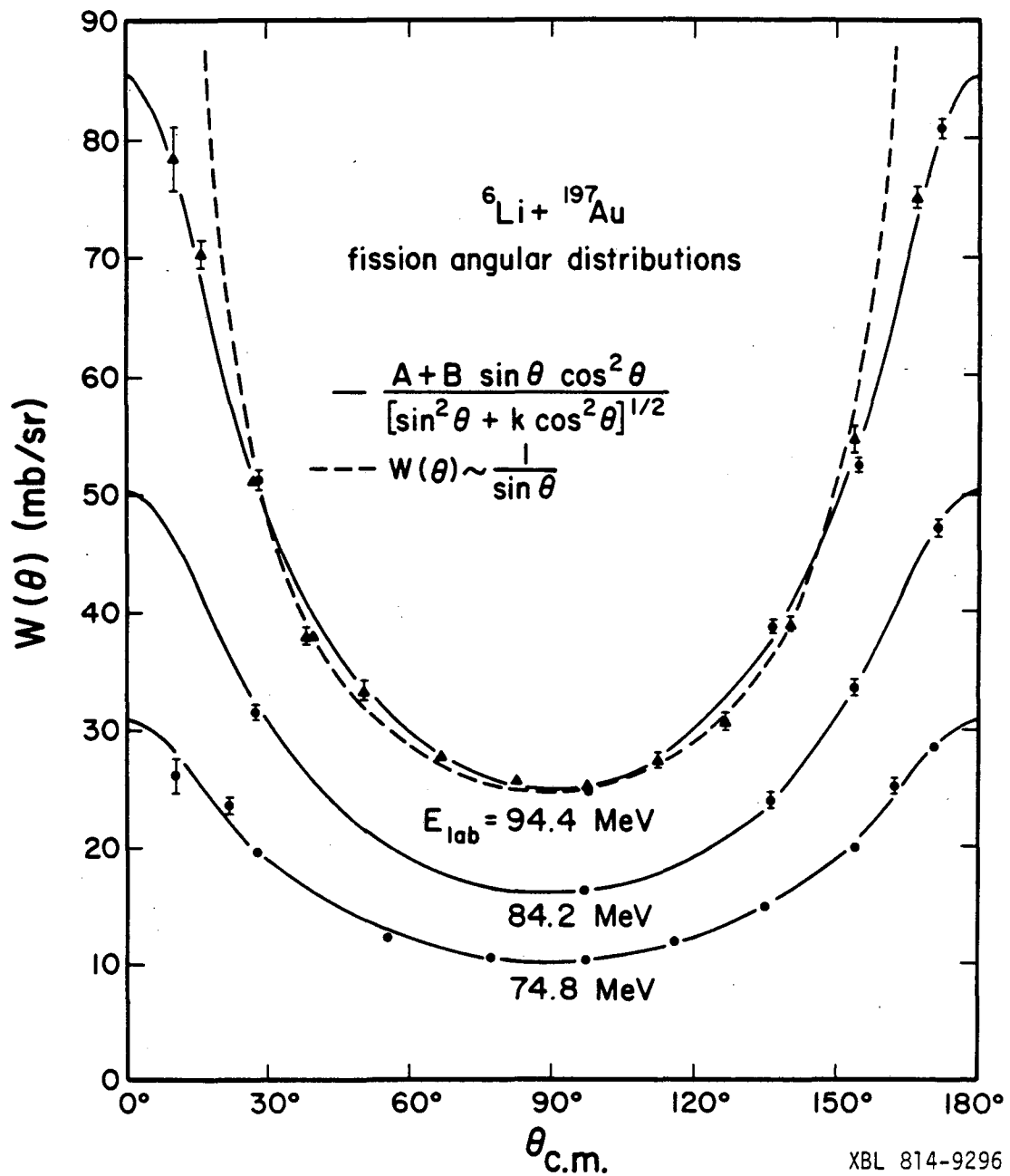
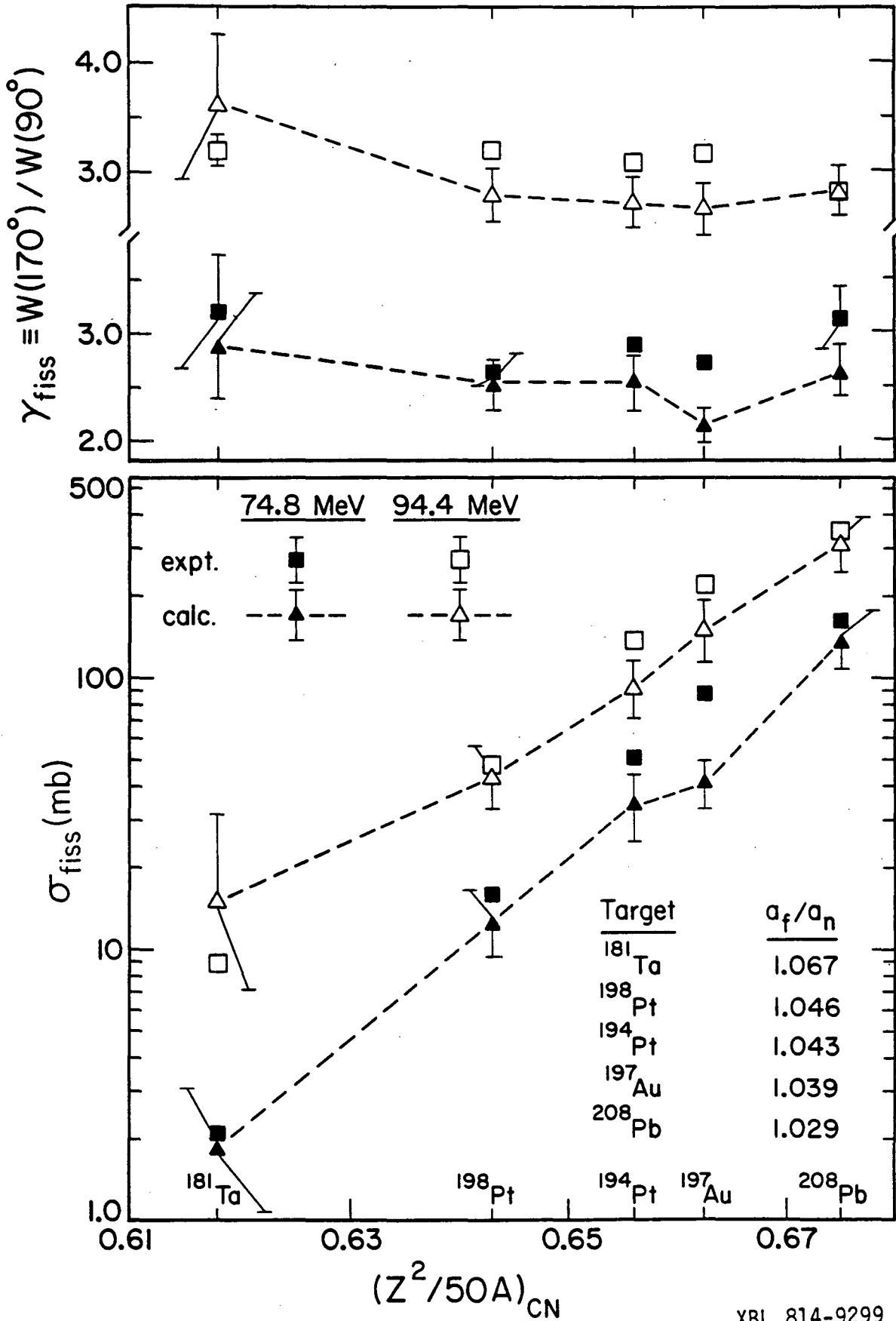


Fig. 42



XBL 814-9299

Fig. 43

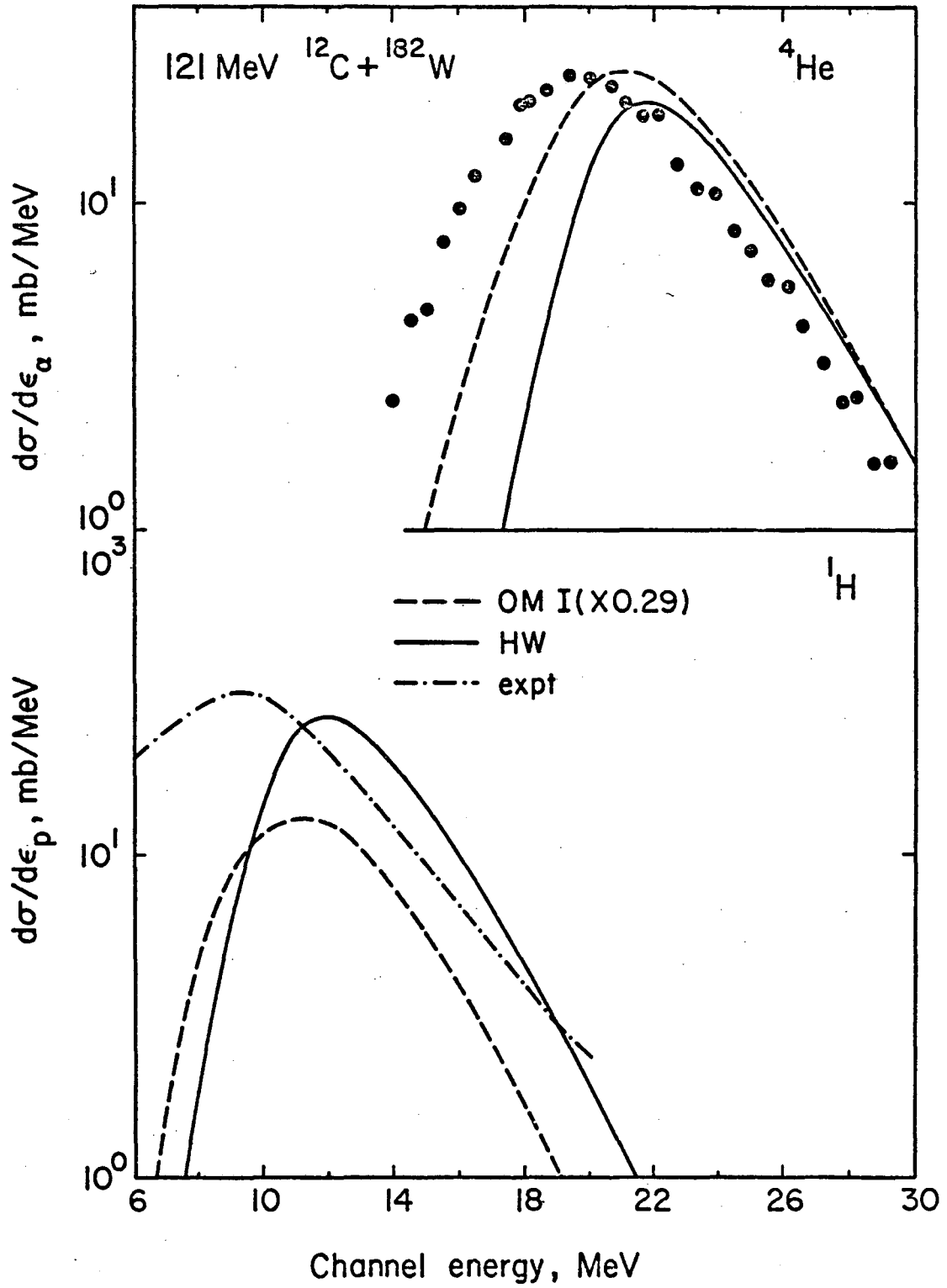


Fig. 44

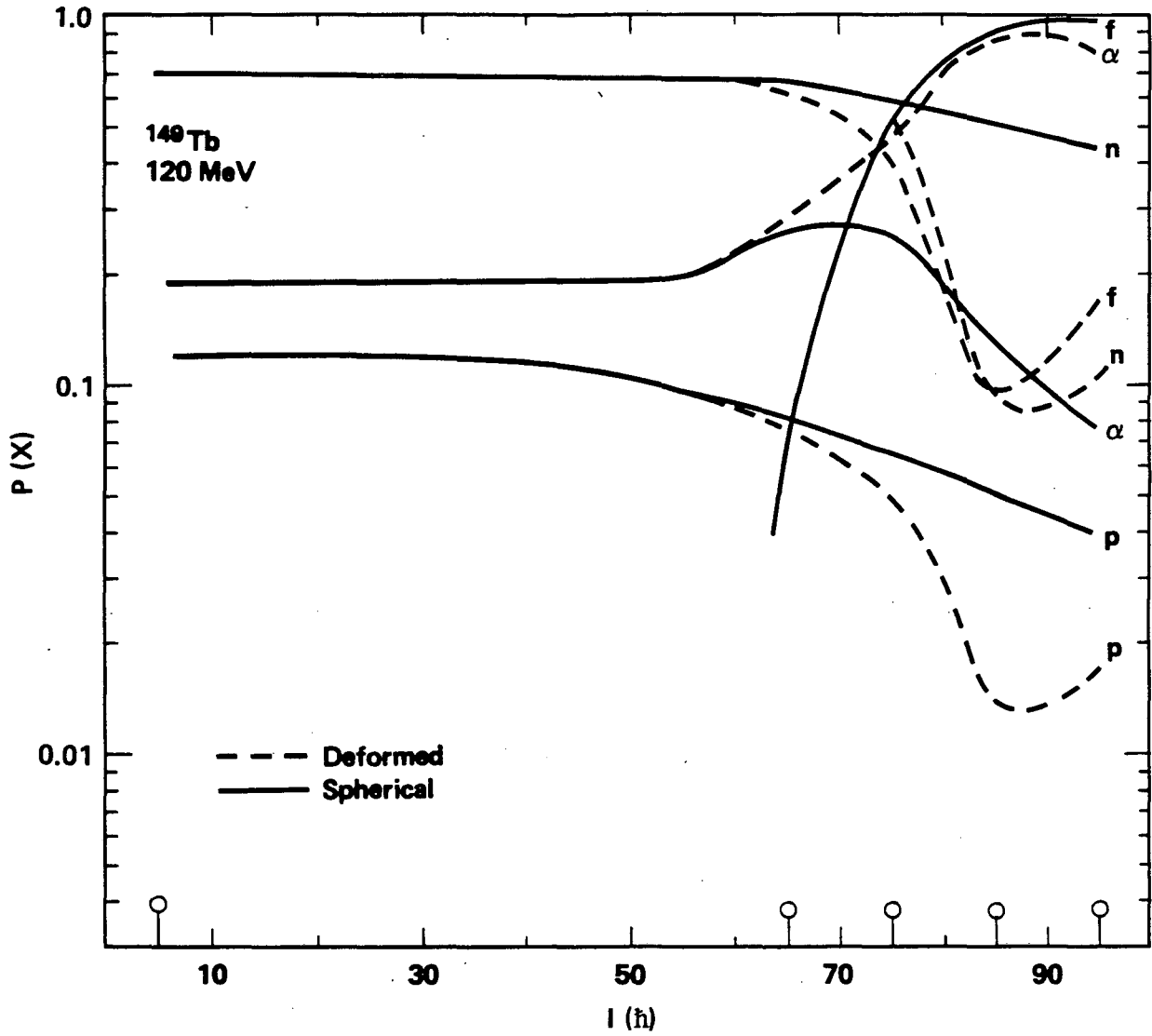


Fig. 45

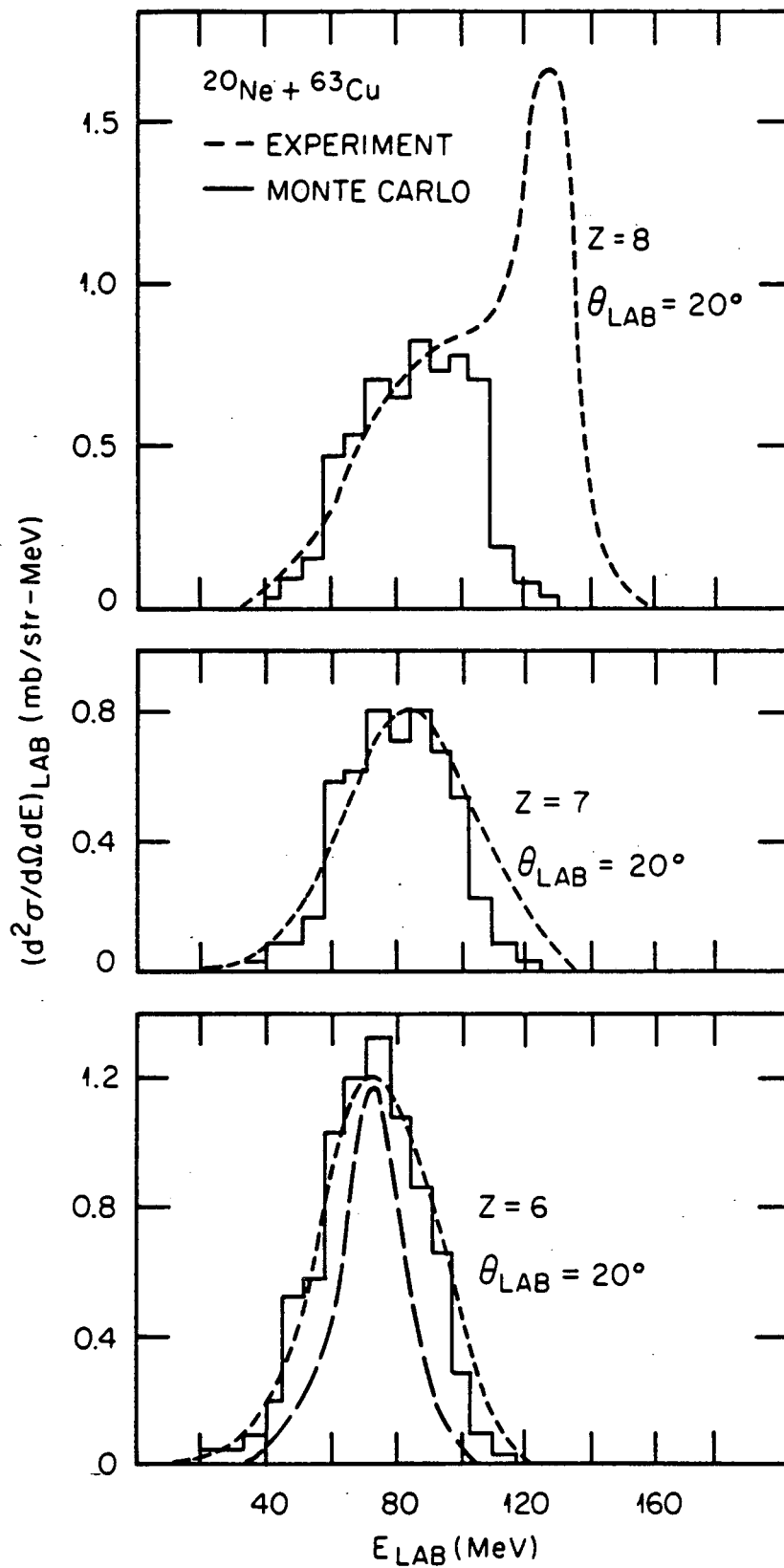


Fig. 47

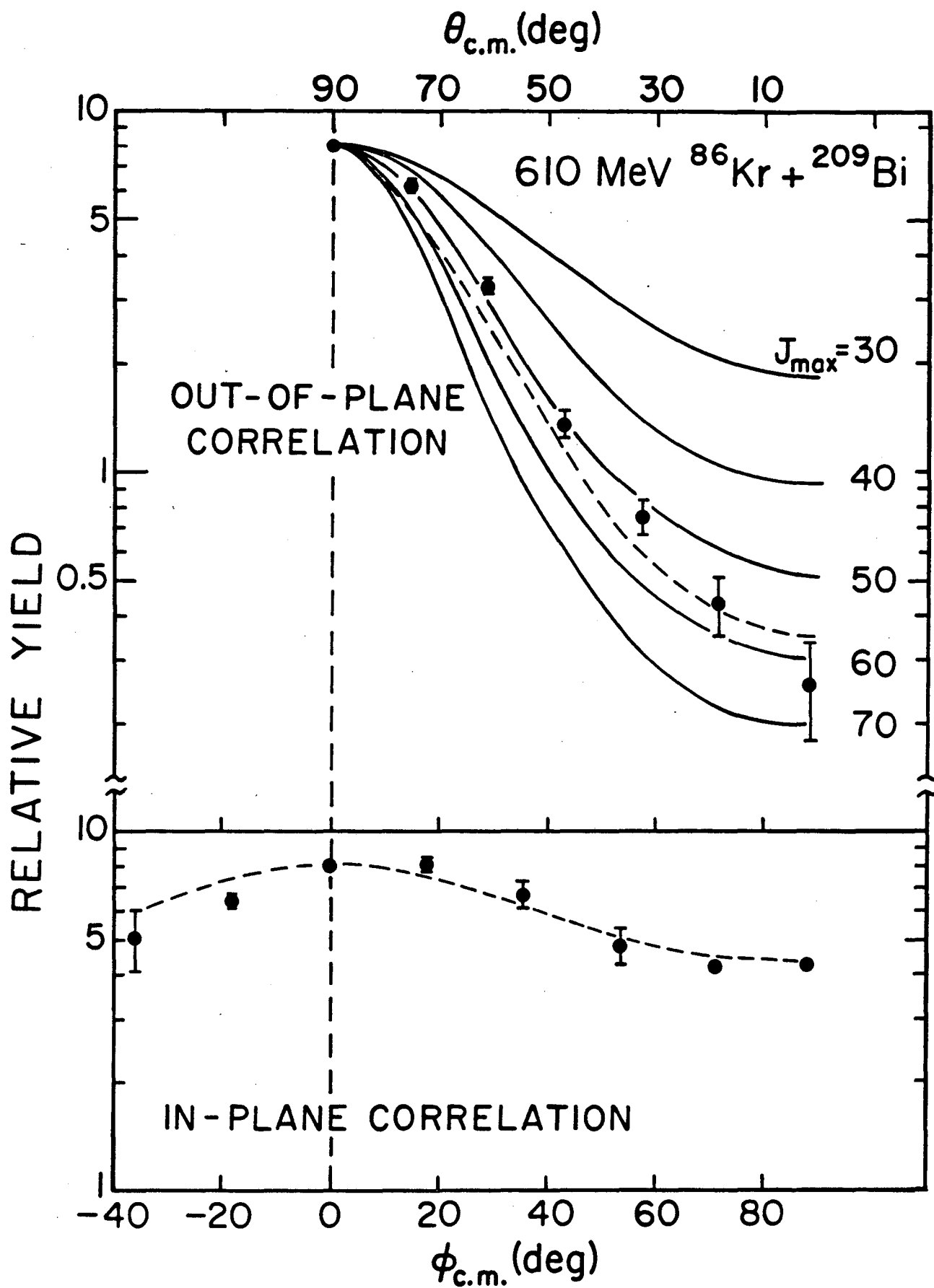


Fig. 48

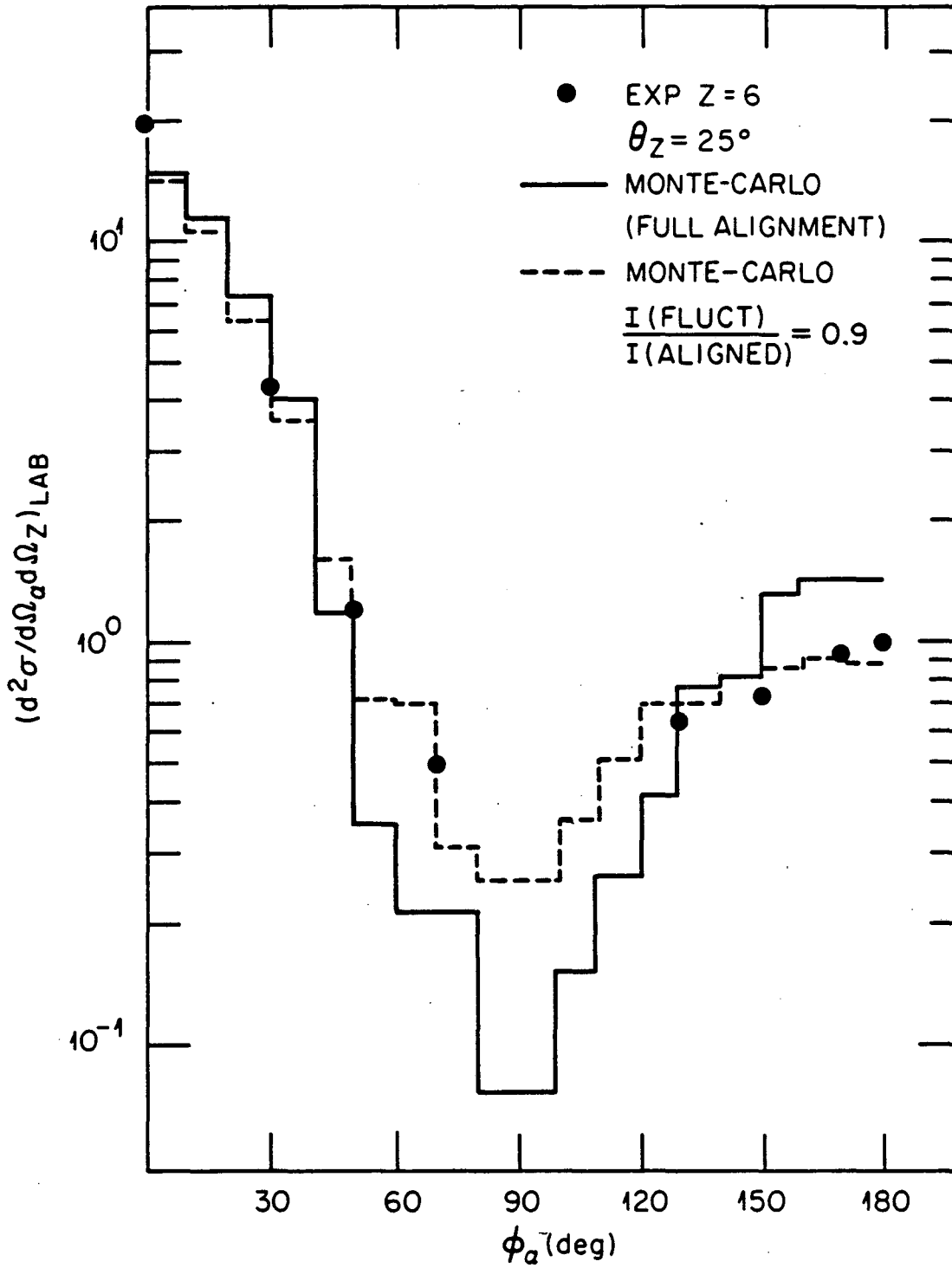


Fig. 49

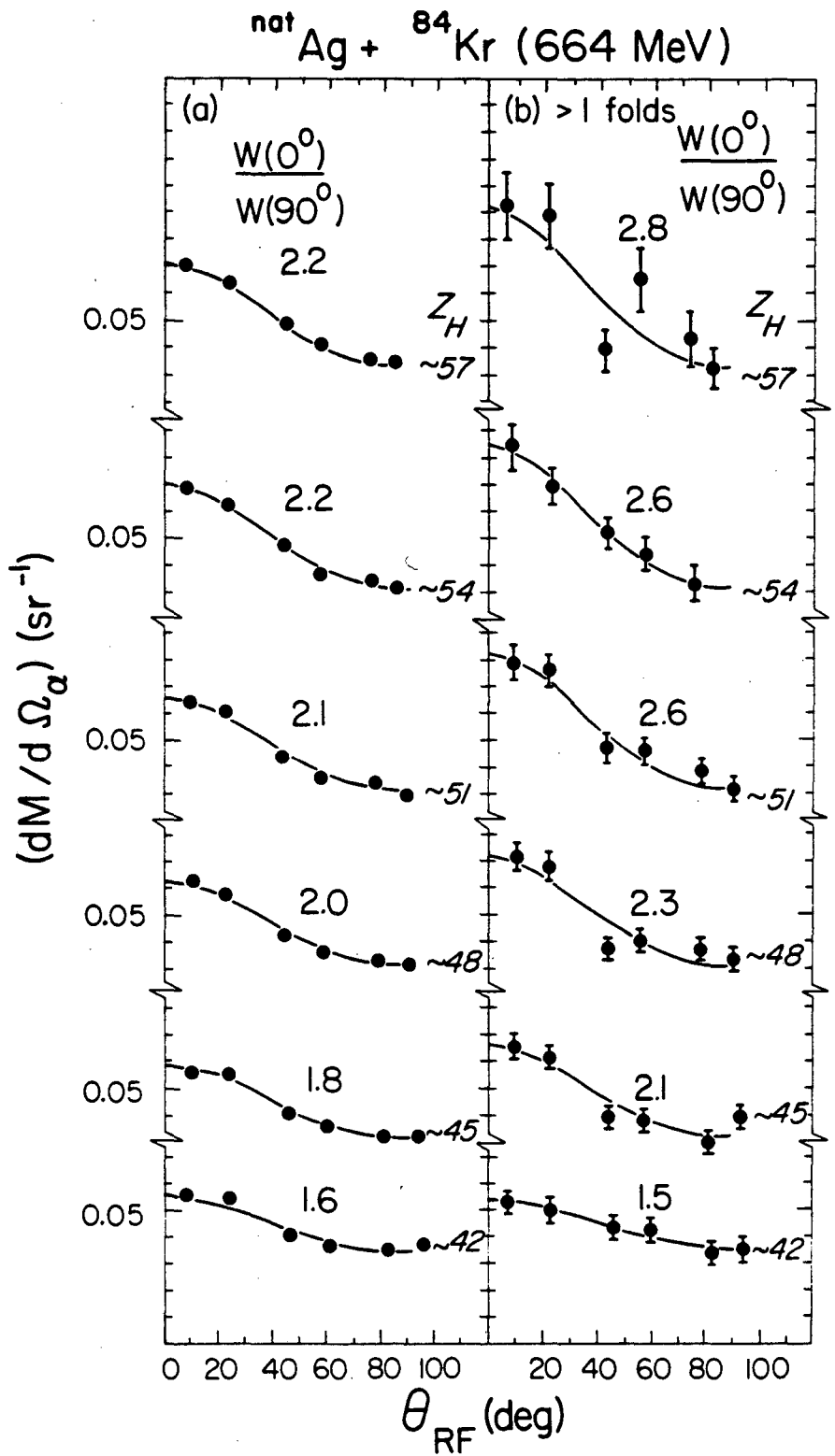


Fig. 50

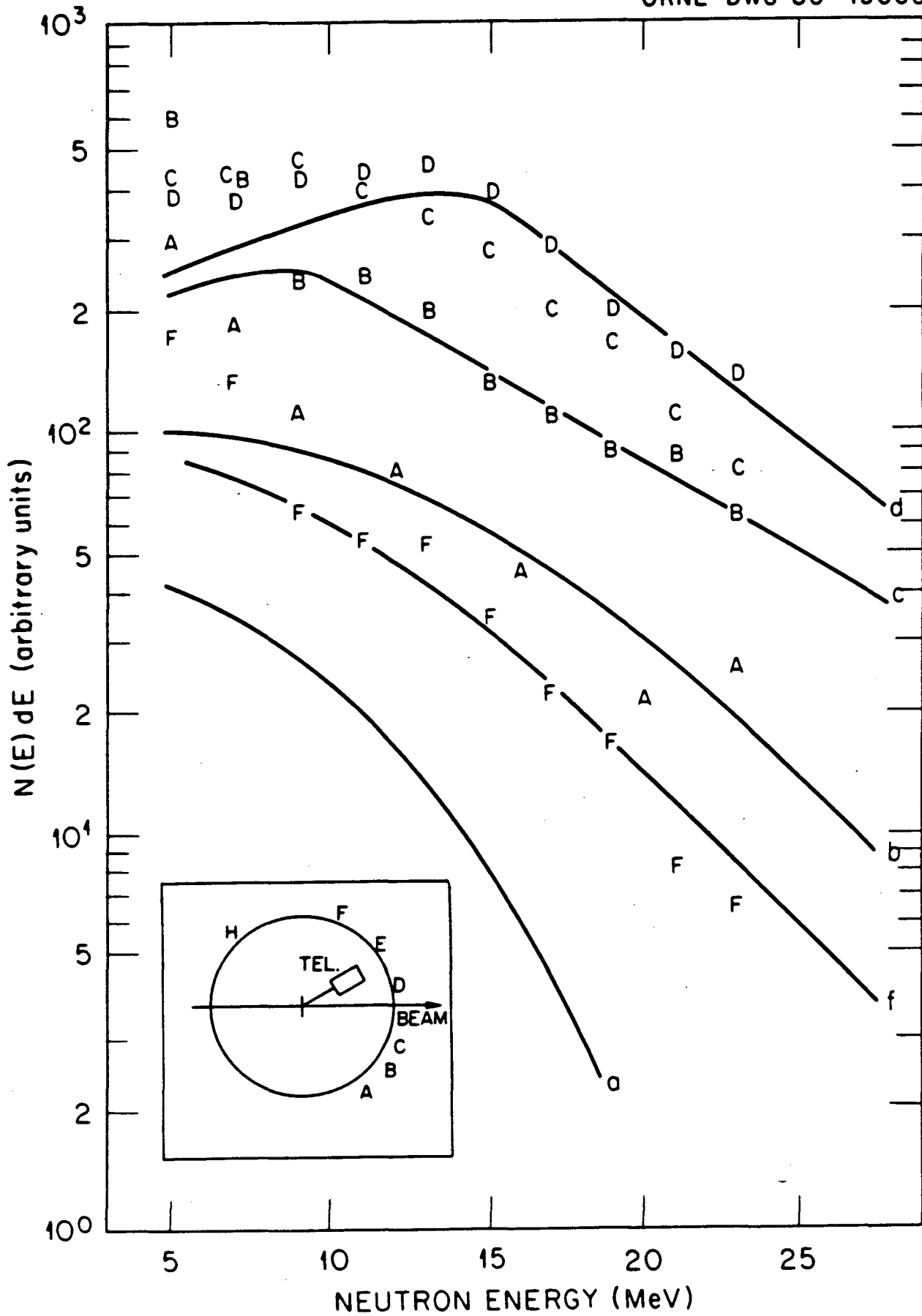


Fig. 51

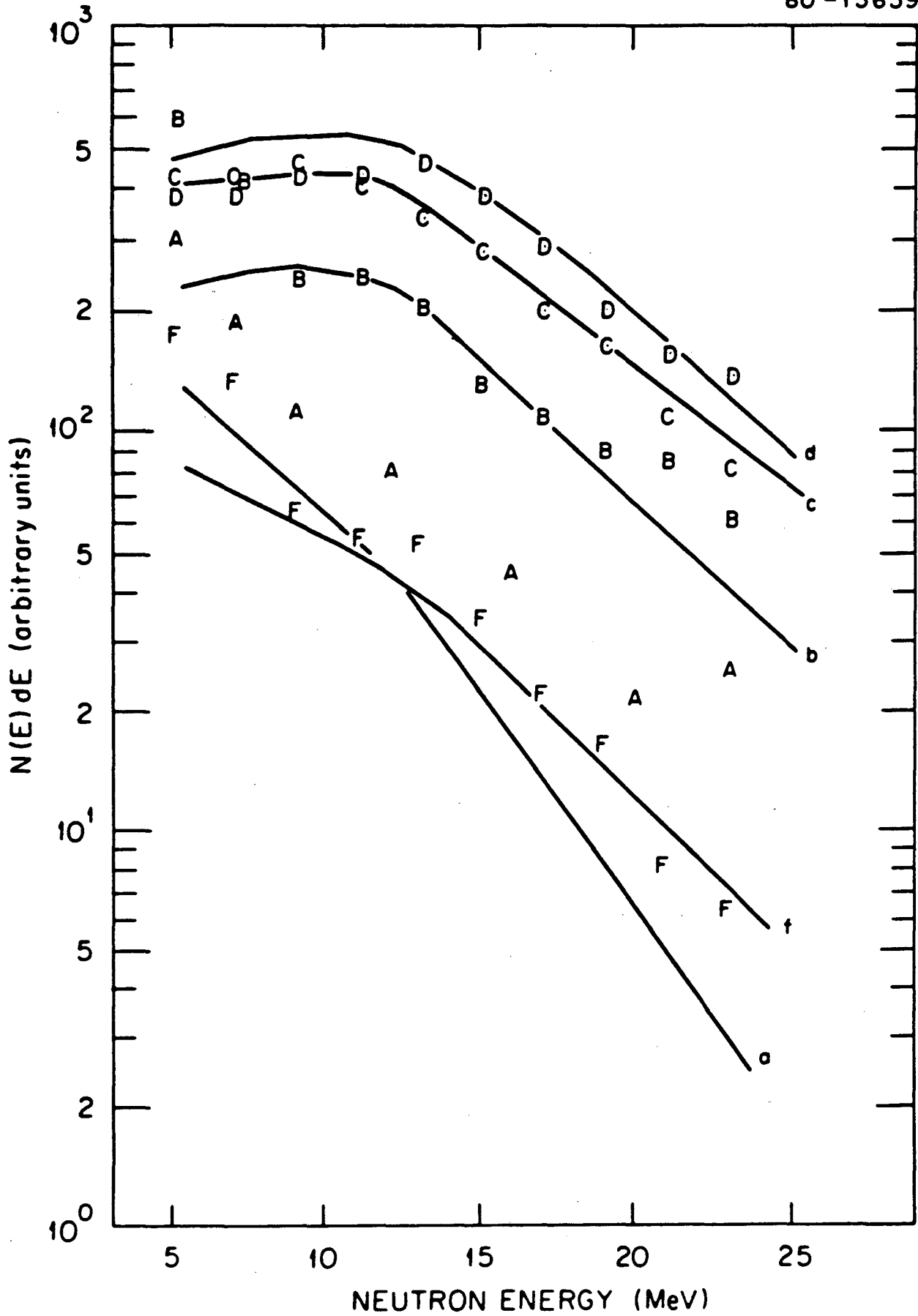
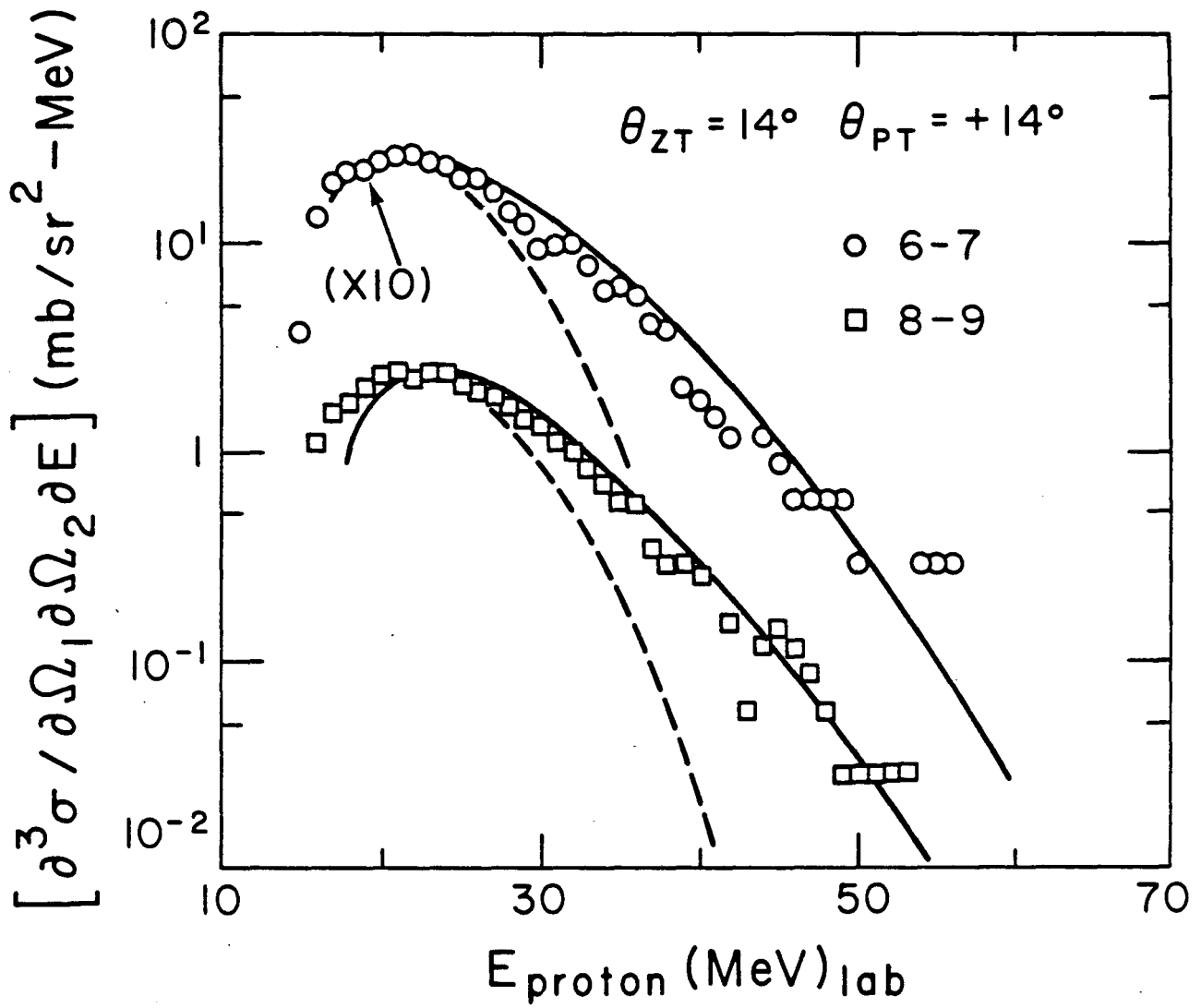
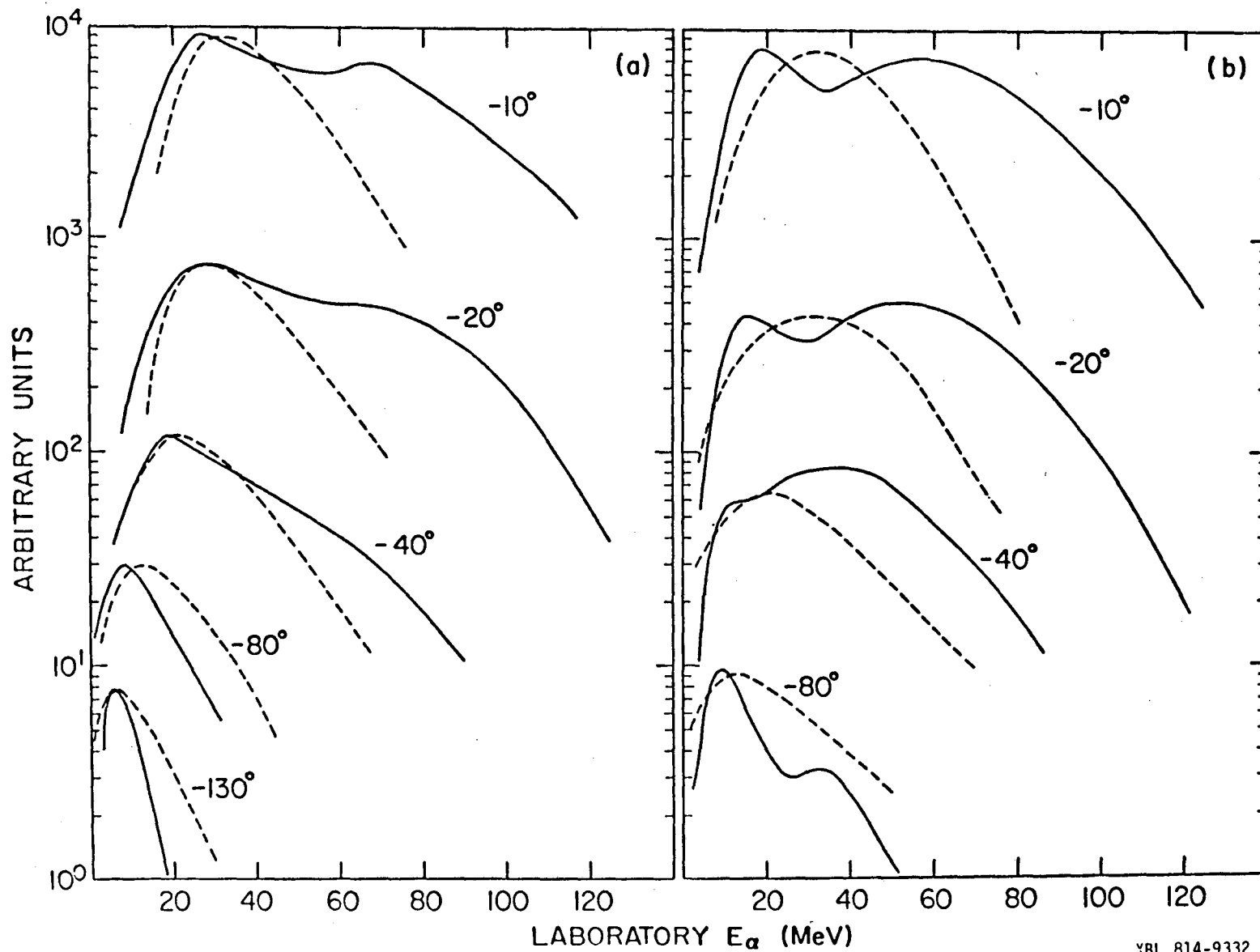


Fig. 52



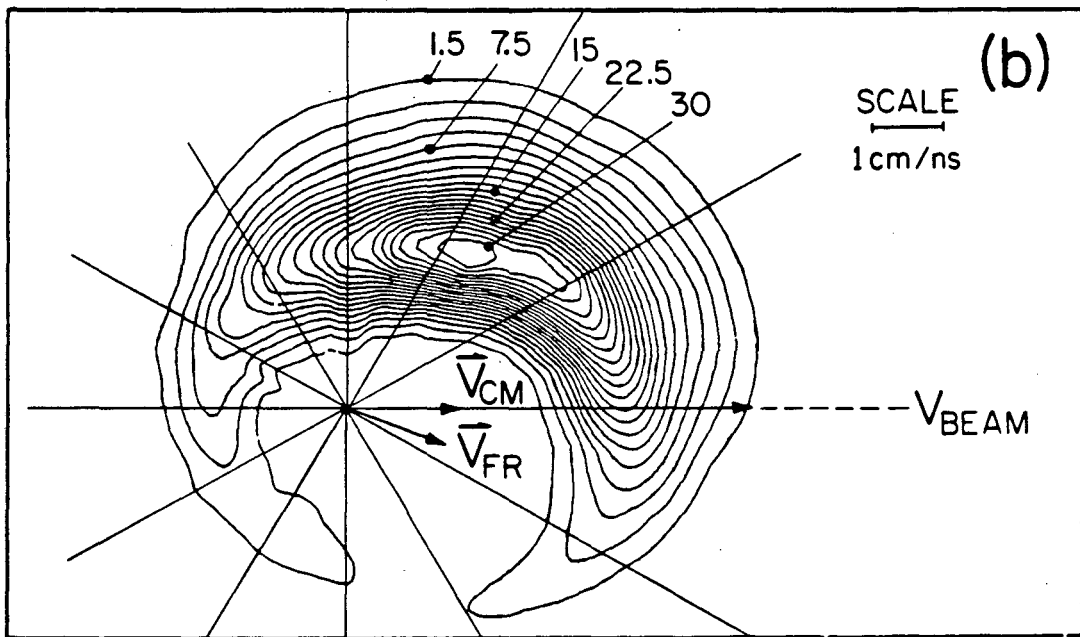
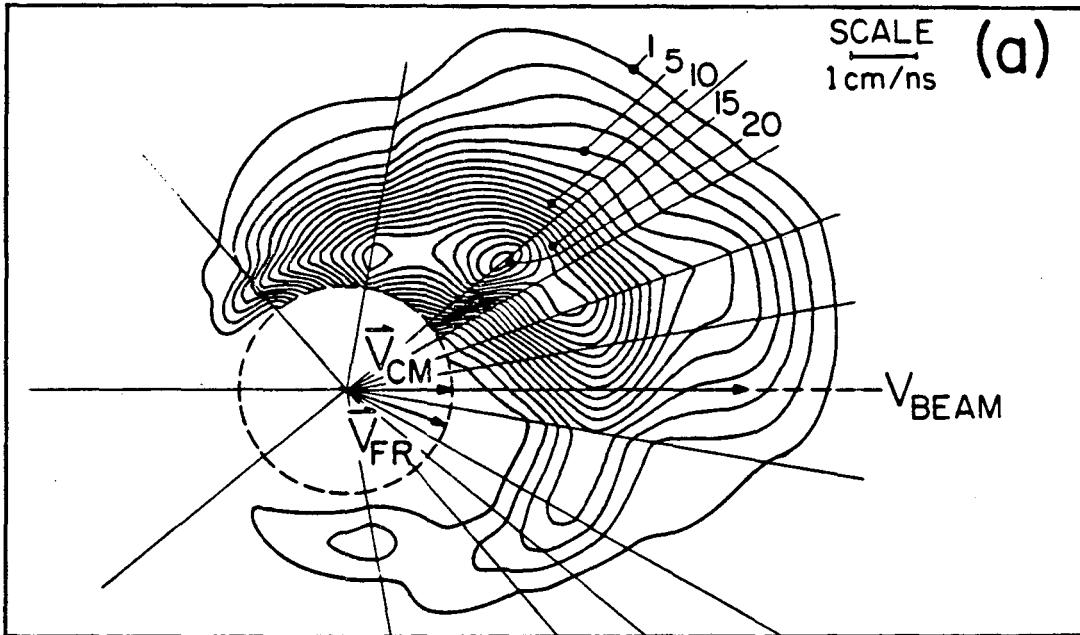
XBL 806-1322

Fig. 53



XBL 814-9332

Fig. 54



XBL 814-9331

Fig. 55

This report was done with support from the Department of Energy. Any conclusions or opinions expressed in this report represent solely those of the author(s) and not necessarily those of The Regents of the University of California, the Lawrence Berkeley Laboratory or the Department of Energy.

Reference to a company or product name does not imply approval or recommendation of the product by the University of California or the U.S. Department of Energy to the exclusion of others that may be suitable.

TECHNICAL INFORMATION DEPARTMENT
LAWRENCE BERKELEY LABORATORY
UNIVERSITY OF CALIFORNIA
BERKELEY, CALIFORNIA 94720

LA RCO OSTI CDL